



**HAL**  
open science

# Methodology for nuclear magnetic resonance and ion cyclotron resonance mass spectrometry

Akansha Sehgal

► **To cite this version:**

Akansha Sehgal. Methodology for nuclear magnetic resonance and ion cyclotron resonance mass spectrometry. Theoretical and/or physical chemistry. Université Pierre et Marie Curie - Paris VI, 2014. English. NNT: 2014PA066491 . tel-01140954

**HAL Id: tel-01140954**

**<https://theses.hal.science/tel-01140954>**

Submitted on 10 Apr 2015

**HAL** is a multi-disciplinary open access archive for the deposit and dissemination of scientific research documents, whether they are published or not. The documents may come from teaching and research institutions in France or abroad, or from public or private research centers.

L'archive ouverte pluridisciplinaire **HAL**, est destinée au dépôt et à la diffusion de documents scientifiques de niveau recherche, publiés ou non, émanant des établissements d'enseignement et de recherche français ou étrangers, des laboratoires publics ou privés.

**THESE DE DOCTORATE DE  
L'UNIVERSITE PIERRE ET MARIE CURIE**

Ecole Doctorale 388: Chimie physique et chimie analytique de Paris Centre

Présentée par

Mlle. Akansha SEHGAL

Pour obtenir le grade de

Docteur en sciences

de l' UNIVERSITE PIERRE ET MARIE CURIE

Sujet de la thèse:

**METHODOLOGY FOR NUCLEAR MAGNETIC RESONANCE AND ION CYCLOTRON  
RESONANCE MASS SPECTROMETRY**

Soutenance publique le 8 octobre 2014

Devant un jury composé de:

Président du jury  
Directeur de thèse  
Rapporteurs

Dr. Sandrine SAGAN  
Prof. Geoffrey BODENHAUSEN  
Prof. Guillaume VAN DER REST  
Dr. Anja BOCKMANN  
Dr. Christian ROLANDO  
Dr. Philippe PELUPESSY

Examineurs

कायेन वाचा मनसेन्द्रियैर्वा ।  
बुद्ध्यात्मना वा प्रकृतिस्वभावात् ।  
करोमि यद्यत् सकलं परस्मै ।  
नारायणायेति समर्पयामि ॥ ॥

*Whatever I perform with my body, speech, mind, limbs, intellect,  
or my inner self, either intentionally or unintentionally,  
I dedicate it all to that Supreme Lord.*

*Masi, it's for you.*

"Sometimes our light goes out but is blown into flame by another human being.  
Each of us owes deepest thanks to those who have rekindled this light."  
Albert Schweitzer

## ACKNOWLEDGEMENTS

---

I would like to take this opportunity to extend my heartfelt gratitude towards the following people whose contributions have made this endeavour possible.

*Prof. Geoffrey Bodenhausen:* I feel truly blessed to have worked under your tutelage. You exposed me to different projects, which helped me to build a broader perspective for research. Time and again, I felt that either it be my scientific troubles or administrative, once they used to come under your notice, with some magical ease they used to either get sorted or you used to assist me in having the means to do so myself. It has been because of your guidance and motivation that I could steer myself forward through the course of my thesis with confidence. I cannot express in words the amount of reverence I feel for you. I will always be indebted to you.

*Prof. Guillaume van der Rest, Dr. Anja Bockmann, Dr. Sandrine Sagan:* for being kind enough to accept the request to be a part of my jury.

*Dr. Philippe Pelupessey:* My thesis could happen because of the ever available guidance and help from you. Whatever I know of NMR, Mathematica, Linux, troubleshooting FT-ICR, precisely everything of my three years here, all comes from you. No amount of "thank you" can suffice for your contribution. I wish I could have learned and imbibed more from you. You are such an ocean of wisdom, knowledge and humility and I hope I will be able to be if not as wise and great a researcher but as humble a human being as you are.

*Dr. Christian Rolando:* I could learn and do FT-ICR because of your patience and the time that you invested in teaching it to me, sitting on the instrument for hours at stretch if the need be or all the discussions that you used to do indulge in so that I never have dearth of ideas to try. I am extremely grateful for your valuable advices and the freedom that you gave me for letting me try new stuffs on the machine and also through my simulations. I thank you immensely for your encouragement and appreciation at every step.

*Dr. Marc Andre Delsuc:* I am grateful for your kind counsel on issues related to coding and 2D FT-ICR. The discussions with you during the ANR meetings have helped in shaping the thesis in a better way.

*Dr. Luminita Duma:* You have been my friend first and colleague second. From the very beginning, you have taken those extra measures to make me feel welcome, happy and sane by opening not just your heart but also your family. From the scared calls while sitting on the spectrometer, to the creativity block while writing, to the self doubts and to the personal woes, you have been there at every step with me, helping, explaining, teaching, encouraging or just listening. I thank you for the science that I learned from you but I think I cannot thank

you for the love that you have bestowed on me. I can just say that I feel blessed to have known you and to have you as a friend.

*Dr. Daniel Abergel:* I would like to thank you immensely for all the valuable discussions and suggestions regarding my subject in particular and science in general. I also owe a thank you to you for keeping me motivated to do science and good science and not give up yet. You were one of the few people in front of whom my truest dumbest streak used to become prominent, thank you for bearing with it and taking it in a fun stride. Your reactions were a reminiscence of my home and used to make me nostalgic but immensely delighted.

*Mr. Fabrice Bray:* I earnestly thank you for your kind and extremely helpful discussions, prompt help from solving the spectrometer issues, to the sample preparation, to data processing. *Team in Lille, Dr. Marie van Agthoven, , Dr. Caroline Tokarski, Dr. Sophie Dalongeville, Dr. Rami Nader, Dr. Azarmidokht Shirazi, Clara and all the people I met on my stay in Lille:* Thank you for your kind hospitality. Your presence helped me to have a productive stay in Lille always.

*Dr. Lionel Chiron:* You have always been too kind to help in any of the coding related issues or explaining the complex work that you do. I thank you for your kind help.

*Dr. Monique Chan Huot:* You have been my first friend here and I have shared the joys of so many firsts of the things with you, from the first trip in Paris with you and your family, to the first salary, and so many more. Thank you for all the good times in and outside the lab. Thank you for not just reassuring but also proving that I always have a bed in your house and I will never be homeless in Paris ;). I will always miss the girl's office fun. I sincerely cherish our friendship and you truly hold a special place in my heart.

*Dr. Enrique Herbert Pucheta:* I landed in Paris to your ebullient smile and warm hug and that made me feel that I am going to be in a wonderful place. Big thanks to you for being my angel.

*Dr. Bruno Vitorge:* My dead computer of two days used to suddenly get started knowing you are in vicinity. Thank you for having such a big influence on my machine also :). Thank you for all the scientific discussions and ideas that you used to lend and for always being so interested in listening to the progress in my work. You are such a nice person. Thank you for everything.

*Shahid:* my veer :), *Cyril:* my grand sucre ami :) thank you for keeping the happy mood high in the lab. The lows are not too lows and the highs are additionally high when one has people like you to share it with. The most awesome lab-mates one could have. *Ching yu:* you are the talent queen of the lab, *Samuel:* my gaba: I wish we could have had spend more time in our office together but whatsoever memories are there, those will always be cherished. Thank you. :). *Dr. Nicolas Birlirakis:* Thank you for all the support and anecdotes for managing the tough times. It indeed used to cheer me up.

*Dr. Piotr Tekeley, Dr. Fabien Ferrage, Dr. Zeinab Serhan, Rudra,* and all other present and past members of the lab: Thank you for the wonderful working atmosphere. All the good people in the lab add to the great science that is performed here. It was a privilege that I was a part of such a great team.

*Eliane:* You have been helping me even before I arrived in France. I can never thank you enough. The small note that you left beside the food that I might need on my arrival here, I still keep it. Since then, to all the paper work, to all the phone calls, to the hassles of visas and tickets and readmissions, you have helped me with everything. You are such a warm person and I am immensely grateful to you.

*Dominique, Anne, Nathalie, Karine and Stephane:* You all have been so kind with your prompt administrative helps. Doing science becomes easier when all such things are well taken care by proficient people like you. Grand merci.

*ANR and ERC Grant:* For the project funding that enabled me to have this PhD.

*Paris:* I came to you knowing not even the language and no person and you gave me some of the best memories ever. Thank you for being so generous in accepting me and thank you for making me meet so many kind hearted people at every step of my stay, some of them ended up being friends for life. I would specially like to thank *Shubhodeep da* (I miss you so much), *Debjaani Di* (the world needs more people like you), *Stephen and co.* (my darling sweetheart, you have been my guardian here, thank you for all the great times), *Saneesh* (you don't need a written thank you and I am not giving you one :P), *Shalini di* (I will make up for all the promises after this, you are adorable), *Lauren* (the world is too small for the people who are close through heart), *Surayya appu* (I wish I get even a part of your energy and enthusiasm, thank you for accommodating me in your life), *Gayatri and Tanmay* (stay exactly as you both are, you both are the kind of friends that everyone would love to have) and everyone from Art of Living, Paris.: Thank you.

*Shruti di:* What should I write for you and how should I thank you? You have been my sister that I never had, the exact replica of the mother I already have and the future mother in law that I will someday have. You have been my confidant and comforter. I looked forward to returning from lab everyday as I knew you were there. Every day of living in Paris would not have been this good if it was not for you. You made my home away from home. I thank God for letting me find you and I love you profusely.

And yes now, my family: *Masi, Mumma, Papa and my babies, Luv and Kush:* Staying away from you people has been the biggest ordeal. But your unconditional support, love and humour made it easier to go through, for me if not always for you all. I have kept my promise of finishing the PhD as still remaining, your happy girl, and I hope I made you all proud. You are the best and the craziest family to have. You all make the epicentre of my world and I am insignificant and incomplete without you all. Whatever I am is all because of you people and also all for you people. I love you all the most.

And last but not the least, *Gurumaharajji*, thank you, everything is because of your omnipresent grace.



## ABSTRACT

---

This thesis encompasses methodological developments in both nuclear magnetic resonance and Fourier transform ion cyclotron resonance mass spectrometry. The NMR section explores the effects of scalar relaxation on a coupled nucleus to measure fast exchange rates. In order to quantify these rates accurately, a precise knowledge of the chemical shifts of the labile protons and of the scalar couplings is normally required. We applied the method to histidine where no such information was available *a priori*, neither about the proton chemical shifts nor about the one-bond scalar coupling constants  $J(^1\text{H}^{15}\text{N})$ , since the protons were invisible due to fast exchange. We have measured the exchange rates of the protons of the imidazole ring and of amino protons in histidine by indirect detection via  $^{15}\text{N}$ . Not only the exchange rate constants, but also the elusive chemical shifts of the protons and the coupling constants could be determined.

For the mass spectrometry section, the ion isolation project was initiated to study the effect of phase change of radiofrequency pulses. Excitation of ions in the ICR cell is a linear process, so that the pulse voltage required for ejecting ions must be inversely proportional to the pulse duration. A continuous sweep pulse propels the ion to a higher radius, whereas a phase reversal causes the ion to come to the centre. This represents the principle of ‘notch ejection’, wherein the ion for which the phase is reversed is retained in the ICR cell, while the remaining ions are ejected. We designed and calibrated pulses, such that the power levels of the ejection pulses are attenuated while the sweep rate is slowed down in the vicinity of the frequencies to be isolated, thereby achieving high resolution and clean isolation.

The manuscript also contains a theoretical chapter, wherein the ion trajectories are plotted by solving the Lorentzian equation for the three-pulse scheme used for two-dimensional ICR. Through our simulations we mapped the ion trajectories for different pulse durations and for different phase relations. We extended our studies to understand harmonics and specifically, to analyze the contribution to harmonics in the 2D spectra due to off-axis excitation, i.e., to ions on trajectories that are not centered in the middle of the ICR cell.

Keywords: histidine, exchange, notch ejection, ion isolation, 2D FT-ICR, pulse schemes.



# CONTENTS

---

<b>Acknowledgements</b>	<b>i</b>
<b>Abstract and keywords</b>	<b>iv</b>
<b>Preamble</b>	<b>1</b>
<b>Part I</b>	
<b>Chapter 1</b>	
<b>Fast proton exchange in histidine: measurement of rate constants through indirect detection by NMR spectroscopy</b>	
1.1 Introduction	4
1.2 Experimental Section	9
1.2.1 Instrumental details	9
1.2.2 Sample preparation	9
1.2.3 Pulse Sequence	9
1.3 Methodology	14
1.4 Results and Discussions	24
1.4.1 Mechanism of Exchange	26
1.4.2 Activation Energy	31
1.5 Conclusions	33
References	34
Glossary Part-I	40

## **Part II**

### **Chapter 2**

#### **High-resolution ion isolation in Fourier transform ion cyclotron resonance (FT-ICR) mass spectrometry by modulating the RF phase during the frequency**

2.1 Introduction	50
2.2 Theory	54
2.3 Experimental Section	59
2.3.1 Pulse Scheme	60
2.3.2 Sample preparation	62
2.4 Results and Discussions	63
2.5 Conclusions and Perspectives	72
References	74

### **Chapter 3**

#### **Spiraling ion trajectories in two-dimensional ion cyclotron resonance mass spectroscopy**

3.1 Introduction	79
3.1.1 History of 2D FT-ICR	79
3.1.2 Similarities and differences between ICR and NMR	81
3.2 2D FT-ICR pulse scheme	84
3.3 Equations of motion	87
3.3.1 Excitation pulse period	89
3.3.2 Encoding period	90
3.3.3 Encoding pulse period	90
3.3.4 Fragmentation period	92

3.4 Trajectory Mapping	92
3.4.1 Case I: $\omega_k t_1 = 2n\pi$ and $\omega_k T = 2\pi$	93
3.4.2 Case II: $\omega_k t_1 < 2n\pi$ and $\omega_k T = 2\pi$	93
3.4.3 Case III: $\omega_k t_1 = 2n\pi$ and $\omega_k T < 2\pi$	94
3.4.4 Case IV: $\omega_k t_1 < 2n\pi$ and $\omega_k T < 2\pi$	94
3.5 Harmonics in 2D spectra	101
3.6 Conclusions and Perspectives	104
References	108
Glossary Part-II	111
Appendix-I	117
Resume de la thèse	119
Curriculum Vitae	131



## PREAMBLE

---

During my PhD, I had an opportunity to work on methodological developments in two completely different fields of spectroscopy: Nuclear Magnetic Resonance (NMR) and Fourier Transform Ion Cyclotron Resonance (FT-ICR) mass spectrometry. As a methodologist, the aim is to find new and better ways of doing old stuff and also to improve existing methods and theories. For NMR, wonderful tools of spin manipulations can be managed by implementing pulse sequences, and for FT-ICR, mass-over-charge ratios of precursors and fragment ions can be obtained through various methods, thus providing solutions to problems in chemistry, biochemistry, and medicine.

This doctoral dissertation comprises of two parts and a total of three chapters. Because of the fragmented nature of the work, each chapter contains its own introduction, methodology, conclusion and references, and can be read independently. There is a glossary included at the end of every part to explain some common definitions and terms used in the text. The first part constitutes the NMR section. In chapter I, we describe an improved method developed previously in the group to study fast exchange of protons by NMR. We applied the method to the complex system of the amino acid histidine where no *a priori* information about the chemical shifts or the one- bond scalar coupling constants is available, which are normally required for the determination of the exchange rate constants. The second part deals with mass spectrometry and comprises of two chapters. In chapter II, we have tried to revive and implement a long-forgotten method of ion isolation by ‘notch ejection’ in Fourier transform ICR mass spectrometry. We have shown how this technique can be applied to high mass-to-charge ratios without losing on the coveted resolution, essential for mass spectrometry. In

chapter III, we sought to achieve a better understanding of the intricacies of the behaviour of ions during the three-pulse scheme used for two-dimensional ICR, especially for pulses of short duration.

## Part-I





## CHAPTER 1

---

# **Fast proton exchange in histidine: measurement of rate constants through indirect detection by NMR spectroscopy**

## **1.1 Introduction**

Molecules in solutions are not rigid structures. They exhibit internal dynamics ranging from fast molecular vibrations, molecular rotations to slow chemical exchange. Chemical exchange can be broadly classified in two categories: i) conformational or intramolecular exchange and ii) chemical or intermolecular exchange. Conformational exchange implies a change in the shape of the molecule due to its environment such as temperature or pH. It includes processes like side-chain motions in proteins, helix-coil transitions of nucleic acids, folding and unfolding of proteins and tautomerization, to mention a few. If the dynamics involve breaking and reforming of bonds, then it is referred to as chemical exchange. This includes processes like binding of ligands to macromolecules, enzyme-catalysed reactions and - the topic of this chapter - protonation/deprotonation, i.e., the exchange of labile protons with the solvent. Most methods used for measuring exchange like fluorescence and absorbance spectroscopy require a perturbation of the system and its return to equilibrium. One can probe the different properties of the two exchanging states during the course of the reaction, e.g. different optical absorptions of exchanging species, or a change in the orientation of a dye attached to a protein involved in conformational exchange. NMR is capable of detecting chemical exchange at atomic resolution even when the system is in chemical and physical equilibrium and when the exchanging moieties are indistinguishable. This is possible because the probes used in NMR are nuclear spins which are located at particular sites in the molecule

and act as spies to detect the motion. So, one detects a perturbation due to exchange of the magnetisation, without disturbing the chemical equilibrium.

Since nuclear magnetic resonance (NMR) is sensitive to chemical bonding, the effect of chemical exchange becomes evident in the spectrum. The exchange of a nucleus between different environments leads to change in NMR parameters like scalar couplings, chemical shifts, etc.<sup>1</sup>

The NMR chemical exchange timescale can be divided into three regimes: slow, intermediate and fast exchange. If we consider exchange between two equally populated sites (A and B), then in the slow regime the exchange rate is much smaller than the separation between the chemical shifts of the two sites, so the normal spectrum is observed with a slight broadening of the lines with increasing dynamics. This broadening continues up to a cross-over point where the lines coalesce as the peaks from the two sites move together and finally merge, so that one speaks of intermediate exchange. As the exchange rate is increased further, it causes narrowing of the coalesced peak. In the limit of very fast exchange, the spins only experience an average chemical shift. The transitions between these three regimes are not very well defined and often one refers to these as slow to intermediate and intermediate to fast exchange.

This whole variation of time-scales of exchange rates can also be illustrated by the case of a nucleus  $S$  that is scalar coupled with an exchanging proton  $I$ . An exchange event can cause a switch between the two lines of the  $J$ -splitting. In the slow exchange regime, the  $S$ -spin spectrum consists of two peaks separated in frequency by  $2\pi J_{IS}$ . In the fast exchange regime, the doublet splitting collapses and the spectrum consists of a single peak at the average of the

two lines in the doublet, i.e., at the chemical shift of the  $S$ -spin, a simplification known as self-decoupling, depicted in Figure 1.1.<sup>2</sup>

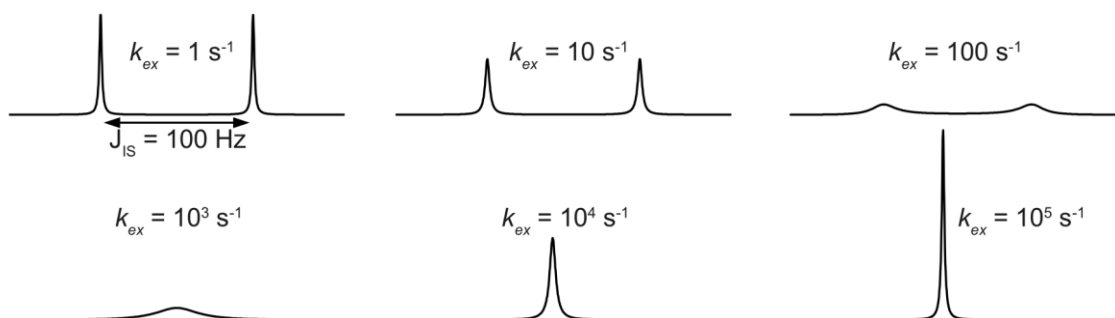


**Figure 1.1.**  $^{15}\text{N}$  spectra for a system where the directly bonded proton participates in exchange (Figure reproduced by permission from *P. Pelupessey, HDR Defense, 2013*).<sup>3</sup>

For the slow to intermediate exchange regime, 2D exchange spectroscopy (EXSY) can be used to obtain maps of cross peaks between exchanging sites.<sup>4</sup> The key parameter in 2D EXSY experiments is the mixing time, which has to be judiciously chosen depending on the exchange rate and the spin-lattice relaxation time  $T_1$ . If the mixing time is too short compared to the inverse of the exchange rate, the cross peaks are very small, while too long a mixing time leads to loss of signal intensity due to  $T_1$  relaxation.<sup>5</sup> Another method employed is the selective inversion-recovery experiment wherein one of the exchanging sites is selectively manipulated while the effects on other sites is observed.<sup>6</sup>

In the fast exchange regime, i.e., beyond the coalescence to a single peak, the contribution to the linewidth due to exchange has to be distinguished from effects of magnetic field inhomogeneity and spin-spin relaxation. The former can be suppressed by the use of a spin echo.<sup>7</sup> The latter can be separated from the exchange rate by varying the delay between the

refocusing pulses in a CPMG (Carr-Purcell-Meiboom-Gill) pulse train.<sup>8-10</sup> Fast exchange rates can also be determined by the measurement of  $T_{1\rho}$ , the spin lattice relaxation time in the rotating frame. The exchange process is characterized by measuring relaxation rates  $1/T_{1\rho}$  when the magnetization is spin-locked using a radio-frequency (*rf*) field.<sup>11</sup> An alternate method for measuring fast exchange is by offset saturation as proposed by Bain *et al.*<sup>12</sup> The offset saturation experiment consists of irradiating the spins with an *rf* field at some offset from resonance, until a steady state is achieved. The *rf* field is then removed and the *z*-magnetisation is measured by an observation pulse. This procedure is repeated for various offsets and the exchange rate is extracted from the curve of  $M_z$  versus the offset.

Proton exchange can be determined by variety of methods in NMR, such as by the analysis of the line-shape of exchanging protons,<sup>13</sup> polarization transfer from the water resonance,<sup>14</sup> decorrelation of longitudinal two-spin order,<sup>15</sup> or measurements of translational diffusion coefficients.<sup>16</sup> Although NMR is unparalleled for the determination of exchange rates due to its capacity to provide site-specific information, its scope is normally limited to moderately fast proton exchange rates (up to few thousand  $s^{-1}$  under favourable conditions).<sup>1,17</sup> We have recently shown how to extend the range of exchange rates that can be measured by NMR by more than an order of magnitude (up to  $10^5 s^{-1}$  for a NH group), using a method that accurately determines the effects on  $^{15}N$  nuclei of scalar relaxation due to exchanging protons.<sup>18</sup> This method relies on monitoring the decay of  $^{15}N$  magnetization under multiple refocusing Carr-Purcell-Meiboom-Gill (CPMG) trains in the presence and absence of proton decoupling.

In the present work, we applied the knowledge acquired for determining fast exchange rates to the challenging system of histidine. Histidine is an essential amino acid that is often found in active sites of enzymes and other proteins that are involved in catalysis,<sup>19</sup> pH regulation,<sup>20</sup>

metal binding<sup>21</sup> and phosphorylation.<sup>22,23</sup> The unique properties of histidine arise from its acid-base characteristics. Indeed, it is the only amino acid with an imidazole side chain that can act either as an acid or as a base in the physiological pH range. This property is of considerable significance for the function of many proteins. For example, NMR confirmed the catalytic role of His-12 and His-119 in RNase A,<sup>24</sup> the regulatory function of His-146 in human haemoglobin,<sup>25</sup> the role of His-37 in shuttling protons into the virion by imidazole protonation and deprotonation, which is facilitated by ring reorientation.<sup>26</sup> Pioneering NMR studies based on direct proton detection have shown that the H<sup>ε2</sup> and H<sup>δ1</sup> protons of the imidazole ring exhibit slow exchange rates in RNase<sup>27</sup> and in human carbonic anhydrase.<sup>28</sup> While NMR spectroscopy has been used to study <sup>15</sup>N chemical shifts and <sup>2</sup>J<sub>NC</sub> and <sup>3</sup>J<sub>NC</sub> in the imidazole rings of histidine over a wide pH range,<sup>29,30</sup> to the best of our knowledge, the exchange rates of labile protons of histidine in aqueous solution had not yet been reported. Solid-state NMR spectroscopy has been used to study <sup>15</sup>N and <sup>13</sup>C chemical shifts of histidine in single crystals and in lyophilized and microcrystalline powders,<sup>31-34</sup> while isotropic and anisotropic <sup>15</sup>N chemical shifts were exploited to investigate the tautomeric and acid-base equilibria of histidine.<sup>31,32</sup> A linear correlation was found between the isotropic <sup>15</sup>N chemical shifts in imidazole and the degree of bond stretching induced by H-bonding.<sup>35</sup> Interestingly, the <sup>13</sup>C chemical shifts of imidazole in histidine lyophilized from solutions with various pH values conserved information about the *pK<sub>a</sub>*'s of the parent solutions.<sup>33</sup>

This chapter describes the measurement of fast exchange rate constants of the H<sup>δ1</sup> and H<sup>ε2</sup> protons of the imidazole ring and of the NH<sub>3</sub><sup>+</sup> protons in histidine as a function of pH and temperature. Furthermore, we determined the elusive one-bond scalar coupling constants <sup>1</sup>J<sub>NH<sub>i</sub></sub> and chemical shifts δ<sub>Hi</sub> of the otherwise invisible H<sup>δ1</sup>, H<sup>ε2</sup> and NH<sub>3</sub><sup>+</sup> protons which could so far not be determined for the range of pH and temperatures under investigation.

## 1.2 Experimental Section

### 1.2.1 Instrumental details

All experiments were performed at 14 T (600 MHz for  $^1\text{H}$ ) using a Bruker Avance III spectrometer equipped with a triple-channel indirect detection probe. Temperature calibration was performed using a mixture of protonated - deuterated (4:96) methanol.<sup>36</sup>

### 1.2.2 Sample preparation and pH measurements

U- $^{13}\text{C}$ ,  $^{15}\text{N}$ -labelled Histidine.HCl.H<sub>2</sub>O was purchased from Cortecnet (France). 20 mM solutions of histidine with a pH ranging from 1.39 to 4.88 were prepared using HCl (1 M, 0.1 M, 0.01 M) or NaOH (1 M, 0.1 M). No buffers have been used in this work to avoid their contributions to hydrogen exchange rates. The pH measurements were performed with a pH meter (Hach Langer) before and after the experiments, retaining the average in the subsequent analysis. Since the experiments were performed without adding any buffer, new NMR tubes were scrupulously cleaned in order to prevent any pH drift, using a Sigma Aldrich NMR tube cleaning apparatus. The tubes were filled with concentrated nitric acid, allowed to stand overnight, and copiously rinsed with water.

### 1.2.3 Pulse sequence

The pulse sequences designed to determine the exchange rate constants of the labile  $\text{H}^{\delta 2}$ ,  $\text{H}^{\delta 1}$  or  $\text{NH}_3^+$  protons of histidine are shown in Figure 1.2. The first and last block of the pulse sequence consists of transferring the magnetisation from suitable ‘spy’ nuclei to the nuclei

being probed and vice-versa. The magnetization of a neighbouring ‘spy’ proton such as  $H^{\delta 2}$ ,  $H^{\epsilon 1}$  and  $H^{\alpha}$  is transferred, via the adjacent carbon-13, to the target nitrogen-15 via two successive coherence transfer steps in the manner of Insensitive Nuclei Enhanced by Polarization Transfer (INEPT).<sup>37</sup>

The first INEPT transforms the longitudinal magnetizations  $H^{\delta 2}_z$ ,  $H^{\epsilon 1}_z$  and  $H^{\alpha}$  into two-spin order terms,  $2H^{\delta 2}_z C^{\delta 2}_z$ ,  $2H^{\epsilon 1}_z C^{\epsilon 1}_z$  or  $2H^{\alpha}_z C^{\alpha}_z$  (indicated by “a” in Figure 1.2) and subsequently the second INEPT leads to  $2N^{\epsilon 2}_z C^{\delta 2}_z$ ,  $2N^{\delta 1}_z C^{\epsilon 1}_z$  or  $2N_z C^{\alpha}_z$  (“b” in Figure 1.2). WALTZ-16 decoupling<sup>38</sup> on the proton channel is used during the INEPT sequences that bring about coherence transfer between  $^{13}\text{C}$  and  $^{15}\text{N}$  so as to reduce the signal losses by preventing the evolution of the scalar coupling due to the protons. The two-spin order terms are converted into antiphase coherences,  $2N^{\epsilon 2}_y C^{\delta 2}_z$ ,  $2N^{\delta 1}_y C^{\epsilon 1}_z$  or  $2N_y C^{\alpha}_z$ , by a  $^{15}\text{N}$   $\pi/2$  pulse. Then these coherences are allowed to decay under a multiple-refocusing CPMG (Carl, Purcell, Meiboom and Gill) pulse train applied to the  $^{15}\text{N}$  nuclei. In experiment *B* continuous wave (*cw*) proton decoupling is applied during the  $^{15}\text{N}$  pulse train, while in experiment *A* decoupling is only applied during a delay of an identical duration as the CPMG pulse train, but before this pulse train, when the nitrogen magnetization is still along the *z*-axis. As it was shown in previous work,<sup>18</sup> the extracted exchange rates are sensitive to the offset (reproduced by permission in Figure 1.3). Therefore *cw* decoupling is used during the *A* and *B* blocks of the two experiments rather than a WALTZ-16 sequence (which is however applied during the second INEPT) to extract the resonance frequency from the offset-dependent results. In principle one could also determine the exchange rate by looking directly at the nitrogen spectrum. For slow exchange, the nitrogen spectrum should feature a doublet separated by the one-bond scalar coupling  $^1J(^1\text{H}, ^{15}\text{N})$  of the exchanging proton with the adjacent atom. For intermediate exchange this doublet coalesces and for fast exchange, the coalesced peak becomes a singlet.

The comparison of coupled and decoupled spectra would not provide a sufficiently accurate measure of the exchange rates if the peaks are affected by long-range couplings  ${}^nJ({}^1\text{H}, {}^{15}\text{N})$  with  $n > 1$  between  ${}^{15}\text{N}$  and remote  ${}^1\text{H}$  nuclei. To overcome this problem, a CPMG block is introduced. The interval in between the  $\pi$  pulses of the CPMG sequence is taken to be such that it prevents the evolution of these long-range couplings, whereas the short-range coupling undergoes scalar relaxation, which allows one to determine the proton exchange rates.

Moreover, using protons for the initial excitation and detection provides higher sensitivity, which cannot be achieved by recording  ${}^{15}\text{N}$ -spectra unless protracted 2D experiments are recorded.

The relaxation of the carbon terms,  $C_z^{\delta 2}$ ,  $C_z^{\epsilon 1}$  and  $C_z^{\alpha}$ , of the antiphase coherences affects both experiments  $A$  and  $B$  equally and does not play any role in subsequent analyses. The remaining coherences are then transferred back to the spy protons. Experiments have been recorded for temperatures between 272.6 and 292.5 K. At each temperature and for each  ${}^{15}\text{N}$  nucleus, about 20 different sets of experiments were performed with variable numbers  $2 < n < 32$  of  $\pi$ -pulses in the CPMG pulse trains, different pulse intervals ( $2\tau = 1.25, 2.5, 5$  ms), different offsets of the *rf* carrier (varied in steps of 2 kHz) and different amplitudes of the *cw* proton decoupling field (from 156 to 5000 Hz). Each set of experiments comprised 4 consecutive pairs of experiments  $A$  and  $B$ , and typically lasted about 3 minutes. From the ratios  $A/B$  of the signal intensities observed in experiments  $A$  (without proton decoupling during the  ${}^{15}\text{N}$  CPMG train) and  $B$  (with proton decoupling), the rate constants of the proton exchange were calculated using a home-written Mathematica program. A small correction was applied to account for the presence of 3%  $\text{D}_2\text{O}$  in the solvent.<sup>18</sup>

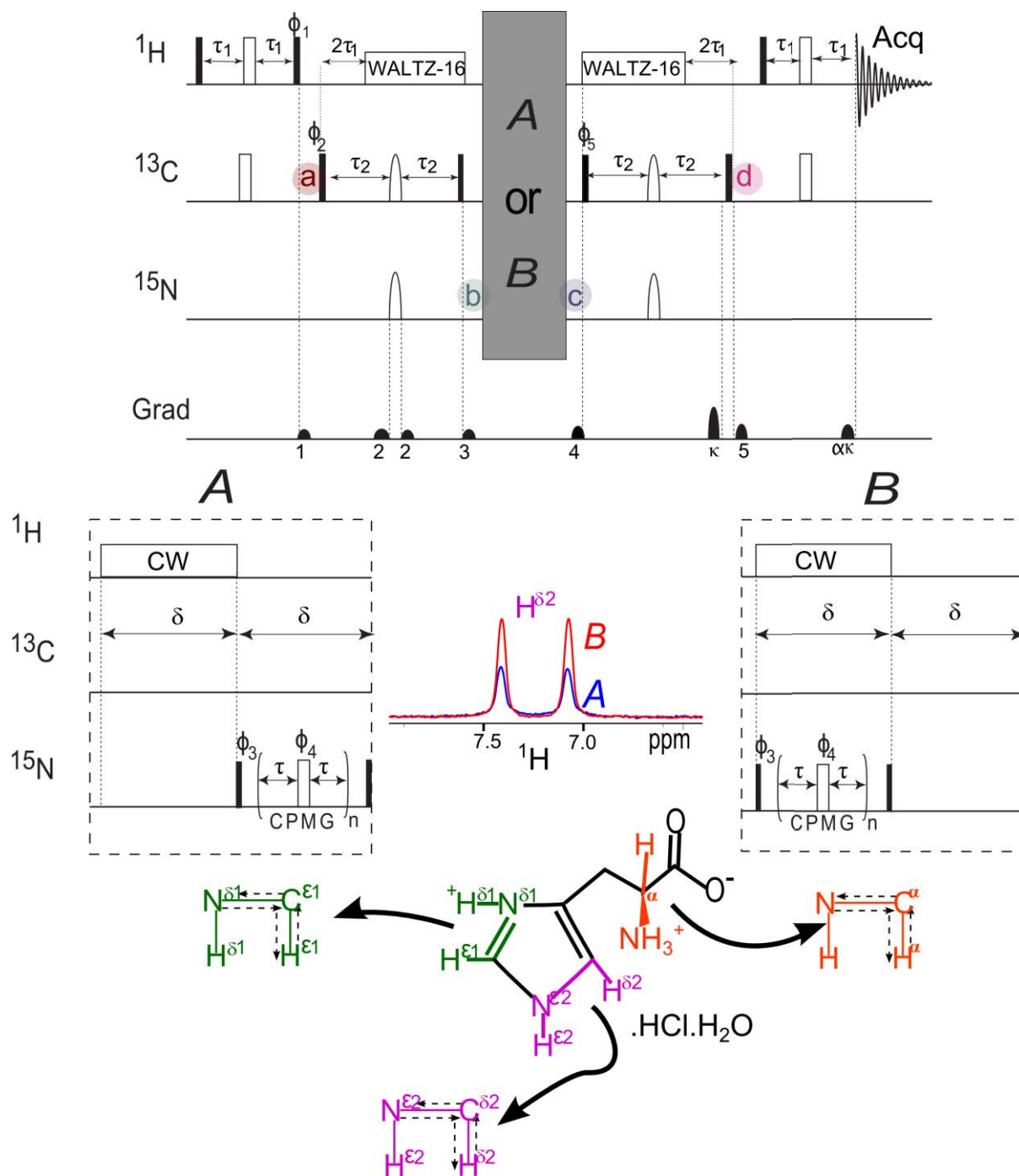


**Figure 1.2.** Pulse sequence designed to measure the proton exchange rates  $k_{ex}$  of the  $\text{NH}^{\delta 1}$ ,  $\text{NH}^{\delta 2}$  and  $\text{NH}_3^+$  groups in histidine. The  $\pi$  and  $\pi/2$  pulses are represented by narrow open and filled rectangles, respectively, while decoupling sequences are represented by wide rectangles. Continuous-wave (cw) proton decoupling is applied in both experiments A and B for a duration  $\delta$ , but the CPMG train, also of length  $\delta$ , is delayed until after the decoupling interval in experiment A, while both are applied at the same time in experiment B. This prevents

differences in temperature induced by decoupling. All  $\pi/2$  and  $\pi$  pulses applied to  $^{13}\text{C}$  in the first and last INEPT blocks were non-selective rectangular pulses, while the  $^{13}\text{C}$  refocusing pulses in the other INEPT blocks had REBURP profiles<sup>39</sup> with a duration of 4 ms. The  $^{15}\text{N}$  inversion  $\pi$  pulse in the INEPT block had a REBURP profile of 2 ms duration for observing  $\text{NH}_3^+$  protons and Q3 profiles<sup>40</sup> with a duration of 30 ms for probing the  $\text{NH}^{\epsilon 2}$  and  $\text{NH}^{\delta 1}$  protons. Continuous-wave proton decoupling was used during the blocks *A* and *B*. The delays were set to  $\tau_1 = 1.69 \text{ ms} \approx 1/(4^1 J_{\text{CH}})$ ,  $\tau_2 = 23.43 \text{ ms} \approx 1/(4^1 J_{\text{NC}})$  for  $\text{NH}_3^+$ ,  $\tau_1 = 1.22 \text{ ms} \approx 1/(4^1 J_{\text{CH}})$ ,  $\tau_2 = 1.10 \text{ ms} \approx 1/(4^1 J_{\text{NC}})$  for  $\text{NH}^{\epsilon 2}$ ,  $\tau_1 = 1.12 \text{ ms} \approx 1/(4^1 J_{\text{CH}})$ ,  $\tau_2 = 2.29 \text{ ms} \approx 1/(4^1 J_{\text{NC}})$  for  $\text{NH}^{\delta 1}$ . All phases were along the *x*-axes unless indicated otherwise. The phases were cycled according to:  $\varphi_1 = 2\{y\}$ ,  $2\{-y\}$ ,  $\varphi_2 = \{x\}$ ,  $\{-x\}$ ,  $\varphi_3 = 4\{x\}$ ,  $4\{-x\}$ ,  $\varphi_4 = y$ ,  $\varphi_5 = 8\{x\}$ ,  $8\{-x\}$  with a receiver phase  $\varphi_{\text{rec}} = \{x, -x, -x, x, -x, x, x, -x, -x, x, x, -x, x, -x, -x, x\}$ . The gradients need to be carefully adjusted so as not to have accidental refocusing. The parameter  $\alpha$  is equal to the ratio  $\gamma_{\text{C}}/\gamma_{\text{H}}$ . The labile  $\text{H}^{\delta 1}$ ,  $\text{H}^{\epsilon 2}$  and  $\text{NH}_3^+$  protons examined in this work are highlighted with colours and the pathways for the transfer of magnetization are indicated on the molecular structure. By way of example, spectra *A* and *B* of the  $\text{H}^{\delta 2}$  proton are shown for indirect detection of  $\text{NH}^{\epsilon 2}$  at pH 3.2 and 292.5 K.

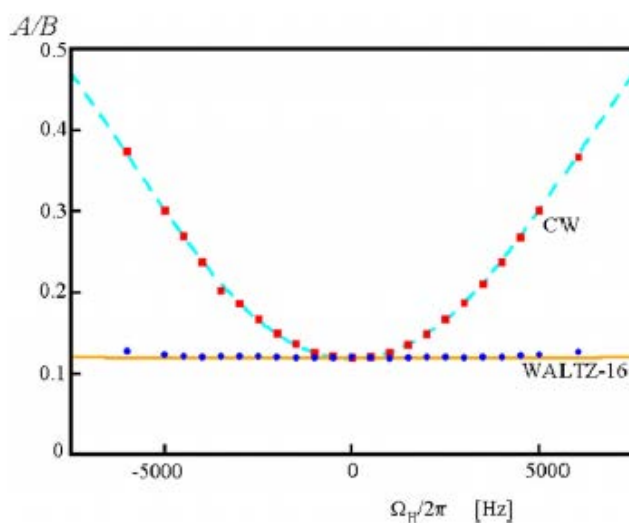


**Figure 1.3.** Experimental (red squares and blue dots) and theoretical profiles (dashed blue and solid orange) of the ratio  $A/B$  versus the offset for *cw* decoupling and WALTZ 16 are shown respectively (Figure reproduced by permission from Kateb *et al.*, *J. Magn. Reson.* 2007).<sup>18</sup>

### 1.3 Methodology

Proton exchange can be mediated either by  $\text{H}_2\text{O}$ ,  $\text{OH}^-$  or  $\text{H}_3\text{O}^+$ . If the incoming and outgoing protons have opposite polarization (which occurs in half of the exchange events), this leads to a flip-flop of the spin attached to the nitrogen. From the point of view of a  $^{15}\text{N}$  nucleus, this amounts to an inter-conversion of the two lines of the doublet, i.e. an exchange of the two single-transition operators:



The exchange constants can be obtained by solving the Liouville–von Neumann equation (equation 1.2) during the CPMG pulse train:

$$\frac{\partial}{\partial t}\rho(t) = -\hat{L}\rho(t) \quad (1.2)$$

where  $\rho(t)$  denotes the density operator and  $\hat{L}$  represents the Liouvillian super-operator,<sup>41</sup> which includes coherent evolution, relaxation and exchange contributions.<sup>42</sup> The solution of this first-order differential equation describes the evolution of the density operator during the CPMG pulse train that contains  $n$   $\pi$ -pulses spaced by intervals  $2\tau$ .

$$\rho(t = 2n\tau) = [\exp(-\hat{L}\tau) \cdot R_N \cdot \exp(-\hat{L}\tau)]^n \rho(0) \quad (1.3)$$

$R_N$  represents the  $\pi_y$  pulse applied to  $^{15}\text{N}$  given as:

$$R_N = \begin{pmatrix} 1 & 0 & 0 & 0 \\ 0 & -1 & 0 & 0 \\ 0 & 0 & -1 & 0 \\ 0 & 0 & 0 & -1 \end{pmatrix} \quad (1.4)$$

For a two-spin system, the density operator  $\rho(t)$  is of dimension  $4 \times 4$ , with 16 elements. Usually the Liouvillian super operator consists of  $4^m \times 4^m$ , where  $m$  represents the number of the spins, i.e., for the present case it should have been a  $16 \times 16$  matrix. But the dimensionality of the matrix can be reduced, since, if we neglect the chemical shift evolution of  $^{15}\text{N}$ , the only possible interconversions of coherences that can occur during the CPMG sequence are:

$$N_y \xleftrightarrow{k_{ex}} 2N_x H_z \xleftrightarrow{\omega_1} 2N_x H_y \xleftrightarrow{\Omega_H} 2N_x H_x \quad (1.5)$$

Therefore, one obtains the following Liouvillian in the basis  $\{N_y, 2N_x H_z, 2N_x H_y, 2N_x H_x\}$ :

$$\hat{L} = \begin{pmatrix} 0 & \pi J_{NH} & 0 & 0 \\ -\pi J_{NH} & k_{ex} & -\omega_1 & 0 \\ 0 & \omega_1 & k_{ex} & \Omega_H \\ 0 & 0 & -\Omega_H & k_{ex} \end{pmatrix} \quad (1.6)$$

Here,  $\omega_1$  is the amplitude of the *rf* decoupling field applied to the protons,  $J_{NH}$  is the relevant one-bond scalar coupling constant and  $\Omega_H$  is the offset between the chemical shift  $\omega_H$  of the exchanging proton ( $\text{H}^{\delta 1}$ ,  $\text{H}^{\delta 2}$  or  $\text{NH}_3^+$ ) and the carrier frequency  $\omega_{ref}$ :

$$\Omega_H = \omega_H - \omega_{ref} \quad (1.7)$$

The ratio  $A/B$  depends on the offset since the decoupling becomes less efficient when the proton carrier frequency is off-resonance.<sup>18</sup> Thus for a given number of pulses and a given duration  $2\tau$  of the inter-pulse delay, the ratio  $A/B$  is minimum when the proton carrier coincides with the chemical shift of the exchanging proton (Figure 1.3).

We have considered the pulses applied to the  $^{15}\text{N}$  nuclei to be instantaneous (in reality they are about  $70 \mu\text{s}$  long, much shorter than the shortest interval  $2\tau = 2.5 \text{ ms}$ ). In equation 1.5,

relaxation is not taken into consideration since the rates either affect both experiments  $A$  and  $B$  equally or can be neglected compared to the exchange rates. During the CPMG pulse trains the in-phase coherence  $N_y$  is refocused, but no antiphase term can evolve when we have  $cw$  decoupling during the CPMG sequence, while in the absence of decoupling, antiphase terms appear between the nitrogen pulses. To obtain the rate constant, the density operator must be evaluated with and without decoupling to get the ratios  $A/B$ .

$$(A/B)^{calc} = \langle N_y(t = 2n\tau; \omega_1 = 0) \rangle / \langle N_y(t = 2n\tau; \omega_1 \neq 0) \rangle \quad (1.8)$$

In this treatment, we considered the exchanging protons to belong to NH groups containing a single proton.  $NH_2$  or  $NH_3$  groups can be treated like NH groups except that one has to take the square or cubic root, respectively, of the experimental  $A/B$  ratios, as shown elsewhere.<sup>43</sup>

In our earlier work, the exchange rate could in principle be determined from only two ratios  $A/B$  obtained with two different intervals  $2\tau$  since the resonance frequencies  $\Omega_H$  and scalar couplings  $J_{NH}$  were known precisely. Under these conditions, the Liouvillian of equation 1.5 has only 1 unknown, but two different experiments are nevertheless necessary since there are two degenerate solutions.<sup>18,43</sup> In the method employed in the previous study, the ratio  $A/B$  versus the exchange rate was plotted for tryptophan in the left panel of Figure 1.4 for different numbers  $n$  of  $\pi$  pulses and a given interval  $2\tau$ . For every ratio  $A/B$  corresponding to different  $n$ , there exist two possible values of  $k$ . To remove the ambiguity, the intervals  $2\tau$  between the  $\pi$  pulses need to be changed. As shown in the right panel of Figure 1.4, for two experiments with the same total relaxation time, there exists only one value of the exchange rate  $k$  that is compatible with both experiments.

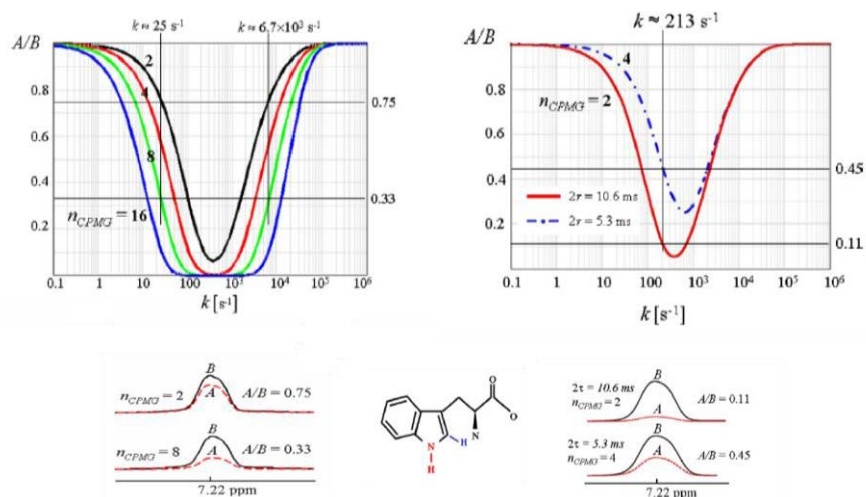


**Figure 1.4.** Left: the bottom figure shows experimental proton spectra of indole protons for  $2\tau = 10.6$  ms,  $^1J_{NH} = 98.6$  Hz and  $\nu = 6$  kHz. The top figure shows the ratio  $A/B$  versus  $k = k_{ex}$  for different values of  $n = n_{CPMG}$ . Right: the effect of changing the delay  $2\tau$  between the  $\pi$  pulses. The bottom figure shows measured ratios for the total relaxation time  $2\tau = 21.2$  ms for two cases. The plot of  $A/B$  versus  $k$  shows that a given experimental ratio intersects with the theoretical curve at four points, but only two of the four crossings are in agreement with a single rate. (Figure reproduced by permission from Kateb *et al.*, *J. Magn. Reson.* 2007).<sup>18</sup>

In this work, the labile protons remain invisible over the entire pH range because they exchange too rapidly. Hence,  $n$ ,  $\tau$ ,  $\omega_{rf}$  and  $\omega_1$  were varied systematically. For all experimental conditions, the ratio  $(A/B)^{calc}$  of equation 1.8 was determined using a home-written Mathematica program. Then, the values of  $\omega_H$ ,  $J_{NH}$  and  $k_{ex}$  were obtained by minimizing  $\chi^2$ , the sum of the squares of the deviations  $(A/B)^{expt} - (A/B)^{calc}$ . Figures 1.5 and 1.6 illustrates that the experiments allow one to accurately determine all three unknown parameters  $k_{ex}$ ,  $J_{NH}$  and  $\delta_H$ : when only two of the unknown parameters are fitted, while the third one is purposely miss-set to  $J_{NH}^{test}$  or  $\Omega_H^{test}$ , significant deviations between the calculated and experimental ratios appear. The procedure described above does not allow one to obtain meaningful exchange rates when the ratio  $A/B$  is close to 1. Indeed, when  $0.9 < A/B < 1.0$  for an entire set

of experiments at a given pH and temperature, the fits become rather imprecise and sensitive to small systematic deviations. Hence, we only applied the three-parameter fit for pH values and temperatures for which  $A/B < 0.9$  in at least one of the experiments recorded at a given pH and temperature. From these fits we obtained scalar coupling constants  $J_{\text{NH}}$  and chemical shifts  $\omega_{\text{H}}$  that are given in Tables 1.1 and 1.2. It is known that  $^1J(^{15}\text{N}^1\text{H}) < 0$ ,<sup>44</sup> but our results do not depend on the sign of the scalar coupling, hence only its absolute value can be deduced. Then, the whole set of experiments was analysed again, assuming that the scalar coupling constants and chemical shifts are constant over the entire pH range. Thus, the exchange rates  $k_{\text{ex}}$  of Table 1.3 were determined by fitting only one single parameter.

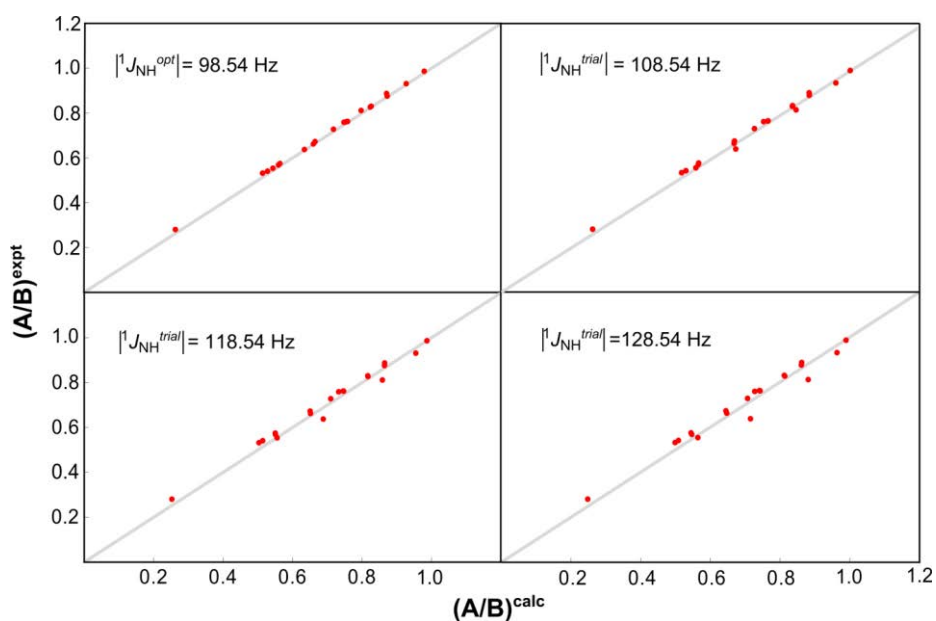


**Figure 1.5.** The scalar couplings  $^1J_{\text{NH}}$  can be postulated to have values  $^1J_{\text{NH}}^{\text{trial}}$  that differ from the optimum value  $|^1J_{\text{NH}}^{\text{opt}}| = 98.54$  Hz, while the chemical shift  $\delta_{\text{H}}$  and exchange rate  $k_{\text{ex}}$  of the  $\text{H}^{\text{e}2}$  proton at 3.2 pH and 292.5 K are fitted. Significant discrepancies are observed when the scalar coupling is deliberately miss-set to  $|^1J_{\text{NH}}^{\text{trial}}| - |^1J_{\text{NH}}^{\text{opt}}| = 0, 10, 20, \text{ or } 30$  Hz. The grey line with a unit slope is merely to guide the eye. Similar results have been obtained for different sites, pH and temperatures.

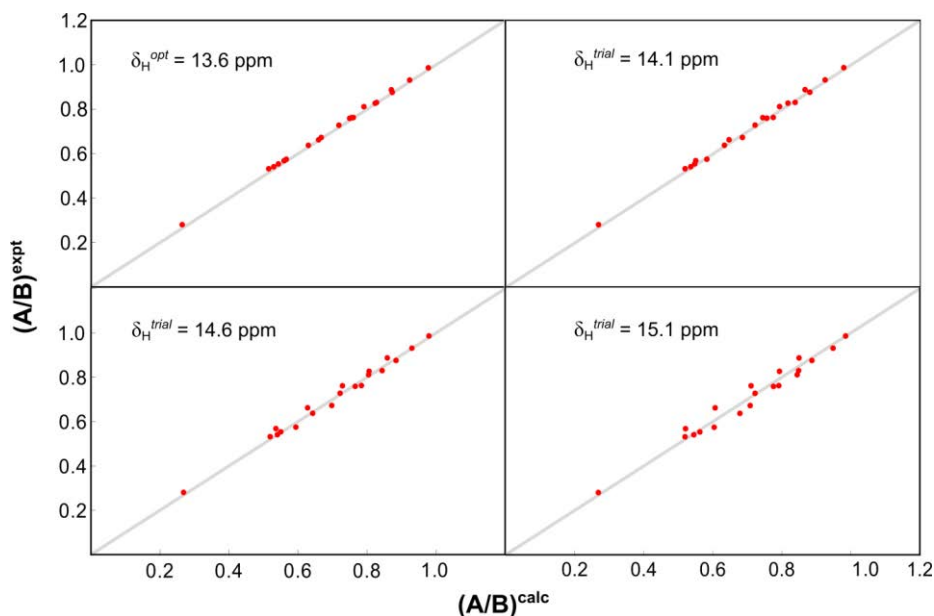


**Figure.1.6.** The chemical shifts  $\delta_{\text{H}}$  of the exchanging  $\text{NH}^{\text{e}2}$  proton can be miss-set deliberately to values  $\delta_{\text{H}}^{\text{trial}}$  that differ from the optimum  $\delta_{\text{H}}^{\text{opt}} = 13.6$  ppm while fitting the one-bond scalar coupling constant  ${}^1J_{\text{NH}}$  and the exchange rate  $k_{\text{ex}}$  at pH 3.2 and 292.5 K. Significant discrepancies are observed when the chemical shift is deliberately miss-set to  $\delta_{\text{H}}^{\text{trial}} - \delta_{\text{H}}^{\text{opt}} = 0, 0.5, 1, \text{ or } 1.5$  ppm. The experimental ratios  $(A/B)^{\text{expt}}$  are plotted against the calculated ratios  $(A/B)^{\text{calc}}$ . The grey line with a unit slope is to guide the eye. Similar results have been obtained for different sites, pH values and temperatures.

The scalar coupling constants determined in this fashion are  $|{}^1J(\text{NH}_3^+)| = 73.2 \pm 0.2$  Hz,  $|{}^1J(\text{NH}^{\text{e}2})| = 98.5 \pm 0.3$  Hz and  $|{}^1J(\text{NH}^{\delta 1})| = 97.2 \pm 1.0$  Hz. The stochastic errors in the ratios  $A/B$  due to noise were very small (on the order of 1‰). Consequently, systematic errors due to  $r_f$  miss-calibration or inhomogeneities, small temperature variations, instrumental instabilities and theoretical simplifications (in particular, cross-correlated relaxation effects were neglected) are expected to be dominant. Hence all  $A/B$  ratios were weighed equally in the  $\chi^2$  minimization. The errors in the scalar coupling constants and chemical shifts were determined from standard deviations of different experiments. In Figure 1.7, the chemical shifts of the different NH protons and one bond scalar coupling constants are plotted as a function of pH.

**Table 1.1.** Absolute values of one-bond scalar coupling constants  $^1J(^1\text{H}, ^{15}\text{N})$  for  $\text{NH}_3^+$ ,  $\text{NH}^{\delta 2}$  and  $\text{NH}^{\delta 1}$ :

$ ^1J(\text{NH}_3^+)  \text{ Hz}$				
Average pH	272.6 K	278.0 K	283.5 K	292.5 K
1.4	73.54	73.64	74.10	73.79
2.4	72.22	73.28	74.28	73.09
2.7	72.84	73.92	73.37	73.70
3.2	72.24	73.47	73.47	72.86
3.6	73.39	73.47	73.73	73.02
3.9	73.78	73.69	73.14	72.51
4.3	72.67	72.02	71.49	72.25
$ ^1J(\text{NH}^{\delta 2})  \text{ Hz}$				
1.4	100.34	100.20	99.90	99.16
2.4	100.25	100.16	97.99	97.36
2.7	99.24	98.51	97.49	97.09
3.2	98.93	98.34	98.10	98.11
3.6	97.97	97.90	98.07	96.50
3.9	99.51	99.07	99.42	99.48
4.3	98.82	95.79	100.71	94.81
$ ^1J(\text{NH}^{\delta 1})  \text{ Hz}$				
1.4	96.71	97.29	101.25	95.06
2.4	93.61	92.27	93.58	102.39
2.7	93.13	92.66	100.91	98.19
3.2	93.31	96.51	97.80	91.99
3.6	92.67	94.38	93.77	97.33
3.9	98.54	103.49	100.86	105.40
4.3	92.08	111.99		

**Table 1.2.** Chemical shifts  $\delta_{\text{H}}$  of  $\text{NH}_3^+$ ,  $\text{NH}^{\delta 2}$  and  $\text{NH}^{\delta 1}$  protons:

$\delta_{\text{H}} (\text{NH}_3^+) \text{ ppm}$				
Average pH	272.6 K	278.0 K	283.5 K	292.5 K
1.39	8.174	8.134	8.113	8.109
2.36	8.120	8.113	8.114	8.075
2.70	8.086	8.057	8.077	8.032
3.17	8.052	8.034	8.027	8.007
3.57	8.045	8.046	8.032	8.009
3.86	8.036	8.033	8.019	8.021
4.30	8.071	8.095	8.045	7.972
$\delta_{\text{H}} (\text{NH}^{\delta 2}) \text{ ppm}$				
1.39	13.777	13.703	13.659	13.677
2.36	13.793	13.697	13.608	13.599
2.70	13.665	13.714	13.702	13.664
3.17	13.704	13.768	13.647	13.628
3.57	13.713	13.686	13.660	13.574
3.86	13.712	13.712	13.662	13.615
4.30	13.760	13.657	13.524	13.898
$\delta_{\text{H}} (\text{NH}^{\delta 1}) \text{ ppm}$				
1.39	13.974	13.965	13.907	13.726
2.36	13.971	13.905	13.855	13.966
2.70	13.980	13.930	13.904	13.914
3.17	13.939	14.045	13.854	14.052
3.57	13.955	14.035	13.961	13.693
3.86	14.038	13.963	13.795	14.113
4.30	13.775	14.257		

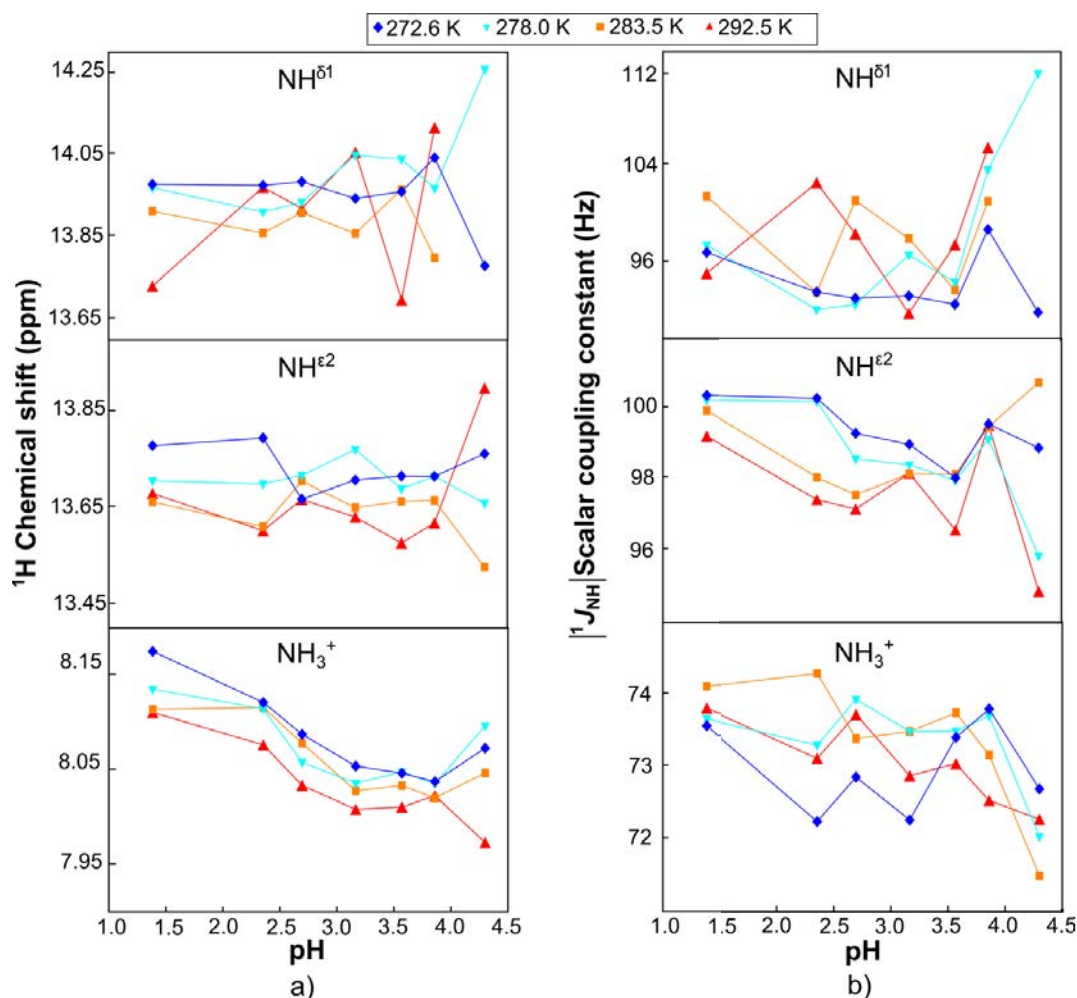


**Figure 1.7.** Variations of the chemical shifts  $\delta_{\text{H}}$  and scalar coupling constants  $^1J_{\text{NH}}$  that have been determined over a range  $1.0 < \text{pH} < 4.5$  and temperatures  $272.6 < T < 292.5$  K, encoded by different colors. The chemical shifts  $\delta_{\text{H}}^{\text{opt}}$  were referenced with respect to the temperature-dependent shift  $\delta_{\text{H}_2\text{O}}$  of the water resonance, as determined by Markley *et al.*<sup>45</sup> The variations are very small (on the order of 0.1 ppm.) For the  $\text{NH}_3^+$  group, the chemical shift appears to have a linear dependence on pH. However, regardless whether one simply assumes an average shift  $\langle \delta_{\text{H}} \rangle$  or a linear pH-dependence of the chemical shifts, the resulting exchange rates are not significantly affected.

To determine the exchange rates, we averaged the scalar coupling constants  $J_{\text{NH}}$  over all temperatures and pH values, while we considered the chemical shifts separately for each

temperature and only averaged them over all pH values. The lowest of the minima of the chi-square minimisation gave the values of the exchange rate as shown in Figure 1.8 for a representative case.

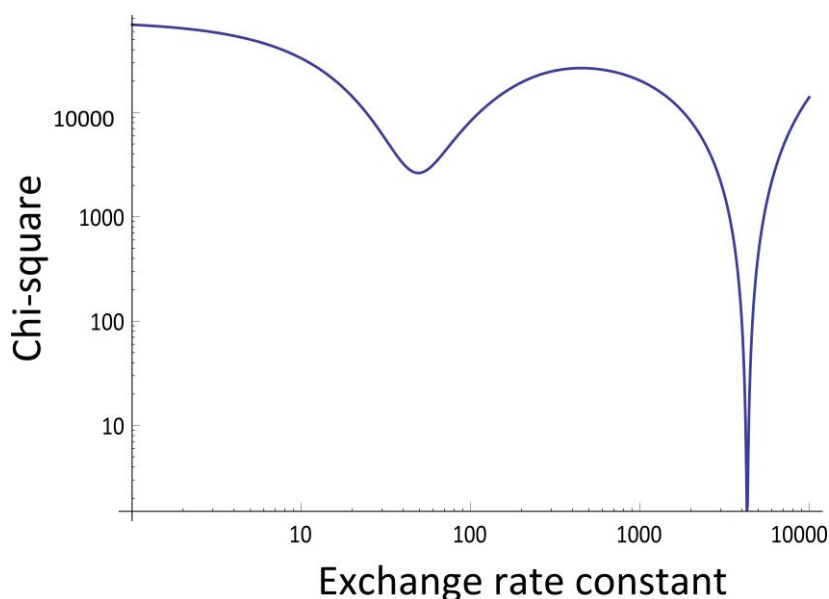


**Figure 1.8.** Plot of exchange rate constant versus chi-square for the representative case of  $\text{NH}_3^+$  at pH 3.57 and 283.5 K. The lowest of the two minima gives the value of exchange rate constant.

The  $^1\text{H}$  chemical shift of the  $\text{NH}_3^+$  group seems to depend slightly on pH, however the fit of the exchange rate is not very sensitive to such small variations which are on order the of 0.1 ppm. Systematic errors in the exchange rates are difficult to assess, while stochastic errors are very small. Therefore, we assumed the error to be the square root of the sum of two sources: a) errors of 1% that are common to all rates, corresponding to an  $r_f$  miss-calibration of about 1%, and b) errors in the fits due to systematic deviations of the ratios  $A/B$  of 1%. Additionally, there may be a contribution due to errors in the scalar coupling. For a given  $A/B$

ratio, the exchange rate is, to a good approximation, proportional to the square of the scalar coupling, which leads to errors of 0.5%, 0.8% and 2% for  $\text{NH}_3^+$ ,  $\text{NH}^{\epsilon 2}$ , and  $\text{NH}^{\delta 1}$ , respectively. The latter errors lead to a synchronous shift of all rates of a particular proton and should therefore be considered apart. In our analysis, we have neglected modulations of the isotropic chemical shifts and scalar couplings induced by de- and re-protonation. Modulations of the nitrogen shifts will affect experiments  $A$  and  $B$  equally but do not affect the ratios  $A/B$ , although such modulations can lead to line-broadening and hence to a decrease of the signal-to-noise-ratio. On the other hand, modulations of the isotropic proton shifts and scalar couplings can in principle affect the ratios  $A/B$ . However, we found an excellent agreement between calculations and experimental values using a single value for these parameters. The values given in Table 1.3 may be interpreted as weighted averages over different conformers.

## 1.4 Results and Discussions

The protons of the  $\text{NH}^{\delta 1}$ ,  $\text{NH}^{\epsilon 2}$  and  $\text{NH}_3^+$  systems have distinct chemical shifts  $\delta_{\text{H}}$ , scalar coupling constants  $J_{\text{NH}}$  and exchange rates  $k_{\text{ex}}$ , but none of these can be observed directly in proton spectra because of fast exchange. We have measured the exchange rate constants of the labile  $\text{H}^{\delta 1}$ ,  $\text{H}^{\epsilon 2}$  and  $\text{NH}_3^+$  protons in histidine over a pH range from 1.39 to 4.88 (Figure 1.9) using the method described in the previous section. The exchange rate constants that could be determined range from  $k_{\text{ex}} = 2.5 \times 10^2 \text{ s}^{-1}$  to  $8.5 \times 10^4 \text{ s}^{-1}$ .

**Table 1.3.** Exchange rate constants  $k_{ex}$  for  $\text{NH}_3^+$ ,  $\text{NH}^{\epsilon 2}$  and  $\text{NH}^{\delta 1}$  protons

$k_{ex}(\text{NH}_3^+) \text{ s}^{-1}$				
Average pH	272.6 K	278.0 K	283.5 K	292.5 K
1.39	252.1±2.5	418.5±4.2	591.9±5.9	1204.9±12.1
2.36	223.8±2.2	366.7±3.7	542.0±5.4	1067.2±10.7
2.70	207.6±2.1	339.1±3.4	486.8±4.9	968.0±9.7
3.17	271.9±2.7	414.1±4.1	613.7±6.2	1257.5±12.6
3.57	377.1±3.8	575.9±5.8	889.5±8.9	1764.0±17.7
3.86	683.0±6.8	1052.0±10.6	1565.7±15.7	2921.2±29.5
4.30	3065.6±31.0	4107.9±41.8	5416.7±55.6	8397.4±88.6
4.88	17791.7±213.7	22581.6±296.7	27490.8±403.7	41970.8±939.3
$k_{ex}(\text{NH}^{\epsilon 2}) \text{ s}^{-1}$				
1.39	1058.6±10.6	1529.5±15.4	2235.7±22.5	3998.0±40.6
2.36	1100.2±11.0	1623.3±16.3	2353.9±23.7	4142.2±42.1
2.70	1103.1±11.0	1648.6±16.6	2427.6±24.4	4218.7±42.9
3.17	1442.4±14.5	2119.9±21.3	3071.7±31.1	5377.7±55.0
3.57	1876.7±18.9	2786.9±28.1	4025.3±40.9	6980.8±72.1
3.86	3627.1±36.8	5131.4±52.4	7080.9±73.2	11562.0±123.3
4.30	12692±136.6	15758±173.9	19474.1±227.7	27363.7±347.7
4.88	68380.8±2725.1	84882.9±5365.4		
$k_{ex}(\text{NH}^{\delta 1}) \text{ s}^{-1}$				
1.39	11656.6±117.8	16099.1±163.5	22531.8±230.5	36719.8±388.6
2.36	12761.7±129.1	17909.5±182.2	24688.3±253.3	40844.1±440.8
2.70	12961.9±131.2	18316.4±186.5	25248.3±259.3	41681.8±451.7
3.17	13639.8±138.2	19072.6±194.3	26759.1±275.6	43864.4±481.7
3.57	14812.1±150.2	20631.6±210.6	28074.7±289.9	46728.2±523.9
3.86	16895.0±208.2	23141.6±236.9	31536.2±328.2	49126.8±561.3
4.30	32657.7±340.7	42538.6±457.0	52583.1±609.0	80903.8±1485.1

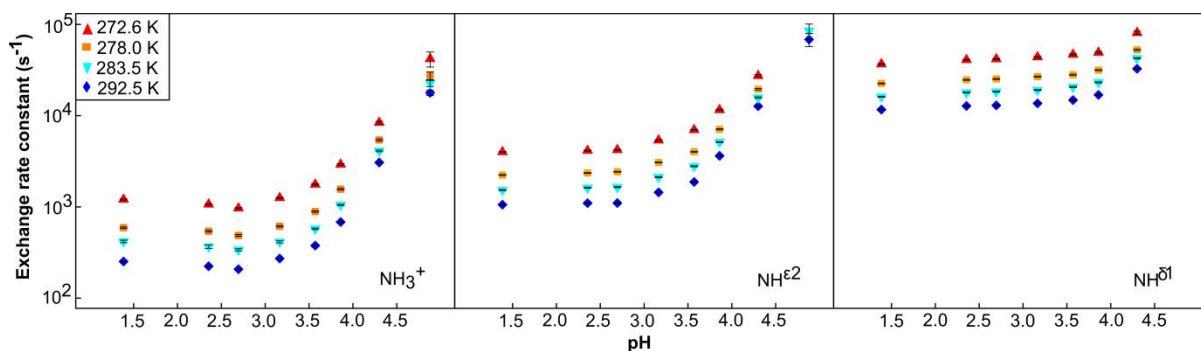


**Figure 1.9.** Proton exchange rate constants  $k_{ex}$  obtained for the  $\text{NH}_3^+$ ,  $\text{NH}^{\epsilon 2}$ ,  $\text{NH}^{\delta 1}$  groups in histidine as a function of  $1.0 < \text{pH} < 4.9$  over the temperature range  $272.6 < T < 292.5$  K. Most error bars are smaller than the symbols. Errors due to the uncertainty of the scalar couplings are not comprised in the error bars and cause a systematic shift of all points, as explained in the text.

### 1.3.1 Mechanisms of Exchange

The range of pH that we probed was well below the  $pK_a$  values of the  $\text{NH}^{\delta 1}$  group of the imidazole ring ( $pK_a = 6.0$ ) and of the  $\text{NH}_3^+$  group ( $pK_a = 9.17$ ) so that the protonated forms of nitrogen atoms  $\text{N}^{\epsilon 2}$  and  $\text{N}^{\delta 1}$  of the imidazole ring and the amino group  $\text{NH}_3^+$  are dominant in the solution. The three relevant forms of histidine in this pH range are shown in Figure 1.10.

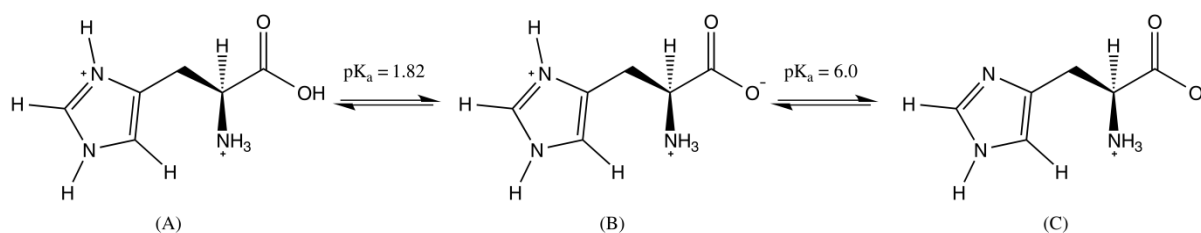


**Figure 1.10.** In the range  $1 < \text{pH} < 5$ , histidine is mainly present in three forms (A, B, C). The  $pK_a$  of the equilibrium between A and B is 1.82, while  $pK_a = 6.0$  for the equilibrium between B and C.

The ability to exchange primarily depends upon the ability to trade a proton between an acceptor and donor. Since the imidazolium nitrogen atoms and the amino group of histidine are protonated over this pH range, the propensity of exchange mediated by a positively charged hydronium ions is expected to be small.<sup>46</sup> For the exchange, a hydrogen-bonded transition-state complex is formed between the donor (histidine) and the acceptor (H<sub>2</sub>O or OH<sup>-</sup>) in two steps: a) redistribution of the proton between the acceptor and donor leading to the elongation of the hydrogen bond and b) breakage of the H-bond and eventual separation from the donor as shown in Figure 1.11. The rapidity of exchange of the protons attached to nitrogen comes from the ability of forming a hydrogen-bonded transition-state complex.

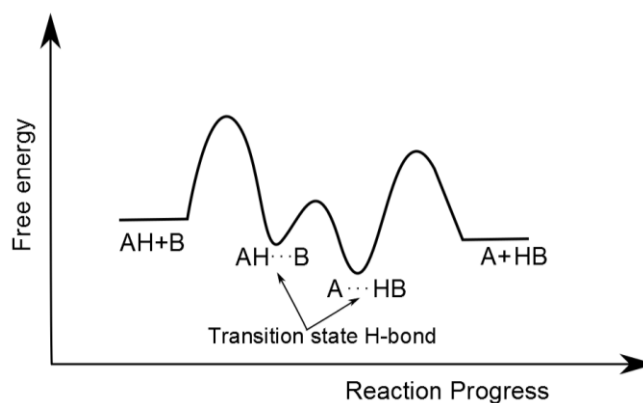


**Figure 1.11.** The free energy versus reaction progress is depicted for a proton donor A, which symbolises histidine, and B, a proton acceptor such as H<sub>2</sub>O and OH<sup>-</sup>.

When plotting the exchange rate as a function of pH, usually a V-shaped curve is observed for amides, which reflects acid and alkaline catalyses. The position of the minimum of this V-curve depends on the relative magnitude of acid and alkaline contributions (the smaller the acid contribution, the more it is shifted towards lower pH). For amino acids, exchange through base catalysis is far more effective than acid catalysis, even by more than 8 orders of

magnitude.<sup>47,48</sup> For the exchange rates of the  $\text{NH}^{\delta 1}$  and  $\text{NH}^{\epsilon 2}$  groups, however, we observed a plateau up to pH 3 and thereafter a gradual increase with pH. This happens because the exchange is water-mediated and obeys pseudo first-order kinetics at low pH, but becomes base-mediated with increasing pH as shown in Figure 1.12,<sup>46</sup> while the acid contribution can be completely neglected for this pH range.

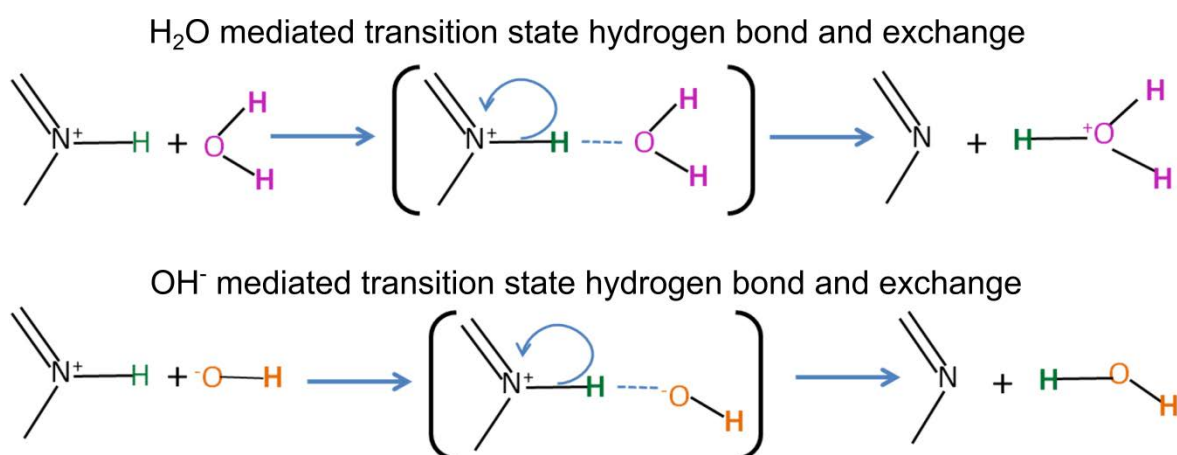


**Figure 1.12.** Mechanisms of exchange via H<sub>2</sub>O and OH<sup>-</sup>.

For  $\text{NH}_3^+$ , when plotting the exchange rate on a logarithmic scale versus pH, we found a U-shaped curve. An additional small contribution due to acid catalysis allows one to explain this shape. We fitted the exchange rate equations averaged over the three distinct forms of histidine in solution (Figure 1.13), the relative concentrations of which are described by the following fractions:

$$\begin{aligned}
 f_A &= (1 + 10^{pH - pK_{a1}} + 10^{2pH - pK_{a1} - pK_{a2}})^{-1} \\
 f_B &= (1 + 10^{-pH + pK_{a1}} + 10^{pH - pK_{a2}})^{-1} \\
 f_C &= (1 + 10^{-pH + pK_{a2}} + 10^{-2pH + pK_{a1} + pK_{a2}})^{-1}
 \end{aligned}
 \tag{1.9}$$

The  $pK_{a1} = 1.82$  refers to the carboxyl group and  $pK_{a2} = 6.0$  corresponds to the  $H^{\delta 1}$  proton of the imidazolium ring.<sup>49</sup> Each of the three forms can have acidic and alkaline contributions to the exchange rates of the three labile  $H^{\delta 1}$ ,  $H^{\epsilon 2}$  and  $NH_3^+$  protons, and a common contribution  $W$  stemming from exchange with neutral water. The solid lines in Figure 1.13 were obtained by fitting the rate constants with the equation:

$$k_{ex} = W + k_{HA}f_A[H^+]_A + k_{OHA}f_A[OH^-]_A + k_{HB}f_B[H^+]_B + k_{OHB}f_B[OH^-]_B + k_{HC}f_C[H^+]_C + k_{OHC}f_C[OH^-]_C \quad (1.10)$$

where  $[H^+] = 10^{-pH}$ ,  $[OH^-] = K_w 10^{pH}$ , and  $K_w$  is the auto-ionization constant of water which depends on the temperature.<sup>50</sup> The results were fitted to equation 1.10 using numerical minimisation with the constraint that the parameters to be fitted must be greater than zero. The alkaline contribution ( $k_{OHA}f_A[OH^-]_A$ ) of form A and the acidic contribution ( $k_{HC}f_C[H^+]_C$ ) of form C can be neglected, since at pH values where  $f_A$  and  $f_C$  are significant these contributions are eclipsed by other terms in equation 1.10. For  $NH^{\delta 1}$ , only two parameters ( $W$  and  $k_{OHB}$ ) were sufficient to explain the trend, since the acid-mediated contributions appear negligible and the ring in the C form has no  $H^{\delta 1}$ . For  $NH^{\epsilon 2}$ , three parameters were needed ( $W$ ,  $k_{OHB}$  and  $k_{OHC}$ ), while the acid-mediated rate constants  $k_{HA}$  and  $k_{HB}$  could not be determined. For  $NH_3^+$ , an additional acid-mediated contribution had to be included to explain the slight increase of the exchange rate at low pH. The same acid-mediated rate constant was assumed for both forms A and B ( $k_{HA} = k_{HB}$ ), since the data do not allow for sufficient discrimination. All exchange constants that could be determined are shown in Table 1.4.

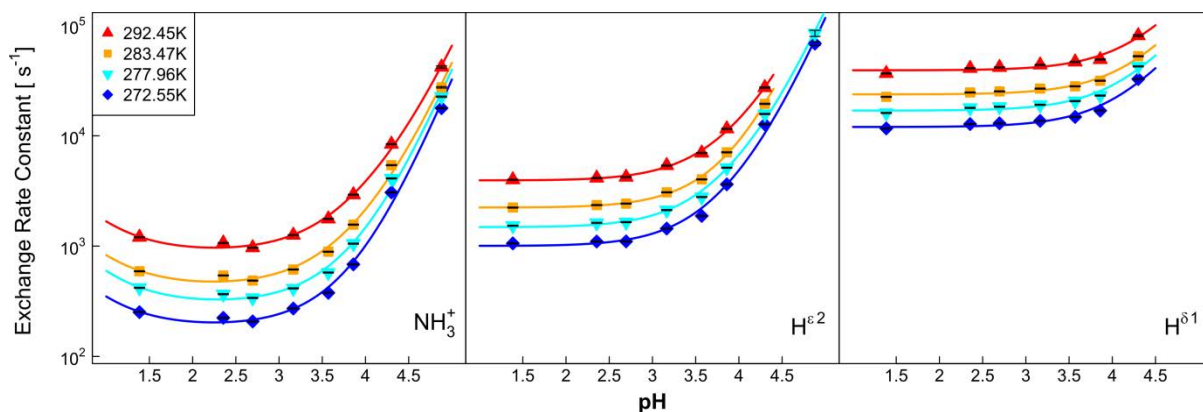


**Figure 1.13.** Proton exchange rate constants  $k_{ex}$  obtained for the  $\text{NH}_3^+$ ,  $\text{NH}^{\epsilon 2}$ ,  $\text{NH}^{\delta 1}$  groups in histidine as a function of  $1.0 < \text{pH} < 4.9$  over the temperature range  $272.6 < T < 292.5$  K. The solid lines result from fits to equations 1.9 and 1.10.

Table 1.4. Exchange rate constants of the protons in the  $\text{NH}_3^+$ ,  $\text{NH}^{\epsilon 2}$  and  $\text{NH}^{\delta 1}$  groups of histidine.

	Temperature (K)	272.6	278.0	283.5	292.5
$\text{NH}_3^+$	$\log(W/[\text{M}^{-1} \text{s}^{-1}])$	2.27	2.48	2.64	2.95
	$\log(k_{HA}/[\text{M}^{-1} \text{s}^{-1}])$	3.21	3.47	3.60	3.90
	$\log(k_{OHB}/[\text{M}^{-1} \text{s}^{-1}])$	13.69	13.68	13.69	13.62
	$\log(k_{OHC}/[\text{M}^{-1} \text{s}^{-1}])$	15.44	15.30	15.11	14.87
$\text{NH}^{\epsilon 2}$	$\log(W/[\text{M}^{-1} \text{s}^{-1}])$	3.01	3.17	3.35	3.60
	$\log(k_{OHB}/[\text{M}^{-1} \text{s}^{-1}])$	14.43	14.38	14.24	14.16
	$\log(k_{OHC}/[\text{M}^{-1} \text{s}^{-1}])$	15.95	15.79	15.86	15.43
$\text{NH}^{\delta 1}$	$\log(W/[\text{M}^{-1} \text{s}^{-1}])$	4.08	4.23	4.38	4.59
	$\log(k_{OHB}/[\text{M}^{-1} \text{s}^{-1}])$	14.94	14.83	14.69	14.51

### 1.3.2 Activation Energy

Additional valuable information which can be extracted from the exchange rate constants is the apparent activation energy defined by the Arrhenius equation.

$$k_{ex} = Ae^{-E_a^\dagger/RT} \quad (1.11)$$

The apparent activation energies of the three  $\text{H}^{\delta 1}$ ,  $\text{H}^{\epsilon 2}$  and  $\text{NH}_3^+$  exchange processes were estimated from the temperature dependence of the proton exchange rates over the relevant range of pH values. The extrapolation of the logarithms of  $k_{ex}$  in the limit  $1/T = 0$  provides the pre-exponential factor  $A$  and the apparent activation energy given in Table 1.5. As expected, the proton exchange rates increase with increasing temperature for all sites (Figure 1.13), and the activation energy can be determined for each NH group at each pH. The apparent activation energies are drawn in Figure 1.14 as a function of pH. We assume that the pH does not depend on the temperature over the limited temperature range considered (we verified this experimentally for the pH 2.55 and 5.10, for a temperature range of 280-312K). The activation energy is roughly constant at low pH and then decreases with increasing pH. These apparent activation energies provide information about the barrier height and thus give insight into the strength of hydrogen bonds. The  $\text{NH}^{\delta 1}$ ,  $\text{NH}^{\epsilon 2}$  and  $\text{NH}_3^+$  groups are involved in hydrogen bonds with partners ( $\text{H}_2\text{O}$  or  $\text{OH}^-$ ) with whom they can exchange a proton. The average chemical shifts of all exchanging protons are below 16 ppm. According to Hong *et al.*<sup>51</sup> this implies that the hydrogen bonds can be described by asymmetric energy wells with unequal populations. As discussed before, the elongation of hydrogen bonds plays an important role in exchange processes.<sup>46,52</sup> The stronger the hydrogen bond, the more energetically expensive its elongation, thus leading to a higher energy barrier and a slower exchange rate. As indicated in the Figure 1.14, the barrier is lowest for  $\text{NH}^{\delta 1}$ , which suggests

**Table 1.5.** Activation energies ( $E_a$ ) and the pre-exponential factors ( $A$ ) of  $\text{NH}_3^+$ ,  $\text{NH}^{\epsilon 2}$ ,  $\text{NH}^{\delta 1}$  groups for different pHs.

	pH	1.39	2.36	2.70	3.17	3.57	3.86	4.30	4.88
$\text{NH}_3^+$	$\ln(A)$	28.17	28.16	27.69	28.06	28.64	27.83	22.81	22.28
	$E_a(\text{kJ/mol})$	51.26	51.51	50.61	50.85	51.46	48.26	33.5	28.34
$\text{NH}^{\epsilon 2}$	$\ln(A)$	26.53	26.47	26.72	26.60	26.81	25.20	20.73	22.23
	$E_a(\text{kJ/mol})$	44.36	44.10	44.66	43.80	43.66	38.52	25.58	25.17
$\text{NH}^{\delta 1}$	$\ln(A)$	26.28	26.53	26.6	26.72	26.44	25.44	23.6	
	$E_a(\text{kJ/mol})$	38.33	38.68	38.81	38.97	38.16	35.57	29.92	

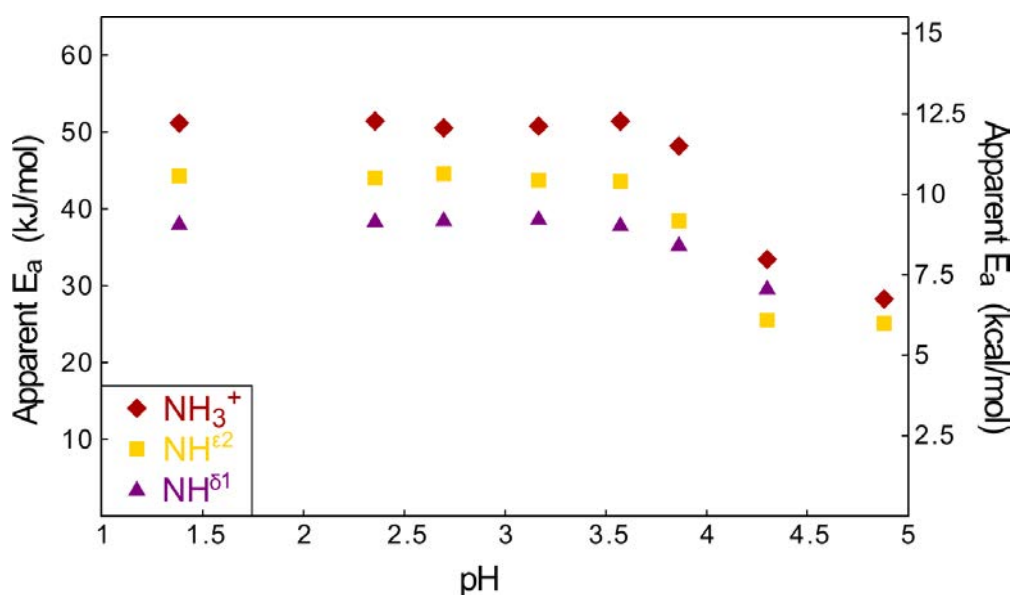


**Figure 1.14.** Apparent activation energies of proton exchange processes in the  $\text{NH}_3$ ,  $\text{NH}^{\epsilon 2}$ ,  $\text{NH}^{\delta 1}$  groups in histidine as a function of pH obtained from the derivatives of the logarithms of the exchange rates of Figure 1.13 with respect to  $1/T$ .

weak hydrogen bonds in the transition states involving H<sub>2</sub>O or OH<sup>-</sup> as partners, thereby facilitating exchange. This corroborates the correlation between the activation energy and the exchange rate. At a given pH and temperature (as shown in Figure 1.13), we obtained  $k_{ex}(\text{NH}_3^+) < k_{ex}(\text{NH}^{\epsilon 2}) < k_{ex}(\text{NH}^{\delta 1})$ . The exchange rates of the three different groups are separated by about an order of magnitude.

## 1.4 Conclusions

We measured the proton exchange rates  $k_{ex}$  of invisible protons in histidine, for NH<sup>δ1</sup>, NH<sup>ε2</sup> and NH<sub>3</sub><sup>+</sup> groups without any prior knowledge of the proton chemical shifts  $\delta_{\text{H}}$  and the one-bond scalar coupling constants  $^1J_{\text{NH}}$ . Our approach permits one to determine these parameters indirectly. The three exchange rates were measured at different temperatures and pH values to determine the apparent activation energies of the exchange processes as a function of pH. The same method can be applied to histidine residues embedded in proteins, provided the transverse relaxation rates of <sup>1</sup>H, <sup>13</sup>C and <sup>15</sup>N are not too fast. Altogether, these results provide valuable information about the role of pH in the chemistry of histidine.

## References

- (1) Bain, A. D. *Prog. Nucl. Magn. Reson. Spectrosc.* **2003**, *43*, 63.
- (2) Levitt, M. H. *Spin Dynamics: Basics of Nuclear Magnetic Resonance*; John Wiley & Sons Ltd.: Chichester, **2001**.
- (3) Pelupessy, P. HDR Defense, Ecole Normale Supérieure, **2013**.
- (4) Jeener, J.; Meier, B. H.; Bachmann, P.; Ernst, R. R. *J. Chem. Phys.* **1979**, *71*, 4546.
- (5) Bain, A. D.; Duns, G. J. *Methods for structural elucidation by high-resolution NMR*; Batta, G.; Kover, K. E.; Szantay, C. J., Eds.; Elsevier B.V., **1997**; pp. 227–263.
- (6) Bain, A. D.; Cramer, J. A. *J. Magn. Reson.* **1993**, *103*, 217.
- (7) Hahn, E. L. *Phys. Rev.* **1950**, *80*, 580.
- (8) Carr, H.; Purcell, E. *Phys. Rev.* **1954**, *94*, 630.
- (9) Meiboom, S.; Gill, D. *Rev. Sci. Instrum.* **1958**, *29*, 688.
- (10) Loria, J. P.; Rance, M.; Palmer, A. G. *J. Am. Chem. Soc.* **1999**, *121*, 2331.
- (11) Deverell, C.; Morgan, R. E.; Strange, J. H. *Mol. Phys.* **1970**, *18*, 553.

- (12) Bain, A. D.; Ho, W. P. Y.; Martin, J. S. *J. Magn. Reson.* **1981**, *43*, 328.
- (13) Grunwald, E.; Loewenstein, A.; Meiboom, S. *J. Chem. Phys.* **1957**, *27*, 630.
- (14) Forsén, S.; Hoffman, R. A. *J. Chem. Phys.* **1963**, *39*, 2892.
- (15) Skrynnikov, N. R.; Ernst, R. R. *J. Magn. Reson.* **1999**, *137*, 276.
- (16) Moonen, C. T. W.; Gelderen, P. van; Vuister, G. W.; Zijl, P. C. M. van. *J. Magn. Reson.* **1992**, *97*, 419.
- (17) Waelder, S. F.; Redfield, A. G. *Biopolymers* **1977**, *16*, 623.
- (18) Kateb, F.; Pelupessy, P.; Bodenhausen, G. *J. Magn. Reson.* **2007**, *184*, 108.
- (19) Fersht, A. R.; Matouschek, A.; Serrano, L. *J. Mol. Biol.* **1992**, *224*, 771.
- (20) Hirst-Jensen, B. J.; Sahoo, P.; Kieken, F.; Delmar, M.; Sorgen, P. L. *J. Biol. Chem.* **2007**, *282*, 5801.
- (21) Puttick, J.; Baker, E. N.; Delbaere, L. T. J. *Biochim. Biophys. Acta* **2008**, *1784*, 100.

- (22) Stock, A. M.; Robinson, V. L.; Goudreau, P. N. *Annu. Rev. Biochem.* **2000**, *69*, 183.
- (23) Tanaka, T.; Saha, S. K.; Tomomori, C.; Ishima, R.; Liu, D.; Tong, K. I.; Park, H.; Dutta, R.; Qin, L.; Swindells, M. B.; Yamazaki, T.; Ono, A. M.; Kainosho, M.; Inouye, M.; Ikura, M. *Nature* **1998**, *396*, 88.
- (24) Bachovchin, W. W.; Roberts, J. D. *J. Am. Chem. Soc.* **1978**, *100*, 8041.
- (25) Kilmartin, J. V.; Breen, J. J.; Roberts, G. C. K.; Ho, C. *Proc. Natl. Acad. Sci. U. S. A.* **1973**, *70*, 1246.
- (26) Hu, F.; Schmidt-Rohr, K.; Hong, M. *J. Am. Chem. Soc.* **2012**, *134*, 3703.
- (27) Patel, D. J.; Woodward, C. K.; Bovey, F. A. *Proc. Natl. Acad. Sci. U. S. A.* **1972**, *69*, 599.
- (28) Gupta, R. K.; Pesando, J. M. *J. Biol. Chem.* **1975**, *250*, 2630.
- (29) Blomberg, F.; Maurer, W.; Rüterjans, H. *J. Am. Chem. Soc.* **1977**, *99*, 8149.
- (30) Kawano, K.; Kyogoku, Y. *Chem. Lett.* **1975**, 1305.
- (31) Harbison, G.; Herzfeld, J.; Griffin, R. G. *J. Am. Chem. Soc.* **1981**, *103*, 4752.

- (32) Munowitz, M.; Bachovchin, W. W.; Herzfeld, J.; Dobson, C. M.; Griffin, R. G. *J. Am. Chem. Soc.* **1982**, *104*, 1192.
- (33) Henry, B.; Tekely, P.; Delpuech, J.; Poincare, H.; Cedex, N. V. *J. Am. Chem. Soc.* **2002**, *124*, 2025.
- (34) Li, S.; Hong, M. *J. Am. Chem. Soc.* **2011**, *133*, 1534.
- (35) Song, X.; Rienstra, C. M.; McDermott, A. E. *Magn. Reson. Chem.* **2001**, *39*, S30.
- (36) Findeisen, M.; Brand, T.; Berger, S. *Magn. Reson. Chem.* **2007**, *45*, 175.
- (37) Morris, G. A.; Freeman, R. *J. Am. Chem. Soc.* **1979**, *101*, 760.
- (38) Shaka, A. J.; Keeler, J.; Frenkiel, T.; Freeman, R. *J. Magn. Reson.* **1983**, *52*, 335.
- (39) Geen, H.; Freeman, R. *J. Magn. Reson.* **1991**, *93*, 93.
- (40) Emsley, L.; Bodenhausen, G. *J. Magn. Reson.* **1992**, *97*, 135.
- (41) Abragam, A. *Principles of Nuclear Magnetism*; Oxford University Press, 1961.
- (42) Binsch, G. *J. Am. Chem. Soc.* **1969**, *91*.

- (43) Segawa, T.; Kateb, F.; Duma, L.; Bodenhausen, G.; Pelupessy, P. *ChemBioChem* **2008**, *9*, 537.
- (44) Grant, D. M.; Harris, R. K., Eds.; *Encyclopaedia of Nuclear Magnetic Resonance, Vol. 5*; John Wiley & Sons Ltd.: Chichester, 1996; p. 3241.
- (45) Markley, J. L.; Bax, A.; Arata, Y.; Hilbers, C. W.; Kaptein, R.; Sykes, B. D.; Wright, P. E.; Wüthrich, K. *Eur. J. Biochem.* **1998**, *256*, 1.
- (46) Englander, S. W.; Downer, N. W.; Teitelbaum, H. *Annu. Rev. Biochem.* **1972**, *41*, 903.
- (47) Dempsey, C. E. *Prog. Nucl. Magn. Reson. Spectrosc.* **2001**, *39*, 135.
- (48) Fersht, A. *Enzyme Structure and Mechanism*; Second.; W. H. Freeman and Company: New York, 1985; pp. 90–92.
- (49) Lundblad, R. L.; Macdonald, F. *Handbook of Biochemistry and Molecular Biology*; Fourth Edi.; CRC Press, 2010; p. 1098.
- (50) Marshall, W. L.; Franck, E. U. *J. Phys. Chem. Ref. Data* **1981**, *10*, 295.
- (51) Hong, M.; Fritzsching, K. J.; Williams, J. K. *J. Am. Chem. Soc.* **2012**, *134*, 14753.

(52) Sterpone, F.; Stirnemann, G.; Hynes, J. T.; Laage, D. *J. Phys. Chem. B* **2010**, *114*, 2083.

## GLOSSARY: Part-I

---

**2D EXSY (Two dimensional exchange spectroscopy):** The method leads to cross peaks which represents spins that are exchanging slowly with one another either conformationally or chemically. The pulse sequence consists of three  $\pi/2$  pulses as shown in the figure below. The fixed mixing time  $\tau_m$  plays a central role in this method. The exchange rate can be determined by following the intensity of cross peaks as a function of the mixing time.

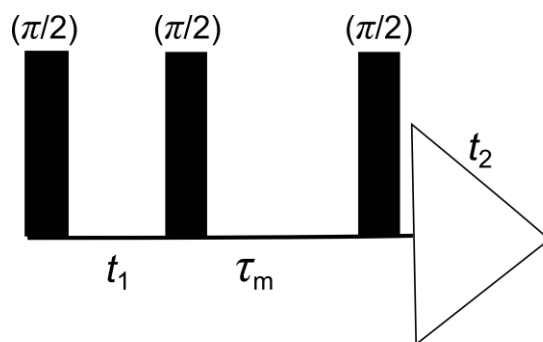


**Figure 1.** 2D EXSY Pulse Scheme

Source: Spin Dynamics: Basics of Nuclear Magnetic Resonance by *M.H. Levitt*, John Wiley and Sons Ltd.,  
NMR Spectroscopy: Basic Principles, Concepts and Applications in Chemistry by *H. Gunther*, John Wiley and  
Sons Ltd.

**Chemical shift:** The local magnetic field experienced by a given nucleus depends on the electrons present in the molecule. The electronic distribution of the same type of nucleus (e.g.  $^1\text{H}$ ,  $^{13}\text{C}$ ,  $^{15}\text{N}$ ) usually varies according to the local geometry (binding partners, bond

lengths, angles between bonds, etc.), and with it the local magnetic field at each nucleus also varies. This effect is called the chemical shift. The chemical shift is defined by a symbol  $\delta$  and is measured as a resonant frequency of a nucleus relative to a reference, expressed in ppm (parts per million).

Source: Spin Dynamics: Basics of Nuclear Magnetic Resonance by *M.H. Levitt*, John Wiley and Sons Ltd., NMR Spectroscopy: Basic Principles, Concepts and Applications in Chemistry by *H. Gunther*, John Wiley and Sons Ltd.

**Chi square ( $\chi^2$ ) minimization:** The chi-square statistic describes the goodness-of-fit of experimental data to a model. Chi-square is calculated by summing up the squares of the differences between the measured data and the expected data (or the theoretical value) divided by the standard error of the data. If the experimentally observed values from a total of  $k$  dataset measurements are  $O_i$ , and the *expected* values from the model are  $E_i(a_M)$ , where  $a_M$  are the  $M$  parameters, then the chi-square is given as:

$$\chi^2 = \sum_{i=1}^k \left[ \frac{O_i - E_i(a_M)}{\sigma_i} \right]^2$$

The standard error of each measurement is  $\sigma_i$ . The appropriate number of degrees of freedom to associate with  $\chi^2$  is  $[k - M]$ . To find the best fit of the  $M$  parameters, these are varied over their allowed ranges until the most probable set of their values are found, represented by the global minimum of chi-square.

Source: <http://www.phys.hawaii.edu/~varner/PHYS305-Spr12/DataFitting.html>, Data Reduction and Error Analysis for the Physical Sciences by *P.R. Bevington, D. K. Robinson*, McGraw-Hill, Inc.

**Coherence:** A weakly coupled two-spin  $\frac{1}{2}$  system  $IS$  can be described by  $2^n$  ( $n = 2$ ) eigenstates. The four-energy level diagram with the eigenstates labelled in the bra-ket notation is shown in the following figure:

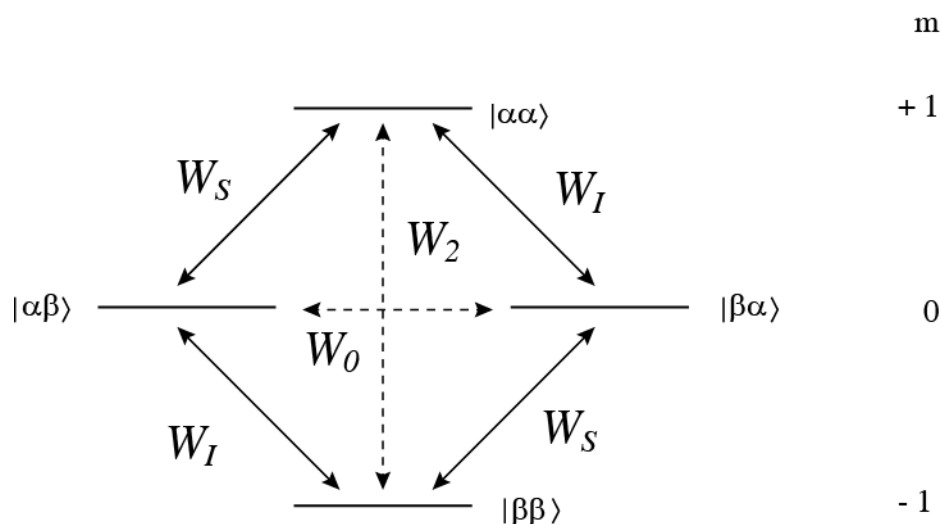


**Figure 2.** Four energy level drawing and product functions of two weakly coupled spins  $1/2$

Each state is characterized by a value of the magnetic quantum number  $m$ , and a selection rule of the angular momentum requires that only transitions between states with  $\Delta m = \pm 1$  can lead to observable magnetization. These are usually called “allowed” transitions, which correspond to  $W_I$  and  $W_S$  (see Figure 2) and are often referred to as single-quantum transitions or coherences. Thus, a coherence corresponds to the transition between two energy levels of spin states, in other words it is the superposition of two eigenstates in a quantum mechanical system. **In-phase magnetisation** refers to coherence of a given set of spins, e.g.,  $I_{1x}$ ,  $I_{1y}$ ,  $I_{1z}$ ,  $I_{2x}$ ,  $I_{2y}$ ,  $I_{2z}$ . **Antiphase magnetisation** represents coherences relative to another spin's polarization. There are four of these coherences:  $2I_{1x}I_{2z}$ ,  $2I_{1y}I_{2z}$ ,  $2I_{1z}I_{2x}$ ,  $2I_{1z}I_{2y}$ .

Source: Understanding NMR Spectroscopy. Class Notes by *J.Keeler*, <http://www-keeler.ch.cam.ac.uk>

**Coupling:** Different spins in a molecule do not precess independently as their energy state can be influenced by nearby spins, leading to the phenomenon of coupling. There are two basic mechanisms by which information between coupled spins is exchanged:  $J$ -coupling and dipolar coupling.

The  **$J$ -coupling (scalar coupling)** is an interaction through chemical bonds that dominates the coupling terms in isotropic liquids. It is an indirect interaction between two nuclear spins which arises from hyperfine interactions between the nuclei and local electrons. It contains information about bond distance and angles and thereby provides information on the connectivity of molecules.

The **dipolar coupling** results from the interaction between two magnetic dipoles. The spins experience the magnetic fields of the spins nearby thus leading to slightly different effective magnetic fields  $\mathbf{B}_{\text{eff}}$ , which also depend on the orientation of both magnetic dipoles. The strength of the dipole-dipole coupling depends strongly on the spin-spin distance  $r^{-3}$  as well as the gyromagnetic ratios of the coupled spins. In isotropic liquids, the dipolar coupling is averaged out however it can still be a source of relaxation.

Source: Spin Dynamics: Basics of Nuclear Magnetic Resonance by *M.H. Levitt*, John Wiley and Sons Ltd., E. L. Hahn and D. E. Maxwell (1952). "Spin Echo Measurements of Nuclear Spin Coupling in Molecules". *Phys. Rev.* 88 (5): 1070–1084.

**CPMG:** It stands for Carr-Purcell-Meiboom-Gill sequence, named after the people who developed it. The sequence is shown in the scheme below. It consists of a first  $90^\circ_x$  pulse that creates transverse magnetisation which starts to precess and relax. In the middle of a variable

time  $\tau$  a  $180^\circ_y$ -pulse is applied to the system. This spin-echo sandwich refocuses the chemical evolution and the heteronuclear scalar coupling of the spins. By increasing the number of  $180^\circ$  pulses one generates a number of spin echoes, which have decreasing intensities. CPMG was initially developed to minimize the losses caused by diffusion of the molecules in an inhomogeneous magnetic field (compared to a single echo). The transverse relaxation time  $T_2$  appears therefore as the decay time of the spin-echo intensities as a function of  $\tau$ .

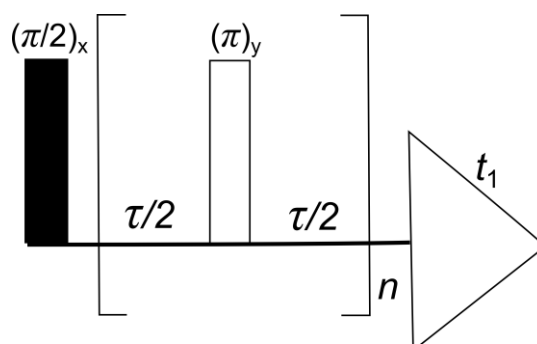


**Figure 5.** CPMG pulse scheme.

Source: Spin Dynamics: Basics of Nuclear Magnetic Resonance by *M.H. Levitt*, John Wiley and Sons Ltd.,  
 NMR Spectroscopy: Basic Principles, Concepts and Applications in Chemistry by *H. Gunther*, John Wiley and  
 Sons Ltd.

**Decoupling:** It is a method used in NMR where a sample to be analyzed is irradiated at a certain frequency or frequency range to prevent, fully or partially, the coherent evolution due to the coupling between certain nuclei. It is achieved by irradiating one spin or spin type with a resonant frequency either continuously or with specially designed decoupling schemes. If the spins being decoupled and being observed by the spectrometer are of the same kind then it is known as **homonuclear decoupling**, and if different kinds of spins are decoupled while one of the

two is observed, this is termed as **heteronuclear decoupling**. In **continuous wave (cw) decoupling**, a continuous monochromatic irradiation is applied and for the **WALTZ-16** sequence the pattern  $90^\circ_x 180^\circ_{-x} 270^\circ_x$  is repeated sixteen times with systematically varied phase shifts.

Source: NMR Spectroscopy: Basic Principles, Concepts and Applications in Chemistry by *H. Gunther*, John Wiley and Sons Ltd.

**INEPT**: The Insensitive Nuclei Enhanced by Polarisation Transfer (INEPT) experiment is used to transfer polarisation from a sensitive nucleus (normally  $^1\text{H}$ ) to a less sensitive nucleus via the scalar coupling. A complete polarisation transfer from *I* to *S* spins is possible if the transfer time is equal to  $1/(2J_{IS})$ . The pulse sequence for the INEPT is drawn below. A  $90^\circ$ -pulse on the *I*-spin creates transverse magnetisation. This is followed by a spin-echo sandwich with  $180^\circ$ -pulses on both spin types. The delay  $\tau=1/(4J_{IS})$ .

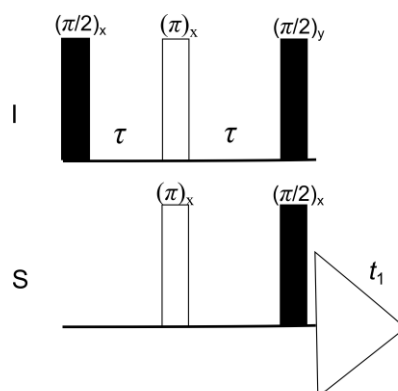


**Figure 3.** INEPT Pulse scheme.

Source: <http://www.chemie.uni-hamburg.de/nmr/insensitive/tutorial/en.lproj/ineptnd.html>, Spin Dynamics: Basics of Nuclear Magnetic Resonance by *M.H. Levitt*, John Wiley and Sons Ltd

**Shaped Pulses:** These are pulses that have an amplitude or/and phase modulation. The advantage over ordinary square pulses is that they have improved offset profile. They are often used for selectively manipulating certain resonances. **Q3** pulses refers to Quaternion cascades and **REBURP** stands for Refocusing Band-Selective Pulse with Uniform Response and Phase. Both of these shaped pulses can be used for selective inversion or refocusing. REBURP profile provides better refocusing while Q3 requires less power for a given bandwidth.

Source: NMR Spectroscopy: Basic Principles, Concepts and Applications in Chemistry by *H. Gunther*, John Wiley and Sons Ltd.

**Spin-echo sandwich:** The spin-echo sandwich consists of an evolution period  $\tau$  with a  $180^\circ$ -pulse in the middle as shown in the pulse scheme below. The spin-echo sequence starts with transverse magnetisation  $-I_y$  that is allowed to freely evolve for half of the evolution period  $\tau/2$  and a  $180^\circ$  pulse which is followed by another period  $\tau/2$ . For the homonuclear case, the offset is refocused while the scalar coupling evolves for time  $\tau$ . In the heteronuclear case, one has three different options. If the  $180^\circ$  pulse affects both the *I*- and the *S*-spins, the result is the same as in the homonuclear case: The chemical shift is refocused while the coupling is not. If the pulse is applied to only the *I*-spins, the chemical shift of the *I*-spins as well as the coupling gets refocused while the *S*-spins evolve normally under the chemical shift. If the pulse is applied to the *S*-spins only, it refocuses the coupling and the chemical shift of the *S*-spins.

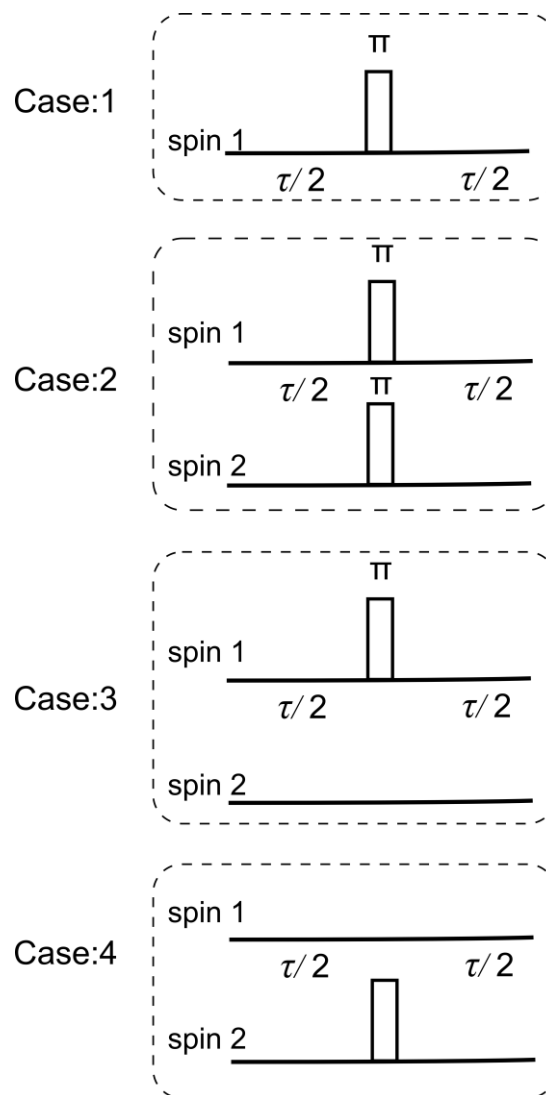


**Figure 4.** Four different spin-echo sequences that can be applied to homonuclear (Case 1) and heteronuclear (Cases 2, 3, 4) spin systems. The open rectangles represent 180° pulses.

Source: Understanding NMR Spectroscopy. Class Notes by *J.Keeler*.

**Spin-lattice relaxation:** This is also known as longitudinal relaxation and is the mechanism by which the  $z$  component of the magnetisation vector comes into thermodynamic equilibrium with its surroundings. Nuclear magnetic resonance was originally used to

examine solids in the form of lattices, hence the name "spin-lattice" relaxation. It is characterized by the **spin–lattice relaxation time**, a time constant known as  $T_1$ . The  $T_1$  relaxation time is a measure of how quickly the net magnetisation vector recovers to its ground state along the direction of the net magnetic field. The length of the net magnetization vector after an inversion of z- magnetisation is given by the following equation:

$$M_t = M_{eq} (1 - 2e^{-t/T_1})$$

Where  $M_t$  is the magnetization at time  $t$ , the time after the  $\pi$  pulse,  $M_{eq}$  is the maximum magnetization at full recovery.

Source: Spin Dynamics: Basics of Nuclear Magnetic Resonance by *M.H. Levitt*, John Wiley and Sons Ltd., NMR Spectroscopy, Spin Choreography: Basic Steps in High Resolution NMR by *R. Freeman*, Oxford University Press

**Spin-spin relaxation time**: It is the mechanism by which  $M_{xy}$ , the transverse component of the magnetisation vector, exponentially decays. It is characterized by the spin–spin relaxation time, known as  $T_2$ , a time constant characterizing the signal decay. It is the time taken for the magnetic resonance signal to irreversibly decay to 37% (= 1/e) of its initial value after its generation by tipping the longitudinal magnetization towards the transverse plane:

$$M_{xy}(t) = M_{xy}(0)e^{-t/T_2}$$

Source: Spin Dynamics: Basics of Nuclear Magnetic Resonance by *M.H. Levitt*, John Wiley and Sons Ltd., NMR Spectroscopy, Spin Choreography: Basic Steps in High Resolution NMR by *R. Freeman*, Oxford University Press

## Part-II



---

## High-resolution ion isolation in Fourier transform ion cyclotron resonance (FT-ICR) mass spectrometry by modulating the *rf* phase during the frequency

### 2.1 Introduction

Mass spectrometry has come a long way since its inception by J. J. Thomson<sup>1,2</sup> in 1912 for the study of a stream of positive neon ions through magnetic and electric fields, measuring its deflection on a photographic plate and observing the isotopes of neon (<sup>20</sup>Ne, <sup>22</sup>Ne), to the formulation of Fourier transform ion cyclotron resonance mass spectrometry (FT-ICR) by Comisarow and Marshall in 1974,<sup>3</sup> and to the present state of FT-ICR, which enables developments in the fields of proteomics,<sup>4-7</sup> metabolomics<sup>8,9</sup> and petroleomics.<sup>10,11</sup> Ion isolation has also come a long way since it was used to study the charge of an isolated droplet of oil or alcohol to determine its charge by Millikan in 1911<sup>12</sup> to modern techniques for selecting and isolating ions in MS/MS experiments, which enable the study of ion/molecule reactions,<sup>13</sup> the analysis of proteins,<sup>14,15</sup> the sequencing of peptides,<sup>16</sup> the elucidation of chemical structures,<sup>17</sup> etc. On a commercial Bruker FT-ICR spectrometer, ion isolation is routinely performed by two techniques that will be discussed below.

Quadrupole mass analysers or linear quadrupole ion traps are used in association with FT-ICR mass spectrometers for selecting precursor ions and for performing tandem analysis of ions that have mass-to-charge ratios within some chosen range. Quadrupole mass analysers uses a simple approach for ion isolation where in the ions are selected by applying suitably modulated potentials to the quadrupolar rods prior to entering the ICR cell. Basically, the direct current (*dc*) and radio-frequency (*rf*) potentials allow only selected ions with stable

trajectories which lie in the Mathieu stability diagram to pass through the four rods. Other ions collide with the rods and are therefore removed.<sup>18,19</sup> A quadrupole mass filter is capable of selectively isolating isotopologues for mono and bi-charged ions with the resolution being routinely around 2000 and up to 10,000. Although the use of this technique is straightforward, the disadvantage of the quadrupole mass filters is the sharp decrease in the transmission efficiency on further attempting to increase the resolution. Recently Hilger *et al.* proposed a new method for ion isolation in quadrupolar ion traps by generating a tailored waveform with single notch which increases the  $m/z$  range that can be probed for isolation as compared to the conventional method.<sup>20</sup> The notch method also enables isolation of a single ion using a quadrupolar mass filter, so the inability to select multiple ions in different  $m/z$  windows in a single experiment remains a disadvantage for this method.

The versatility of ICR mass spectrometers comes from the fact that trapped ions can be manipulated at will by radio-frequency (*rf*) pulses.<sup>21, 22</sup> This leads to the second method for ion isolation that is available on FT-ICR mass spectrometers: the in-cell isolation technique, introduced as correlated sweep excitation (COSE)<sup>14</sup> and now more commonly known as the correlated harmonic excitation fields technique (CHEF),<sup>23,24</sup> which utilises suitable *rf* excitation pulses to select ions. In this method, a radiofrequency chirp excitation is used to excite all unwanted ions to orbits of increasing radii, until they collide with the walls of the cell, i.e., with the detection or excitation plates. Instead of using a chirp pulse with a monotonous sweep of the frequency, the frequency is made to 'skip' the cyclotron frequency of the ion to be isolated. The disadvantage of this process is that sidebands inherent to radio frequency sweeps can lead to off-resonance excitation of ions that are to be isolated if their mass-to-charge ratios are close to those of the ions to be ejected.<sup>25</sup> CHEF is applied on the commercial FT-ICR mass spectrometers for routinely studying fragmentation of multiply

protonated complexes of metal with peptide ions,<sup>26</sup> for selectively isolating single isotopic peaks of heavy proteins like apomyoglobin,<sup>27</sup> doubly protonated bradykinin<sup>28</sup> with high front-end resolution and mass accuracy. The method had been applied to study the fragmentation pathways of single isotopic peaks of substances like Suwannee river fulvic acid (SRFA) for which isolation was performed using CHEF and single shot ejection,<sup>29</sup> for isolating peaks for measuring the amino acid isotopomer distribution for biological systems and studying their metabolic pathways.<sup>30</sup> CHEF technique was further developed by Kruppa et al, to isolate multiple ions in a single experiment using tailored waveforms simultaneously isolating analyte and calibrant ions and also multiple charged states of protein drug complex to analyse the site of covalent drug bonding.<sup>15</sup> This procedure is referred to as multi-CHEF (multiple correlated harmonic excitation fields). This technique had also been applied for absolute quantification of proteins.<sup>31</sup>

Isolation by this method is not very suitable to study the fragmentation of precursor ions by either infrared multiphoton dissociation (IRMPD) or electron capture dissociation (ECD) techniques. The ions gain some axial kinetic energy during the resonant ejection process and start to move off-centre, thereby making IRMPD fragmentation techniques difficult since the laser is applied in the center of the cell and poor overlap of the electron beam with the off-axis precursor ions interferes with fragmentation by ECD.<sup>32,33</sup>

A method which overcomes the disadvantages of both quadrupolar isolation (QI) and in-cell isolation, developed by Marshall and co-workers in 1985, is the 'stored waveform inverse Fourier transform' (SWIFT) technique.<sup>34</sup> An excitation pulse with a suitable wave-form is created in time-domain by an inverse Fourier transform of the desired frequency- (or mass-) domain profile which is then applied to the ion trap cell. SWIFT method generates arbitrary frequency-domain excitation magnitude spectrum with flat and uniform power over the entire

mass range of interest. For isolation, ions to be ejected are excited with flat power over all but one or more specified  $m/z$  ranges and with zero-power windows to prevent excitation of the  $m/z$  to be retained and these selected ions are then subsequently excited to be fragmented or observed. This can provide accurate ion isolation.<sup>35</sup> SWIFT has been used for isolation prior to MS/MS analysis for a single isotopologue of ubiquitin and carbonic anhydrase<sup>36</sup> and for analysis of 18+ charge state of intact bovine histone H4 with a mass selectivity of 0.1  $m/z$  unit.<sup>37</sup> Although by using the SWIFT method, isotopologues can be isolated with high resolution but the arbitrary waveform synthesizer needed for this technique is not implemented in commercially available FT-ICR mass spectrometers.

Another method which allows one to avoid off-resonance excitation was initially proposed by Noest and Kort in 1983. The details of this method, which came to be known as the “notch ejection” technique, are discussed in the PhD thesis of A. J. Noest and was published later.<sup>38</sup> The work was applied on a commercial MS instrument to study hydrogen–deuterium exchange by isolating hydroxides of small molecules like phenyl ethers.<sup>39</sup> Applications were described by Vulpius *et al.*<sup>40</sup> and by Farrell *et al.*<sup>41</sup>. Vulpius *et al.* were able to isolate low-abundant ions with a high signal-to-noise ratio and a resolving power that was better than 1 Da on fragment ions of 1-nonene ( $m/z$  68 and 54) generated by electron impact ionization. Farrell *et al.* applied a combination of notch ejection and selective ion partitioning in a dual cell and isolated ions of  $m/z$  183 in protonated triethyl phosphate.

This simple method for ion isolation does not appear to be very popular, since it could not be applied to high  $m/z$  samples without loss of resolution. In principle, it requires excitation of ions during the first half of the sweep followed by de-excitation of the ions after inversion of the *rf* phase. It was assumed that the method needs a symmetric power distribution over the

selected bandwidth, which is difficult to achieve due to unfavourable characteristics of the *rf*-transmitters.

In this study we have tried to overcome the above-mentioned shortcomings of the notch ejection technique, and we improved the method by modifying the *rf* amplitude profile during the frequency sweep. We thus obtained high resolution for high mass samples with efficient and clean isolation. We could easily implement this technique on FT-ICR mass spectrometers, without requiring any special software or hardware.

## 2.2 Theory

Fourier transform ion cyclotron resonance (FT-ICR) mass spectrometry uses pulsed excitation to manipulate ions by generating coherent motions of ensembles of ions. Frequency swept or chirp pulses are the usual method applied in the infinity cell of the Penning trap of commercial ICR instruments to excite, analyze and detect ions.<sup>35,42</sup> The theory of the swept excitation and the response of the ions to it have been covered in detail by Marshall *et al.*<sup>43</sup> Stepwise frequency-swept excitation is preferred over continuous swept frequency excitation for synchronizing the phase of the sweep and for maintaining phase stability. Such a pulse is defined by the sum of exponential wave function given in equation 2.1-2.2.

$$\psi_n = E_0 \exp[i (\omega_n (t - (n-1)\Delta T) + \phi_n)] \quad (2.1)$$

where,  $E_0$  is the amplitude of the applied wave ( $=V_{p-p}/d$ ). The frequency  $\omega_n$  and the phase  $\phi_n$  of the  $n^{\text{th}}$  step are given by:

$$\begin{aligned} \omega_n &= \omega_1 + (n-1)2\pi\Delta\nu \\ \phi_n &= \frac{n\Delta T}{2} [2\omega_1 + (n-1)2\pi\Delta\nu] \end{aligned} \quad (2.2)$$

where,  $\omega_1$  is the initial frequency,  $\Delta T$  is the duration of each step and  $\Delta\nu$  is the step size. This allows chirp pulses to be used for very frequency-selective excitation. A way of selecting the frequency and not exciting certain selected ions can be achieved by zeroing the magnitude profile of the chirp for which the frequency needs to be suppressed, or in other words for the ion that needs to be isolated. This is performed by inverting the phase of the pulse at the desired frequency as:

$$\varphi_m = \begin{cases} E_0 \exp[i(\varphi_m(t - (m-1)\Delta T) + \varphi_m)], & 1 < m < p \\ E_0 \exp[i(\varphi_m(t - (m-1)\Delta T) + \varphi_m + \pi)], & p < m < n \end{cases} \quad (2.3)$$

The number of the steps in the chirp pulse goes from 1 to  $n$  and the phase is reversed when the loop counter reaches  $p$ , which corresponds to the frequency of the ions to be isolated as shown in Figure.2.1.

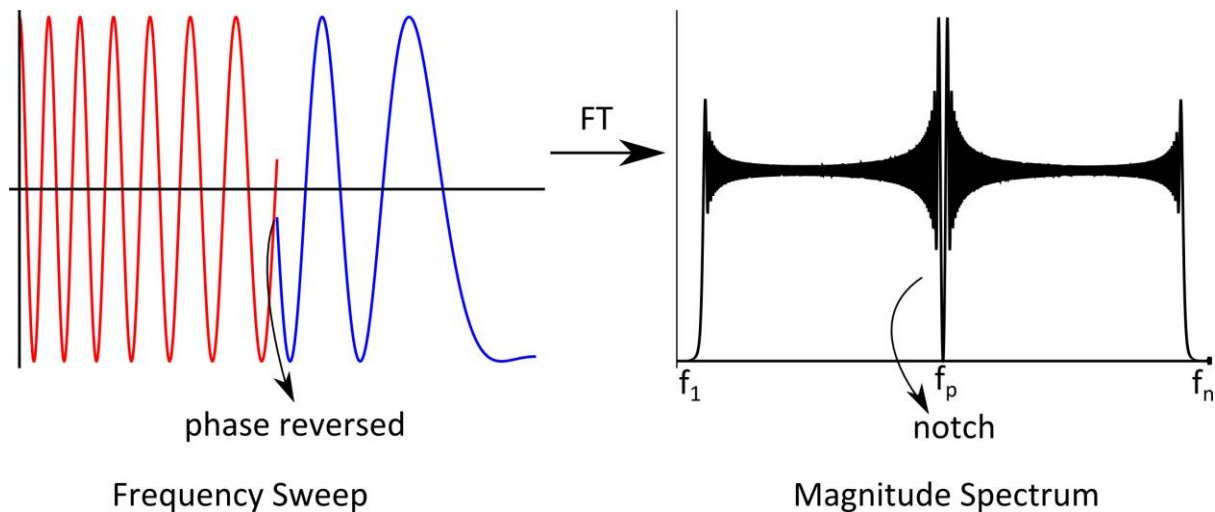


**Figure 2.1.** Houriet's scheme for notch ejection and spectral contents of a frequency sweep from  $f_1$  to  $f_2$  with a phase shift at the frequency  $f_n$ .

In the notch ejection method, the phase of the radio frequency ( $rf$ ) pulse is inverted (i.e., undergoes a sudden  $\pi$  phase shift) when the sweep reaches the cyclotron frequency corresponding to the  $m/z$  ratio of the ions that one wishes to isolate. The notch allows one to

bring the desired ions to the center of the ICR cell while all other ions are ejected<sup>44</sup>. The ions that must be isolated experience little or no excitation by the RF pulse. The width  $\Delta m$  of this notch is related to the mass  $m$ , charge  $z$  and sweep rate (SWR) as in equation. 2.4.<sup>40</sup>

$$\frac{m}{\Delta m} \propto \frac{z}{m \times (SWR)^{1/2}} \quad (2.4)$$

As the  $m/z$  ratio increases, the resolution of ion isolation decreases. Therefore, the notch ejection method as it was originally suggested could not be used for samples with high  $m/z$  ratios. Another limitation of this method is the limited mass range as high power is required to eject the ions from the cell. To overcome these limitations, particularly for high  $m/z$  ratios, we modified the sweep rate of the pulses which depends on both the power and the duration of the pulse. The excitation profile of the ions depends on the product of the voltage and pulse duration.<sup>45</sup> The radii of the ion trajectories increase after the application of a pulse as:

$$r = \frac{V_{p-p} \times T}{2 \times d \times B}$$

(2.5)

where  $V_{p-p}$  and  $T$  refer to the peak to peak voltage and the duration of the *rf* pulse respectively and  $d$  is the diameter of the ICR cell and  $B$  refers to the magnetic field applied. We performed experiments on ubiquitin (MW = 8.6 kDa) and obtained an optimum working range for the length of the ejection pulse for low powers for such high mass samples. The intensity variation of the most abundant peak of  $MH_9^{9+}$  and  $MH_{11}^{11+}$  was observed for a constant voltage of  $V_{p-p} = 10$  V and varying pulse duration from 10  $\mu$ s to 370  $\mu$ s. The maximum intensity was achieved for a pulse of duration of 50  $\mu$ s and voltage 10 V for both ions.

It is evident from equation 2.5 and from the response of ubiquitin (Figure 2.2) that the highest intensity and the point where all ions are ejected (marked by shaded lines in Figure 2.2) occur at the same values if the product of the pulse length and voltage is constant. This happens

because the radius of the ions after excitation does not depend on the  $m/z$  ratio and also because the excitation magnitude vs. frequency profile in chirp excitation does not change dramatically if the product of the duration and amplitude of the excitation is kept constant.<sup>34</sup>

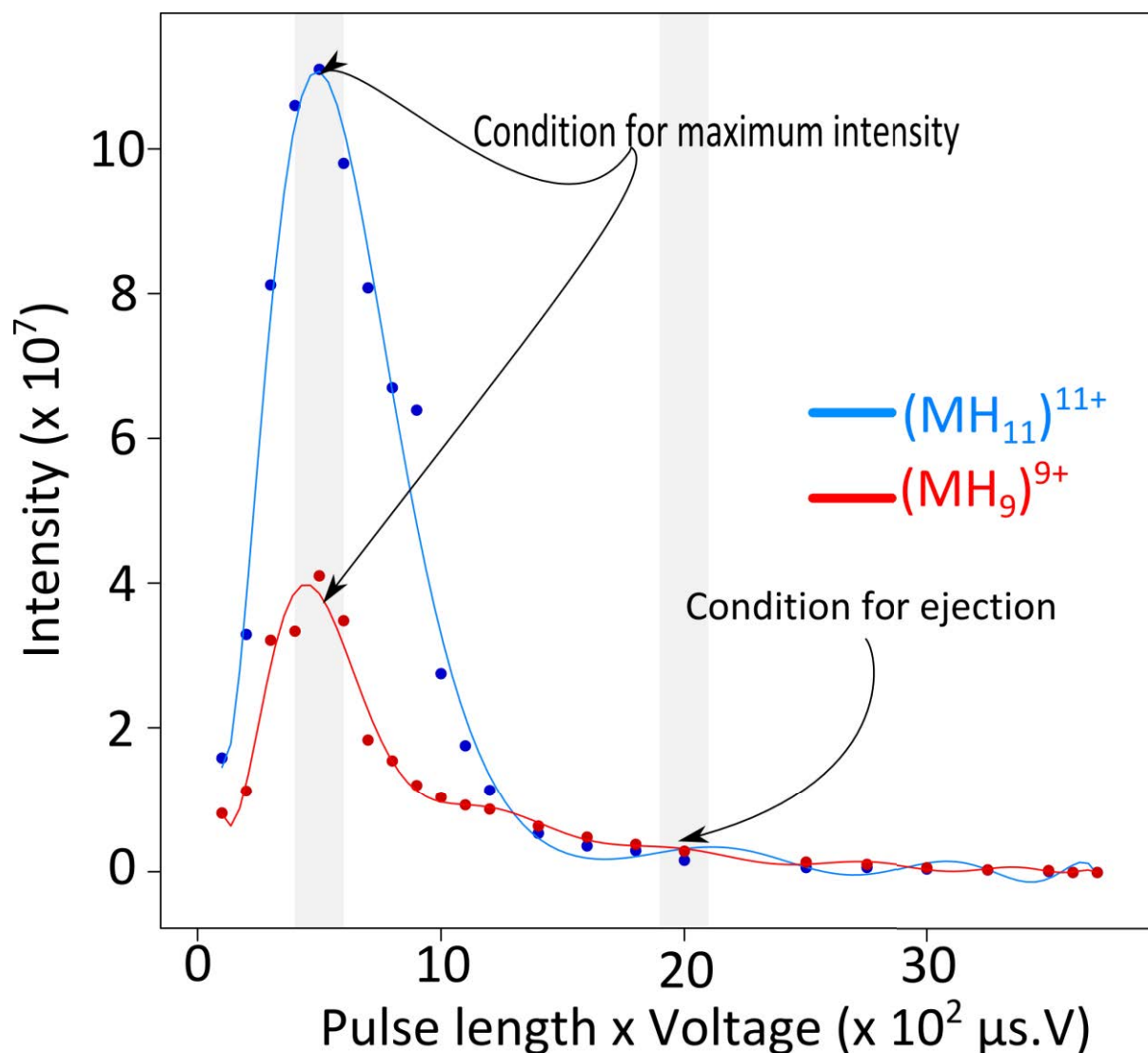


**Figure 2.2.** Intensity of the most abundant peak of ubiquitin as a function of the product of pulse length and voltage. The lines are the polynomial fits of the experimental data.

Therefore, a 10<sup>2</sup>-fold reduction of the voltage could be obtained by increasing the pulse duration while maintaining an intensity which could be observed. This allows one to change

the sweep rate. There is another feature of the frequency sweep, i.e. the frequency step; the adjustment of this parameter enables one to avoid an unreasonable increase in the pulse length and thereby of the experimental time. If one takes the smallest possible step in the frequency list, the pulse duration that yields the maximum signal intensity decreases from 20 to 1  $\mu\text{s}$  at the default peak to peak voltage  $V_{p-p} = 78 \text{ V}$ . For enhancing the spectral range and also dramatically increasing the number of the frequencies that could be probed, the frequency step size was taken to be the minimum allowed on the spectrometer, i.e.,  $\Delta\nu = 62.5 \text{ Hz}$ . The use of small steps allows one to have several frequencies in a selected range and thereby a chance of handling the cyclotron frequencies of several ions. The stepped variation of frequency sweep excitation is shown in Figure 2.3.

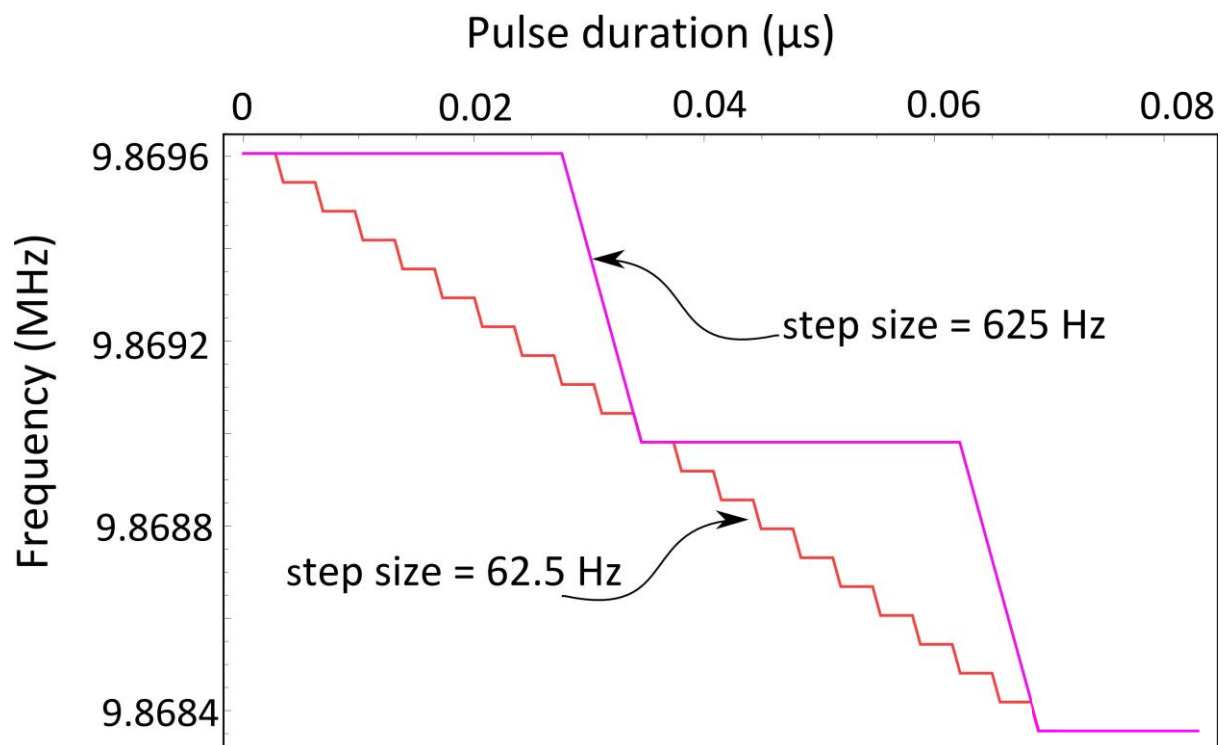


**Figure 2.3.** Frequency sweep as a function of pulse duration when changing the frequency in a step-wise fashion with step sizes  $\Delta\nu = 625$  (purple) and  $62.5$  (red).

We incorporated these features to probe high  $m/z$  samples without any loss of resolution by decreasing the sweep rate. We did this by attenuating the power levels of the ejection pulses in the vicinity of the frequencies to be isolated as:

- (i) high level voltage, high scanning rate, stepped twice
- (ii) low level voltage, low scanning rate,
- (iii) reversal of the phase during the lowest scanning rate,
- (iv) same as (i) to accelerate data acquisition, as compared to using single sweep rate in the conventional technique (as shown in Figure. 2.4).

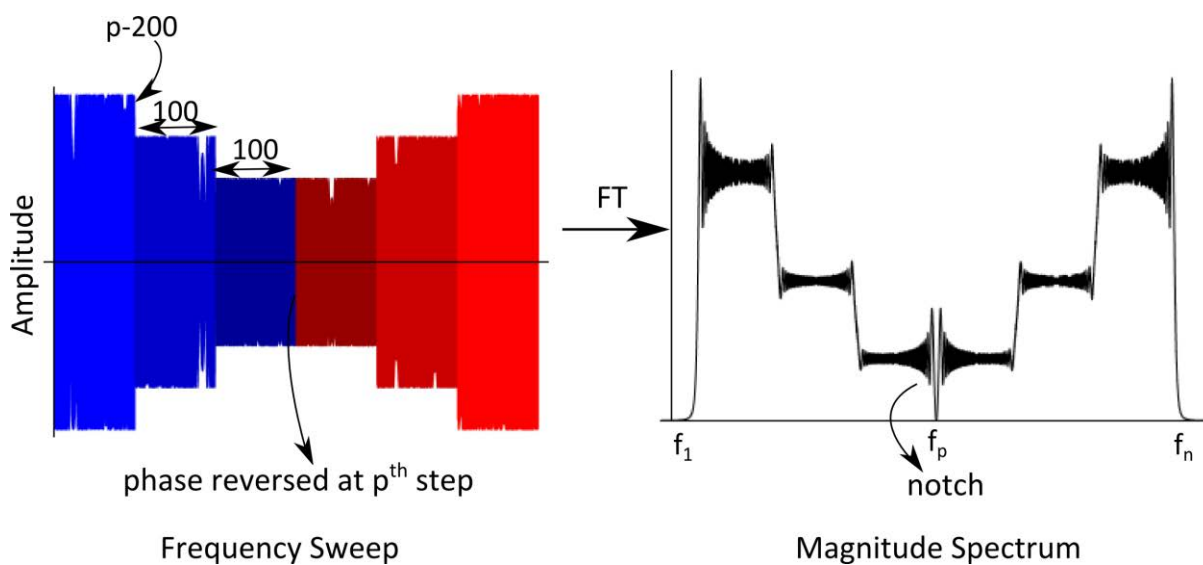


**Figure 2.4.** Modified scheme for notch ejection (left) and spectral contents (right) of a frequency sweep from  $f_1$  to  $f_2$  with a phase shift at the frequency  $f_p$ .

### 2.3 Experimental Methods

All experiments were performed with a Bruker Apex QE Fourier transform ion cyclotron resonance mass spectrometer (Bruker Daltonics, Bremen, Germany), equipped with a 9.4 T

magnet, and a positive nano-ESI ion source. The pressure in the ICR cell was maintained at  $10^{-10}$  mbar.

### 2.3.1 Pulse Scheme

The power levels were optimized for different samples and experiments, to control the ejection of the desired ions and achieve higher isolation efficiency. The experiments require the application of only two radiofrequency pulses for isolation of the desired ions from a mixture of ions with mass values varying over a wide range. We refer to these two pulses as ‘ejection-isolation pulse’ and ‘detection pulse’. The various pulse schemes applied are shown in the Figure 2.5.

**Ejection-isolation pulse:** The power level is attenuated so that a slower sweep rate, which is essential for high resolution of high  $m/z$ , acts only in the vicinity of the  $m/z$  ratio of the ion to be retained. For ions other than the ones which are retained, ejection of the ions is achieved by adjusting the duration and voltage of the pulse such that their cyclotron orbit radii exceed the dimensions of the cell. We attenuated the power level starting from the default voltage value of the spectrometer of 7 dB ( $V_{p-p} = 78$  V) and a duration of 10  $\mu$ s. For the second step we lowered the power level to 15 dB ( $V_{p-p} = 31$  V) and increased the duration to 150  $\mu$ s. The last step is the most crucial for adjustment as it determines the resolution of the ejection process. It has to be adjusted depending on the  $m/z$  of the ion to be isolated. For samples with

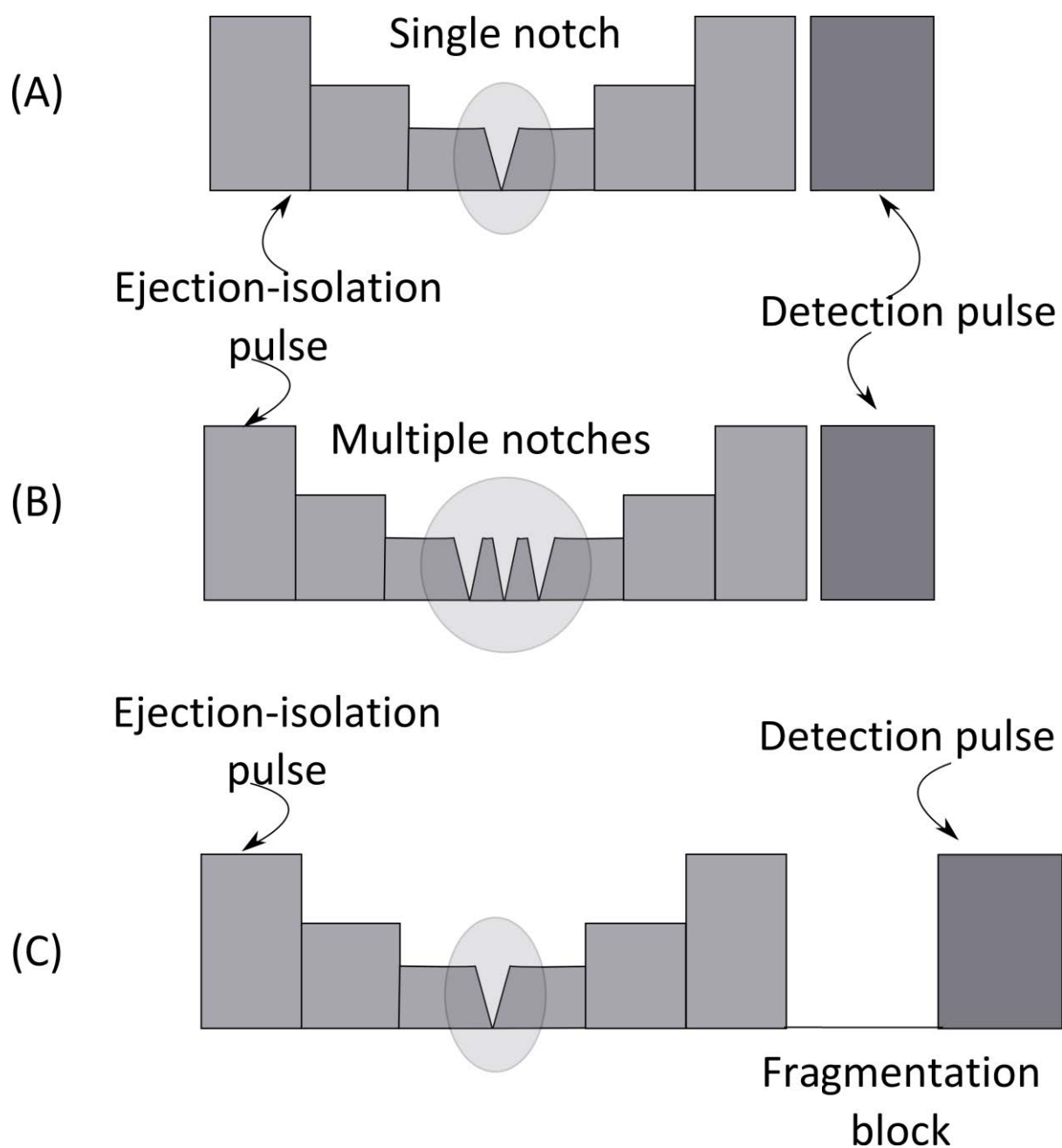


**Figure 2.5.** Improved schemes for ion ejection by lowering the sweep rate for part of the ejection pulse: (A) for one ion, (B) for multiple ions, (C) including an interval for ion fragmentation.

$m/z \leq 1000$ , a pulse attenuation of 25 dB (voltage  $V_{p-p} = 10$  V) is applied for a duration ranging from 400- 8000  $\mu$ s and for samples with  $m/z \geq 1000$ , 43 dB ( $V_{p-p} = 1$  V) power is applied for about 12000-14000  $\mu$ s. If  $p$  is the value of the loop counter at the time of the inversion of the frequency, then the first transition of the voltage and pulse duration is performed at a value of

the loop counter  $p-200$  in the frequency list. The second transition is after 100 steps and the third transition is optimized to occur after 200 steps for the case of single ion isolation, when the frequency of the ion to be isolated is in the middle of the pulse (as shown in Figure 2.4). Multiple notches can also be accommodated for multiple ion isolation.

**Detection Pulse:** This pulse is required for observing the ion that was isolated during the previous pulse. For the minimum frequency increment of 62.5 Hz, the default detection pulse of length 1  $\mu$ s has an attenuation 7dB ( $V_{p-p} = 78$  V).

The parameter “XBB” controls the step size within the frequency list of the  $rf$  chirp. It has a value of 100 as a default on the instrument. We increased the value to 1000 for all experiments recorded which corresponds to the frequency step of 62.5 Hz.

In between these two pulses, blocks of infrared multiphoton dissociation (IRMPD) or electron capture dissociation (ECD) can be inserted to induce fragmentation. IRMPD as a fragmentation mode is applied using a continuous CO<sub>2</sub> laser with a 10.6  $\mu$ m wavelength and power 25 W. The laser power and the pulse length were computer controlled. Experiments were conducted at 50% of the maximum laser power and the laser pulse was applied for 1.2 s. Experiments for fragmentation by electron capture dissociation (ECD) after ion isolation were carried out with a 1.3 A electron emission current for 0.12 s.

### 2.3.2 Sample Preparation

Samples of the proteins substance P, insulin B chain, insulin, ubiquitin and trioleate were purchased from Sigma-Aldrich (Saint Louis, MO, USA) and were used as received. AQUA peptide: the retinol binding protein (RBP) 4 labeled peptide was obtained from ThermoFischer (San Diego, USA).

The protein samples were dissolved in 1:1 water:methanol with 0.1% formic acid at concentrations between 1 pm/ $\mu$ l and 5 pm/ $\mu$ l. The initial flow rate was 20-30  $\mu$ l/h, which was lowered to 4-6  $\mu$ l/h after generation of for 15 minutes in the nanoESI ion source. The AQUA peptide samples were prepared by dilution with the same solution used for electrospray. The AQUA 1 and 2 samples were obtained by “in-solution” digestion of 5  $\mu$ g of commercial RBP4 using trypsin.

## 2.4 Results and Discussions

The conventional scheme, as suggested by Houriet *et al.*, with a single low power level with a low sweep rate can be optimized for samples of low mass. But if the conventional scheme is used for both excitation and detection of higher masses, the experimental time becomes protracted because of the low sweep rate. For complex samples with high masses, we therefore developed a scheme as discussed before with three distinct power levels. The power was reduced to a very low level, while the length of pulse increased, but only over a small window of 12.5 kHz width which encompasses the frequency where the phase must be inverted in the three step ejection-isolation pulse. All other ions are ejected, except for the one corresponding to the frequency where the phase is reversed. The improved scheme with three power levels was employed for initial experiments on Substance P (1.4 kDa) with ion isolation and further fragmentation by ECD and IRMPD. We isolated the mono-isotopic ion of  $(MH_2)^{2+}$ . Similar results were obtained on isotopologues of  $(MH_2)^{2+}$  containing up to three  $^{13}C$  isotopes, as shown in Figure 2.6. The cyclotron frequency of the ions being isolated ( $f_c$ ) and the frequency at which the phase is reversed ( $f_p$ ) for substance P is shown in Table 2.1. The pulse parameters employed for substance P were {78 V for 10  $\mu$ s, 31 V for 115  $\mu$ s, 10 V for 400  $\mu$ s} for the ejection-isolation pulse and {78 V for 1  $\mu$ s} for all the experiments,

changing only the loop counter corresponding to the frequency to be inverted. The resolution of separation for these isotopologues of doubly charged ions of substance P is 1350 ( $\approx 675/0.5$ ), with an isolation efficiency of about 10%. The ion resolution was over 20000 for the first  $^{12}\text{C}$  isotopologue isolated for substance P.

After isolation, the mono-isotopic ion of  $\text{MH}_2^{2+}$  was fragmented by electron capture dissociation (ECD) and infrared multiphoton dissociation (IRMPD) as shown in Figures 2.7 and 2.8 respectively. As shown in the top spectra of both figures, the isolated precursor ion contained only  $^{12}\text{C}$  atoms and was free from interference of any  $^{13}\text{C}$  isotopes. And because of such a clean isolation, the fragmented peaks did not contain any other isotopes and fragments arising due to electron capture in ECD, such as  $(\text{MH}_2)^{+}$ , which could be distinguished from the  $^{13}\text{C}$  isotope of  $\text{MH}^+$ . The bottom spectra in the Figures 2.7 and 2.8 depict isolation and fragmentation of isotopologues of  $(\text{MH}_2)^{2+}$  with one  $^{13}\text{C}$  isotope. We observed that the fragments contain peak with  $^{13}\text{C}$  isotope and a contribution of peak containing all  $^{12}\text{C}$  isotope. For samples with higher masses, on performing experiments with the same pulse duration and power level as for  $m/z < 1000$ , we could neither obtain clean isolation nor could maintain the intensity of the isolated peaks to  $1/10^{\text{th}}$  of the mass spectra.

We, using the equation 2.3 (which represents a single step notch), simulated the notches for a *rf* pulse voltage of 1V and a duration varying from 18000  $\mu\text{s}$  to 6000  $\mu\text{s}$  pulse and plotted the full width at half depth of the notch against the pulse duration, of the Fourier transformed frequency profile of the pulse representing the magnitude mode, as shown in Figure 2.9. The figure indicates that the width of the notch decreases with the pulse length. For a slower sweep rate, the notch width is narrow and this enables probing samples with higher separation resolution, so that we could isolate ions of higher  $m/z$ . We also observed that rather than a sharp V-shaped notch at a given frequency, the notch is U-shaped, as shown in

the zoomed inset of Figure.2.9, which allows us to be a little off in frequency for inverting the phase without sacrificing isolation. This is helpful from an instrumental point of view as due to a preset frequency list on the machine we were unable to revert the phase at the exact frequency.

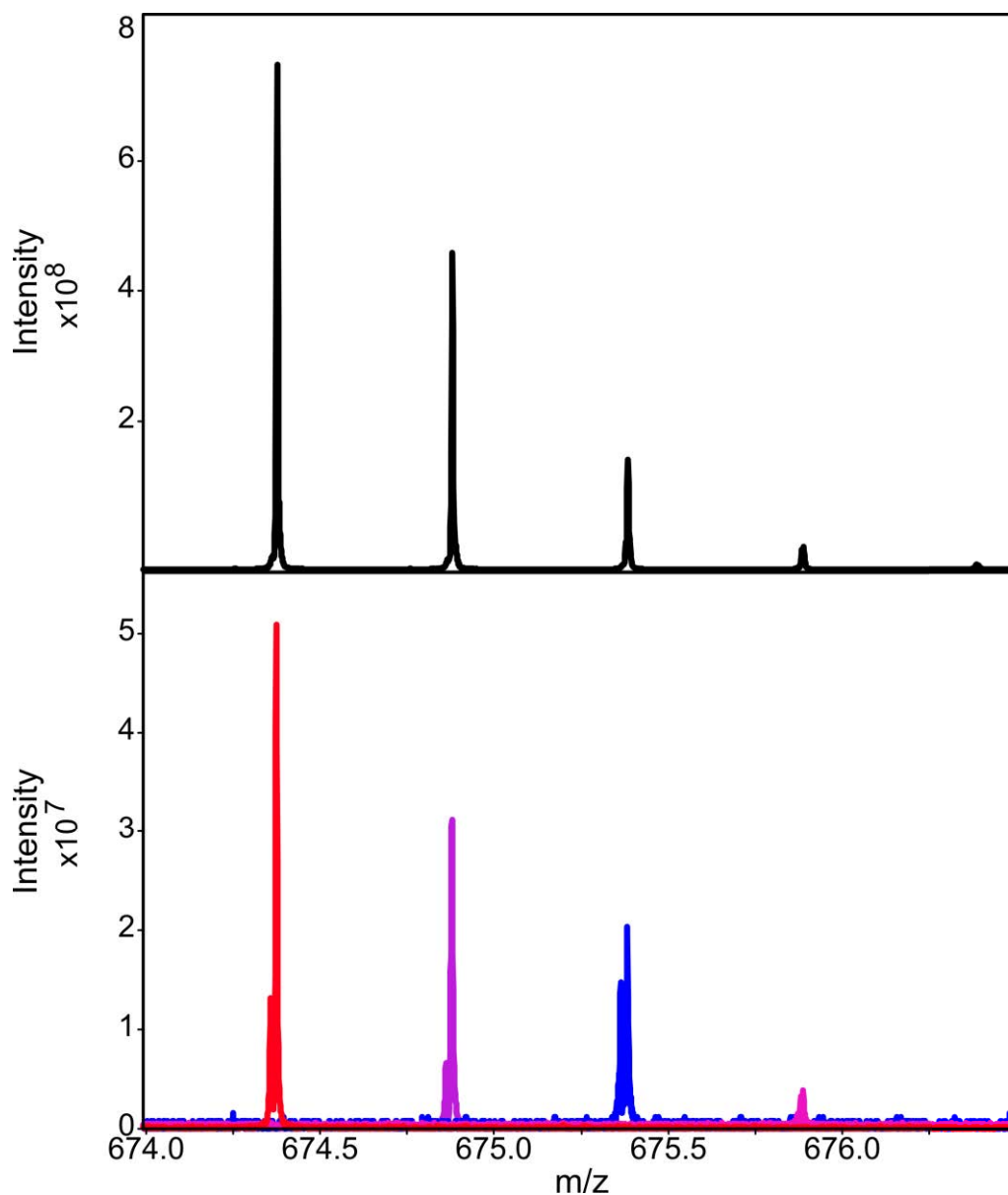


**Figure 2.6.** Mass spectra of substance P measured with a 9.4 T FT-ICR spectrometer: top spectrum under standard conditions without isolation, and bottom spectrum with notch ejection isolation of the mono-isotopic peak of  $MH_2^{2+}$  with the modified ejection pulse scheme.

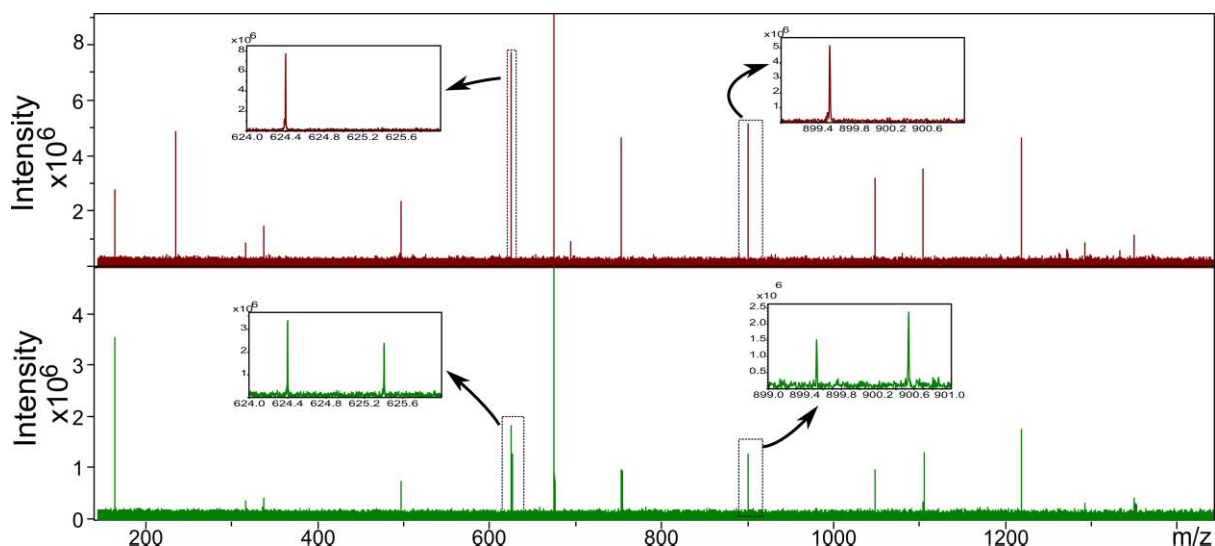


**Figure 2.7.** Fragmentation using ECD of the peaks of  $MH_2^{2+}$  with the improved scheme. The upper panel indicates isolation and fragmentation of the isotopologue of  $MH_2^{2+}$  with only  $^{12}C$  isotopes and the lower panel shows isolation and fragmentation of  $MH_2^{2+}$  with one  $^{13}C$  isotope. The zoomed peaks shows representative fragment peaks of  $c_5$  ( $m/z = 624.4$ ) and  $c_7$  ( $m/z = 899.4$ ), with resolutions of approximately 100000. All other fragments  $c$  and  $z$  can be seen in the spectra.

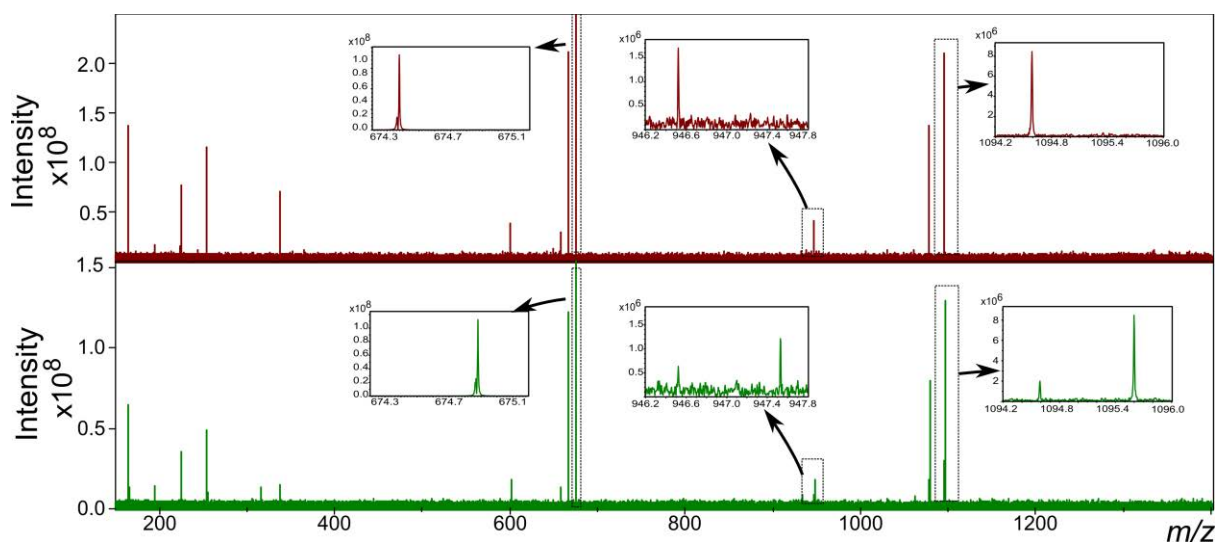


**Figure 2.8.** Fragmentation with IRMPD of the peaks of  $MH_2^{2+}$  with the improved scheme. The upper panel indicates isolation and fragmentation of the isotopologue of  $MH_2^{2+}$  with only  $^{12}C$  isotopes (first zoomed window) and the lower panel shows isolation and fragmentation of  $MH_2^{2+}$  with one  $^{13}C$  isotope (first zoomed window). The zoomed peaks show representative fragments of  $KPQQFFGL$  ( $m/z = 946.6$ ), with a peak

resolution of 94652 and  $\gamma_9$  ( $m/z = 1094.2$ ), with a peak resolution of. All other fragments  $b$  and  $y$  can be seen in the spectra.

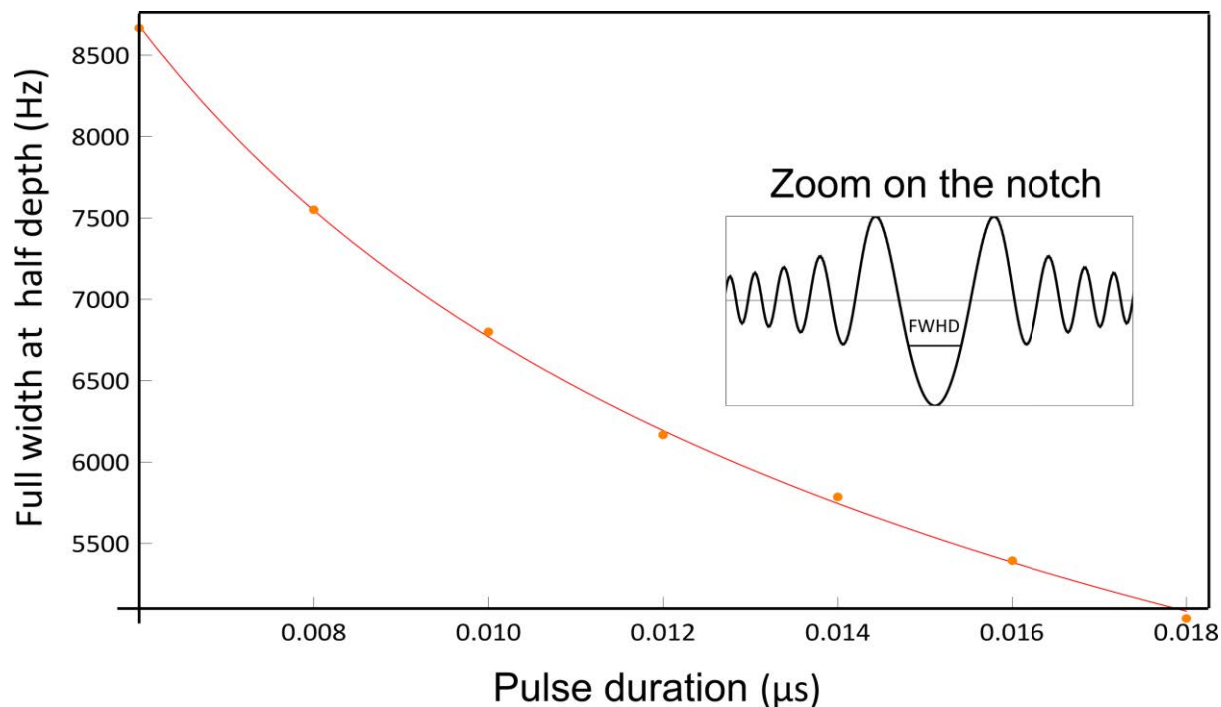


**Figure 2.9.** The curve indicates the variation of the width of the notch for different pulse lengths such that the product of the voltage and pulse duration stays constant, with the inset showing a zoomed view on the notch.

In the inset, the vertical axis represents the magnitude mode (absolute value) of the  $rf$  excitation, obtained from the analytical formula for Fourier transform of the time domain signal. The depth of the peak is calculated from the width at half the minimum height of the vertical axis.

In order to isolate ions without loss of resolution and sensitivity, the sweep rate and the exact frequency of the phase shift needed to be optimized. To go further on higher masses and to probe the validity of the isolation for complex systems, we performed experiments with the improved three-level pulse scheme on samples of insulin B chain (3.5 kDa) and insulin (5.7 kDa) and with a slower sweep rate. The attenuated power level for experiments on both samples of insulin and insulin B chain was 43 dB ( $V_{p-p} = 1$  V) for an optimized pulse length

of 14 ms, for a sweep, which ‘encloses’ the ion to be isolated and rest of the parameters were as discussed before. Most multiply charged states (e.g.,  $z = 4+$ ,  $5+$  for insulin B chain and  $z = 4+$ ,  $5+$ ,  $6+$  for insulin) could be isolated along with their all isotopologues. The isolated peaks of  $MH_5^{5+}$  for insulin B chain and  $MH_6^{6+}$  for insulin are shown in Figure 2.10. The resolution of separation for insulin B chain is bigger than 3537 ( $\approx 707.534:0.2$ ) and for insulin is bigger than 5740 ( $\approx 956.6:0.17$ ).

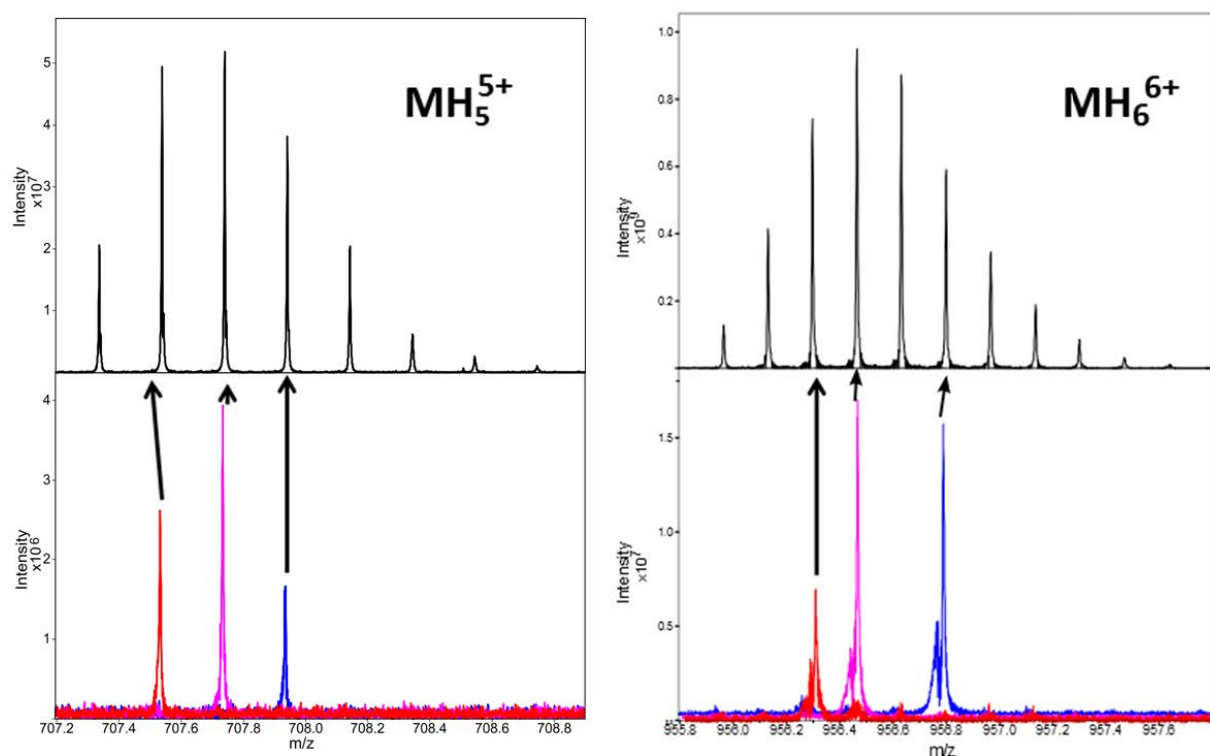


**Figure 2.10.** The top spectra shows the isotopic distributions and the bottom figure the stacked spectra of some isolated peaks, for  $MH_5^{5+}$  in Insulin B chain on the left, and for  $MH_6^{6+}$  in Insulin on right. (The frequency parameters for which the ions are isolated are given in Table 2.1)

When the preset frequency is too far from the cyclotron frequency of multiple charged or high mass ions, an interference with other peaks occur during isolation (due to the small difference in their respective frequencies). This leads to an insufficiently clean separation.

The issue was resolved by shifting the mass range. In this manner, we could shift the frequency where we can invert the phase, such that it is around  $\pm 30$  Hz with respect to the actual frequency of the desired ion. All the phase reversal frequencies given in Table 2.1 for the respective ion being observed were optimized by shifting the mass range of the experiment thereby obtaining the conditions for the most efficient isolation. Though this can be a tedious task, once this technique becomes accepted and is frequently used by the community, an auto-generated frequency list could be set up with the ion to be isolated kept in focus, and applied for clean isolation of isotopologues of multi-charged ions.

For isolating more than one ion simultaneously, we created several notches during the low-power sweep and inverted the phases several times, keeping the same pulse parameters as for single notches, but by changing the loop counters. We could efficiently isolate the isotopic peaks of AQUA peptide 1 and 2 samples as shown in Figure 2.11, by reversing the phase at several points. We isolated the  $^{12}\text{C}$  isotope and one  $^{13}\text{C}$  isotope, corresponding to  $m/z = 585.284$  and  $585.783$  respectively of AQUA peptide 1 and  $m/z = 603.827$  and  $604.328$  respectively of AQUA peptide 2. The pulse parameters taken for the experiment were: {78 V for 10  $\mu\text{s}$ , 31 V for 115  $\mu\text{s}$ , 10 V for 500  $\mu\text{s}$ }

Absolute Quantification (AQUA) methods are based on comparisons of protein expression levels between isotopically labeled and non labeled samples. Mass spectrometry in conjunction with liquid chromatography is used for such proteomic studies particularly for post translational protein modifications (e.g. ‘liquid-chromatography-selected reaction monitoring’ (LC-SRM) and ‘liquid-chromatography multiple reaction monitoring’ (LC-MRM)). Ions need to be isolated for performing the quantification and built-in methods are used for this purpose.

**Table 2.1** Frequency parameters for the ions isolated for different samples

	$m/z$	$f_c$ (kHz)	$f_p$ (kHz)	$ f_c - f_p $ (Hz)
Substance P				
Monoisotopic $MH_2^{2+}$	674.38	214.0591	214.0734	14.3
$MH_2^{2+}$ with 1 $^{13}C$	674.88	213.8959	213.9159	20
$MH_2^{2+}$ with 2 $^{13}C$	675.38	213.7371	213.7284	8.7
$MH_2^{2+}$ with 3 $^{13}C$	675.88	213.5786	213.6034	24.8
Insulin B chain				
$MH_5^{5+}$ with 3 $^{13}C$	707.54	204.0220	204.0454	23.4
$MH_5^{5+}$ with 4 $^{13}C$	707.74	203.9641	203.9823	18.2
$MH_5^{5+}$ with 5 $^{13}C$	707.94	203.9063	203.9332	26.9
Insulin				
$MH_6^{6+}$ with 3 $^{13}C$	956.256	150.9450	150.9615	16.5
$MH_6^{6+}$ with 4 $^{13}C$	956.422	150.9188	150.9415	22.7
$MH_6^{6+}$ with 6 $^{13}C$	956.755	150.8663	150.8791	12.8
AQUA peptide 1 and 2				
AQUA 1	585.284	246.6396	246.6519	12.3
	585.786	246.4295	246.4019	27.6
AQUA 2	603.827	239.0650	239.0269	38.1
	604.328	238.8670	238.8394	27.6

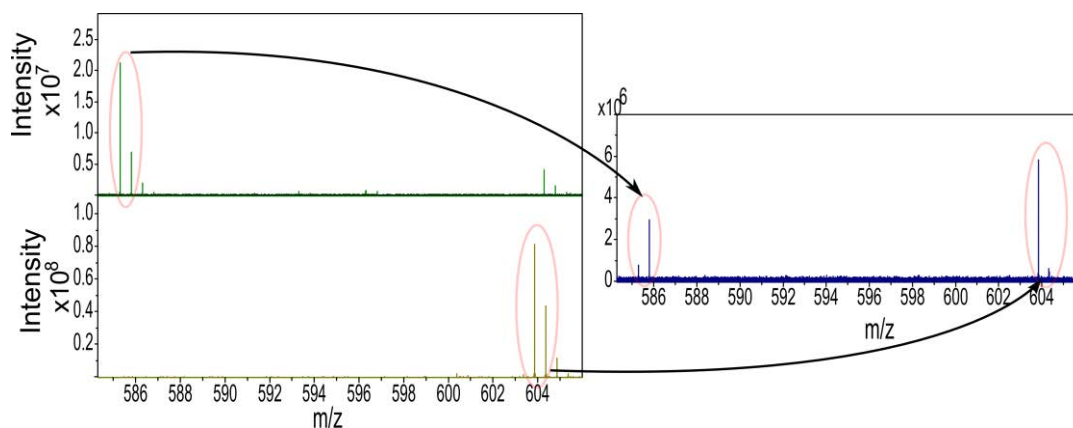


**Figure 2.11:** Multiple ions isolated for AQUA peptide: The left top and bottom spectra show the ms spectra of AQUA peptide 1 and 2 respectively. The right figure indicates the multiple isolated peaks of the mixture of AQUA 1 and 2.

We did a comparative analysis of ion isolation techniques available on the spectrometer with the notch isolation method. As can be seen from Figure 2.12, both quadrupolar and CHEF isolation fail to provide a clean single isotopologue peak of a relatively simple sample of mono lithiated trioleum ion,  $[M+^7\text{Li}]^+$ . For this comparison, the ion isolation by notch was performed by using a single-power and pulse duration ejection-isolation pulse rather than the more elaborated three-stepped pulse. As can be seen from the figure, the isotopologue with a  $^6\text{Li}$  ion disappears easily even with the traditional notch technique while the intensity of the main isolated peak is comparable with CHEF. The number of frequency sweeps utilized for ion isolation is just two,<sup>15</sup> whereas for conventional techniques like CHEF several chirp and/or single-frequency excitations are required. Notch ejection possesses the ability to become the state of art technique for ion isolation.

The protocol for ion isolation was optimized for several samples. Details of these samples and the peaks that were isolated are reported in Appendix 1.

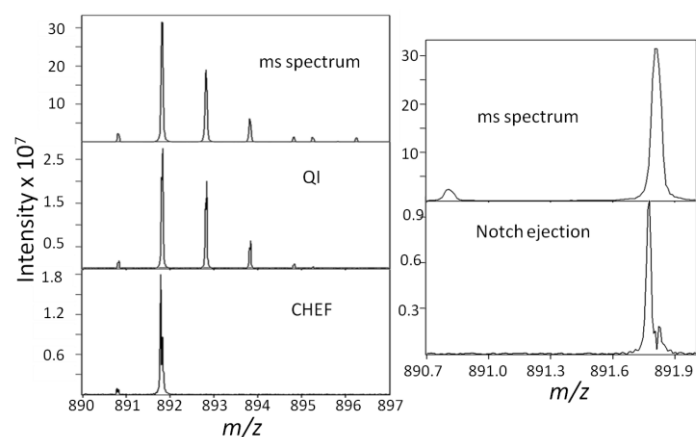


**Figure 2.12:** Comparison of the notch method with QI and CHEF. Left figure: The top spectrum is the mass spectrum of  $[\text{trioleate}+\text{Li}]^+$ ; Middle spectrum represents the isolation by quadrupolar isolation (QI), showing all isotopic masses after isolation; the bottom spectrum shows isolation by correlated harmonic excitation fields (CHEF) where the  $[\text{M}+^6\text{Li}]^+$  peak is also present. Right top figure is the mass spectrum of  $[\text{trioleate}+\text{Li}]^+$  and right bottom figure is the spectrum obtained through notch ejection. For CHEF the  $m/z = 891.82$  was isolated with an excitation power of 42 % and the safety belt parameter of  $0.055 m/z$ . For notch ejection, the ejection pulse was of a low sweep rate of 31V and  $100 \mu\text{s}$  and the detection pulse of 78 V for  $1 \mu\text{s}$ . The cyclotron frequency of  $m/z= 891.81[\text{M}+^7\text{Li}]^+$  is 161.862 kHz and the phase is reversed at 161.886 kHz.

## 2.5 Conclusions and Perspectives

The improved technique is based on the phase reversal of the radio frequency pulse near the cyclotron frequency of the ion to be selected, resulting in high resolution and clean isolation, without much loss in intensity in an proficient and simple way. Efficient isolation of a single isotope peak prior to fragmentation reduces the complexity of fragment ion spectra, thus enabling easier identification of fragments, as has been shown for substance P. By using three power levels, the experimental time was reduced to minutes, compared to hours when using the conventional scheme with a single power level. This reduction in experimental time provides more freedom for manipulating a manifold of ions and also improves the isolation

efficiency. This tool for ion isolation can be easily used in commercial spectrometers without the need of additional hardware or software. With better insight into the behavior of ions in the cell upon inversion of the phase, better optimization of the conditions could be achieved which would enable an improvement of the proposed technique.

We observed high resolution on both precursor and fragment ions with clean isolation and multi isolation, as the need be. We could isolate the desired ions in a complex mixture of labeled proteins and we plan to extend the method for the quantitation of peptides without chromatography using the AQUA (Absolute Quantification) method. As done in an AQUA experiment where we mix peptides labeled with stable isotopes with an unlabeled native peptide produced during proteolytic cleavage of the target protein, we plan to perform such selective isolation with our multiple notch ejection technique. In the lab recently an absolute AQUA strategy of RBP4 had been developed, to study the methods for preserving the transfusion quality of blood plasma by SRM-MS, LC/MS based technique. This quantification relies on the precise measurement of the concentration of three proteotypic peptides of the protein RBP4: YWGVASFLQK (AQUA 1), FSGTWYAMAK (AQUA 2) and DPNGLPPEAQK (AQUA 3) which are obtained by the enzymatic digestion of the target protein trypsin and of their isotopically labeled counterparts. We could isolate the isotopologues of a sample of mix of AQUA 1 and AQUA 2 by the notch ejection experiment and plan to further perform the analysis of the proteolyzed samples with the isotopically labeled AQUA internal standard peptide. We believe that notch ejection thus would be able to provide a faster substitute of the protracted analysis of LC/MS for SRM and MRM based techniques for studying proteomics.

## References

- (1) Thomson, J. J. *Philos. Mag.* **1912**, *24*, 209.
- (2) Thomson, J. J. *Proc. R. Soc.* **1913**, *A 89*, 1.
- (3) Comisarow, M. B.; Marshall, A. G. *Can. J. Chem.* **1974**, *52*, 1997.
- (4) Smith, R. D.; Anderson, G. A.; Lipton, M. S.; Pasa-Tolic, L.; Shen, Y.; Conrads, T. P.; Veenstra, T. D.; Udseth, H. R. *Proteomics* **2002**, *2*, 513.
- (5) Shen, Y.; Toli, N.; Zhao, R.; Paa-Toli, L.; Li, L.; Berger, S. J.; Harkewicz, R.; Anderson, G. A.; Belov, M. E.; Smith, R. D. *Anal. Chem.* **2001**, *73*, 3011.
- (6) Qian, W.-J.; Camp, D. G.; Smith, R. D. *Expert Rev. Proteomics* **2004**, *1*, 87.
- (7) Gygi, S. P.; Aebersold, R. *Curr. Opin. Chem. Biol.* **2000**, *4*, 489.
- (8) Brown, S. C.; Kruppa, G.; Dasseux, J.-L. *Mass Spectrom. Rev.* **2005**, *24*, 223.
- (9) Taylor, N. S.; Weber, R. J. M.; Southam, A. D.; Payne, T. G.; Hrydziuszko, O.; Arvanitis, T. N.; Viant, M. R. *Metabolomics* **2009**, *5*, 44.
- (10) Lobodin, V. V.; Rodgers, R. P.; Marshall, A. G. *Pet. Compr. Environ. Mass Spectrom.* **2012**, *18*, 415.

- (11) McKenna, A. M.; Williams, J. T.; Putman, J. C.; Aeppli, C.; Reddy, C. M.; Valentine, D. L.; Lemkau, K. L.; Kellermann, M. Y.; Savory, J. J.; Kaiser, N. K.; Marshall, A. G.; Rodgers, R. P. *Energy & Fuels* **2014**, *28*, 2454.
- (12) Millikan, R. A. *Phys. Rev.* **1911**, *32*, 349.
- (13) Sleno, L.; Volmer, D. A.; Marshall, A. G. *J. Am. Soc. Mass Spectrom.* **2005**, *16*, 183.
- (14) Lavanant, H.; Derrick, P. J.; Heck, A. J. R.; Mellon, F. A. *Anal. Biochem.* **1998**, *255*, 74.
- (15) Kruppa, G.; Schnier, P. D.; Tabei, K.; Orden, S. Van; Siegel, M. M. *Anal. Chem.* **2002**, *74*, 3877.
- (16) Kirkpatrick, D. S.; Gerber, S. a; Gygi, S. P. *Methods* **2005**, *35*, 265.
- (17) Shi, S. D.; Hendrickson, C. L.; Marshall, A. G. *Proc. Natl. Acad. Sci. U. S. A.* **1998**, *95*, 11532.
- (18) Belov, M. E.; Nikolaev, E. N.; Anderson, G. A.; Auberry, K. J.; Harkewicz, R.; Smith, R. D. *J. Am. Soc. Mass Spectrom.* **2001**, *12*, 38.
- (19) March, R. E. *J. Mass Spectrom.* **1997**, *32*, 351.
- (20) Hilger, R. T.; Santini, R. E.; Luongo, C. a.; Prentice, B. M.; McLuckey, S. a. *Int. J. Mass Spectrom.* **2014**, *In Press*.

- (21) Marshall, A. G.; Hendrickson, C. L. *Int. J. Mass Spectrom.* **2002**, *215*, 59.
- (22) Marshall, A. G.; Schweikhard, L. *Int. J. Mass Spectrom. Ion Process.* **1992**, *118-119*, 37.
- (23) Koning, L. J. de; Nibbering, N. M. M.; Orden, S. L. van; Laukien, F. H. *Int. J. Mass Spectrom.* **1997**, *166*, 209.
- (24) Johnson, H.; Wong, S. C. C.; Simpson, D. M.; Beynon, R. J.; Gaskeua, S. *J. Am. Soc. Mass Spectrom.* **2008**, *19*, 973.
- (25) Heck, A. J. R.; Koning, L. J. De; Pinkse, F. A.; Nibbering, N. M. M. *Rapid Commun. Mass Spectrom.* **1991**, *5*, 406.
- (26) Liu, H.; Håkansson, K. *J. Am. Soc. Mass Spectrom.* **2006**, *17*, 1731.
- (27) Heck, A. J. R.; Derrick, P. J. *Eur. J. Mass Spectrom.* **1998**, *4*, 181.
- (28) Heck, A. J. R.; Derrick, P. J. *Anal. Chem.* **1997**, *69*, 3603.
- (29) Witt, M.; Fuchser, J.; Koch, B. P. *Anal. Chem.* **2009**, *81*, 2688.
- (30) Pingitore, F.; Tang, Y.; Kruppa, G. H.; Keasling, J. D. *Anal. Chem.* **2007**, *79*, 2483.
- (31) Johnson, H.; Wong, S. C. C.; Simpson, D. M.; Beynon, R. J.; Gaskell, S. *J. J Am Soc Mass Spectrom* **2008**, *19*, 973.
- (32) Zhang, H.; Cui, W.; Wen, J.; Blankenship, R. E.; Gross, M. L. *J. Am. Soc. Mass Spectrom.* **2010**, *21*, 1966.

- (33) Zhang, H.; Cui, W.; Wen, J.; Blankenship, R. E.; Gross, M. L. *Anal. Chem.* **2011**, *83*, 5598.
- (34) Guan, S.; Marshall, A. G. *Int. J. Mass Spectrom. Ion Process.* **1996**, *157-158*, 5.
- (35) Chen, L.; Marshall, A. G. *Int. J. Mass Spectrom. Ion Process.* **1987**, *79*, 115.
- (36) O'Connor, P. B.; McLafferty, F. W. *J. Am. Soc. Mass Spectrom.* **1995**, *6*, 533.
- (37) Guan, S.; Burlingame, A. L. *J. Am. Soc. Mass Spectrom.* **2010**, *21*, 455.
- (38) Noest, A. J.; Kort, C. W. F. *Comput. Chem.* **1983**, *7*, 81.
- (39) Kleingeld, J. C.; Nibbering, N. M. M. *Tetrahedron* **1983**, *39*, 4193.
- (40) Vulpius, T.; Houriet, R. *Int. J. Mass Spectrom. Ion Process.* **1989**, *88*, 283.
- (41) Farrell, J. T.; Lin, P.; Kenttamaa, H. I. *Anal. Chim. Acta* **1991**, *246*, 227.
- (42) Baykut, G.; Eyler, J. R. *Trends Anal. Chem.* **1986**, *5*, 44.
- (43) Marshall, A. G.; Roe, D. C. *J. Chem. Phys.* **1980**, *73*, 1581.
- (44) Marshall, A. G.; Wang, T.-C. L.; Ricca, T. L. *Chem. Phys. Lett.* **1984**, *105*, 233.

- (45) Marshall, A. G.; Hendrickson, C. L.; Jackson, G. S. *Mass Spectrom. Rev.*  
**1998**, *17*, 1.

# Spiralling ion trajectories in two-dimensional ion cyclotron resonance mass spectroscopy

## 3.1 Introduction

### 3.1.1 History of 2D FT-ICR

Two-dimensional nuclear magnetic resonance (NMR) has inspired the development of 2D techniques in many fields like infrared (IR),<sup>1</sup> electron spin resonance (ESR),<sup>2</sup> ion cyclotron resonance (ICR) spectroscopy,<sup>3</sup> and very recently electron spectroscopy (ES)<sup>4</sup> and femtosecond spectroscopy.<sup>5</sup> Though till date, these 2D techniques have not been able to provide the remarkable feats of NMR. Two-Dimensional Ion Cyclotron Resonance Mass Spectroscopy (2D FT-ICR-MS) was introduced about 27 years ago by a joint effort of an NMR group led by Prof. Bodenhausen and an MS group led by Prof. Gäumann.<sup>3</sup> The idea was inspired by two-dimensional exchange spectroscopy (2D EXSY) or nuclear Overhauser exchange spectroscopy (NOESY),<sup>6</sup> which are used to obtain information regarding dynamic processes like chemical exchange and isomerisation or structural information. In 2D FT-ICR, single frequency and dual frequency methods were used initially to map ion-molecule reactions of small molecules.<sup>3</sup> To overcome bandwidth limitations of monochromatic pulses, the experiments were extended using frequency swept *rf* (chirp) pulses. The dependence on the indirect evolution interval  $t_1$  of the ICR signal of ions of methane ( $\text{CH}_3^+$ ,  $\text{CH}_4^{*+}$  and  $\text{CH}_5^+$ ) and deuterated methane ( $\text{CHD}_2^+$ ,  $\text{CHD}_3^+$  and  $\text{CD}_3^+$ ) was observed.<sup>7</sup> Pfändler et al. recognized that 2D FT-ICR MS was not limited to gas fragmentation techniques like collision induced dissociation (CID) and in a subsequent study, they recorded a 2D FT-ICR mass spectrum

using infrared multi-photon dissociation (IRMPD) as a fragmentation mode.<sup>8</sup> Two other methods were proposed for performing multidimensional MS experiments: a) 2D Hadamard Transform/Fourier Transform (HT/FT) and b) the use of Stored Waveform Ion radius Modulation (SWIM.) In Hadamard transform (HT) methods,<sup>9,10</sup> about half of the precursor ions are selected and dissociated simultaneously by a comb excitation; the process is repeated for a total of  $N$  times, selecting a different half of the precursors each time ( $N$  being also the number of precursors). Ross *et al.*<sup>11</sup> developed the SWIM technique, wherein they combined features of both HT/FT ICR and the Bodenhausen-Gaumann sequence. While Pfändler *et al.* used two frequency sweeps to modulate the cyclotron radii of the ions, Ross *et al.* combined these two pulses in one and varied the magnitude of the pulse sinusoidally as a function of frequency, following a principle similar to McLafferty *et al.* In this technique, the frequency of the variation is designed to increase linearly. For each frequency spectrum, the inverse Fourier transform is calculated and the resulting *rf* voltage is applied to the excitation plates for  $N$  different waveforms before injecting the gas into the ICR cell, re-exciting the ions and recording the time-domain transient. Instead of calculating the Fourier transform as a function of the evolution interval  $t_1$ , it is calculated as a function of the waveform number  $n = 1, 2, \dots, N$ . In 2001, van der Rest *et al.* used the SWIM FT/FTMS method to study complex mixtures, namely, proton-bound dimers and sodium-bound dimers of amino acids.<sup>12</sup> In 2002, Ross *et al.* applied SWIM to products of combinatorial synthesis of pharmaceutical interest and to samples of interest for automotive industries.<sup>13</sup>

In 2010, 2D FT-ICR experiments were revived by a team led by Dr. Rolando, using the IRMPD method for fragmentation of peptides.<sup>14</sup> Subsequently, the ECD fragmentation technique was also incorporated for 2D analysis of complex peptides samples.<sup>15</sup> Denoising algorithms like Cadzow's and RQR, which are frequently used in NMR data handling, were

adapted for 2D FT-ICR in view of reducing scintillation noise in the indirect dimension.<sup>16</sup> While 2D FT-ICR/MS has the potential to become a viable method for chemical analysis, not much references are available in the literature, except for the paper by Guan and Jones<sup>17</sup> on the theory of 2D FT-ICR. The latter work finds elegant solutions for the description of the ion trajectories under assumptions that turned out in practice not to lead to optimal sensitivity (in particular the assumption of long *rf* pulses). Herein, we try to formulate a theory for the behaviour of ions in the cases of small pulses which were recently optimized experimentally.<sup>18</sup>

### **3.1.2 Similarities and differences between ICR and NMR**

As the inspiration for performing 2D FT-ICR comes from 2D NMR, developing simple models to explain the ion behaviour in analogy to the classical models of NMR and exploring their similarities and differences becomes pertinent.

On the one hand, 2D ICR allows one to correlate pairs of frequencies that are characteristic of precursor and fragment ions before and after a modification of their mass-to-charge ratio by fragmentation, protonation, loss of neutral fragments, etc. These modifications can be induced by collisions with neutral molecules or by irradiation with infrared or electron beams. On the other hand, in applications to NMR, 2D EXSY allows one to correlate pairs of chemical shifts that are characteristic of the environments of nuclei before and after a chemical reaction or cross-relaxation processes. The magnetic field leads to circular motion of spins and ions manifested and measured as Larmor precession of magnetic moment for NMR and cyclotron rotation of ion for ICR, where the sense of rotation is determined by the

magnetogyric ratio and charge of ion respectively which are observed by applying linearly polarised radio frequency (*rf*) pulses.<sup>19,20</sup>

In its most basic form, two-dimensional exchange spectroscopy (2D EXSY) which provided the inspiration for two-dimensional ICR, uses a sequence comprising three pulses:  $\beta - t_1 - \beta' - \tau_m - \beta'' - t_2$ . The pulse scheme is shown in Figure 3.1. For ICR, the pulse sequence is like:  $P_1 - t_1 - P_2 - \tau_m - P_3 - t_2$ . In NMR, the three radio-frequency (*rf*) pulses are characterized by the ‘nutations angles’  $\beta$ ,  $\beta'$  and  $\beta''$  that are determined by the product of their durations  $\tau_p$ ,  $\tau_p'$  and  $\tau_p''$  and their *rf* amplitudes,  $t_1$  represents the evolution time,  $t_2$  represents the detection period and  $\tau_m$  represents the mixing time. On the other hand, in ICR the three radio-frequency (*rf*) pulses are characterized by the energy they confer to the ions (acceleration or deceleration) that is likewise determined by the product of their durations  $T_1$ ,  $T_2$  and  $T_3$  and their amplitudes. In NMR, the frequency range is usually in the order of parts per million (ppm), so that the three *rf* pulses can have the same monochromatic carrier frequency to cover the bandwidth, chosen in the vicinity of the Larmor frequency of the nuclei under investigation. In contrast, in ICR to cover a broad range of spectral widths, ranging from a few kHz to many MHz, needs to be covered and frequency swept chirp pulses are used. In their most common forms, 2D EXSY and 2D NOESY use three equal nutation angles  $\beta = \beta' = \beta'' = \pi/2$ . Similarly, in the initial 2D ICR experiments, three pulses with the same amplitude were considered.

If 2D EXSY experiments are performed using three pulses with identical flip angles  $\beta = \beta' = \beta'' = \pi/2$ , the fate of the magnetization can be readily described. The first pulse  $\beta$  converts the longitudinal magnetization  $M_z^k$  into a transverse component  $M_x^k$ , the second pulse  $\beta'$  has the opposite effect and generates a  $t_1$ -dependent longitudinal component  $M_z^k(t_1)$ , which, after

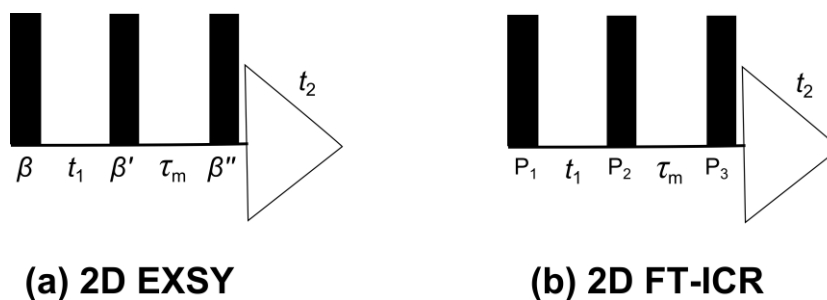


**Figure 3.1.** The conventional (a) 2D EXSY sequence, i.e.:  $\beta - t_1 - \beta' - \tau_m - \beta'' - t_2$ , (b) 2D FT-ICR sequence  $P_1 - t_1 - P_2 - \tau_m - P_3 - t_2$  with pulses  $P_1, P_2$  and  $P_3$  of pulse length  $T_1, T_2$  and  $T_3$  rather than flip angles  $\beta, \beta'$  and  $\beta''$ .

a partial conversion of  $M_z^k(t_1)$  into  $M_z^l(t_1)$  through exchange or cross-relaxation, is again converted by the third pulse  $\beta''$  from  $M_z^l$  into  $M_x^l$  that induces a signal in the second interval  $t_2$ . Unlike many other 2D NMR experiments that involve a transfer of coherence, and therefore require a quantum-mechanical treatment, most applications of 2D EXSY and 2D NOESY can be discussed purely in classical terms. Thus 2D EXSY NMR and 2D ICR share a reassuring common ground.

Signal generation and detection are linear if the amplitude of the response is proportional to the amplitude of the excitation i.e if the nutation/ flip angles are very small such that  $\sin(\beta) = \beta$ .<sup>21</sup> This represents the pole of the conventional Bloch sphere. So, the response is linear only for small angles. The response to excitation in ICR is always linear. The trajectories of ions in 2D ICR also exhibit a linear response if the perturbations are weak, but these trajectories are not confined to a restricted part of the ICR cell. As a result, concepts such as phase-cycles cannot be readily transferred from NMR to ICR. There is no analogy in ICR for a distinction of longitudinal and transverse components, as if we neglect so-called ‘magnetron motions’,

the motion of the ions is limited to a plane perpendicular to the applied magnetic field  $B_0$ , so that one cannot make a distinction between transverse and longitudinal components.

In the now widely accepted parlance of 2D NMR, the evolution interval  $t_1 = n_1 \Delta t_1$  is incremented in  $N_1$  steps with  $n_1 = 0, 1, 2, \dots, (N_1-1)$ , where the increment  $\Delta t_1$  determines the spectral width  $\Delta \nu_1 = 1/\Delta t_1$  in the  $F_1$  domain, also known as  $\nu_1$  or  $\omega_1$  domain. The maximum duration  $t_1^{\max} = (N_1-1) \Delta t_1$  determines the digital resolution  $\delta \nu_1 = 1/t_1^{\max} = \Delta \nu_1/(N_1-1)$  in the  $F_1$  domain. Likewise, the signal is observed in the detection interval  $t_2$  by taking  $N_2$  samples at intervals  $\Delta t_2$  that determine the spectral width  $\Delta \nu_2 = 1/\Delta t_2$  in the  $F_2$  domain, also known as  $\nu_2$  or  $\omega_2$  domain. The duration  $t_2^{\max} = (N_2-1)\Delta t_2$  determines the digital resolution  $\delta \nu_2 = 1/t_2^{\max} = \Delta \nu_2/(N_2-1)$  in this domain. The same technique is applied for obtaining 2D FT-ICR spectra which will be discussed in detail in the next section.

To what extent coherently resonating ions in ICR can be expected to behave like transverse magnetization in NMR still remains a question of debate. And this work attempts a step forward towards understanding the behaviour of single ions with simple monochromatic pulses, neglecting the complexities of space charges and magnetron motions.

### **3.2 2D FT-ICR pulse scheme**

The 2D FT-ICR allows one to map correlations between precursor and fragment ions without ion isolation and without any a-priori information about the sample, thus making it a sample-independent technique.

The conventional 2D spectrum can be represented by a contour plot of intensities as a function of two frequencies ( $\omega_1$  and  $\omega_2$ ) which are obtained by the Fourier transformation of the data recorded as a function of two time variables ( $t_1$  and  $t_2$ ). The position of each peak is specified by two co-ordinates. By convention, the spectrum is arranged so that  $\omega_1$ , which represents the evolution in the indirect dimension, is plotted along the vertical axis, while the evolution in the direct dimension  $\omega_2$  is along the horizontal axis. The general scheme for obtaining such a spectrum for FT-ICR MS is given in Figure 3.2(A). The preparation time consists of encoding period ( $t_1$ ), sandwiched between excitation ( $T_1$ ) and encoding ( $T_2$ ) pulses. In an ICR cell, we wish to monitor the conversion of a precursor ion  $I^k$  into a fragment ion  $I^l$ .

Usually this comes about through fragmentation that may be induced by an electron beam like electron capture dissociation (ECD)<sup>22</sup> and electron transfer dissociation (ETD),<sup>23</sup> by infrared light like infrared multiphoton dissociation (IRMPD)<sup>24</sup> and blackbody infrared radiative dissociation (BIRD),<sup>25</sup> or by collisions with neutral molecules like collision induced dissociation (CID)<sup>26</sup> during the fragmentation period  $\tau_m$ , similar to the mixing time of NMR. After this period, there follows an excitation pulse ( $T_3$ ) which brings the ions to the periphery of the ICR cell, where they are detected during the detection period ( $t_2$ ).

The encoding period  $t_1$  is sequentially incremented and the data is recorded like free induction decay (FID) as a function of  $t_2$  for each value of  $t_1$ . The usual 2D spectrum can be denoted as in Figure 3.2. (B). In ICR, the conversion of a fraction  $f_{kl}$  of precursor ions  $I^k$  into fragment ions  $I^l$  in the fragmentation period (mixing interval)  $\tau_m$  leads to a cross-peak at coordinates ( $\omega_1 = \Omega^k$ ,  $\omega_2 = \Omega^l$ ), with a cross-peak amplitude  $f_{kl}$ . Fragmentation of this

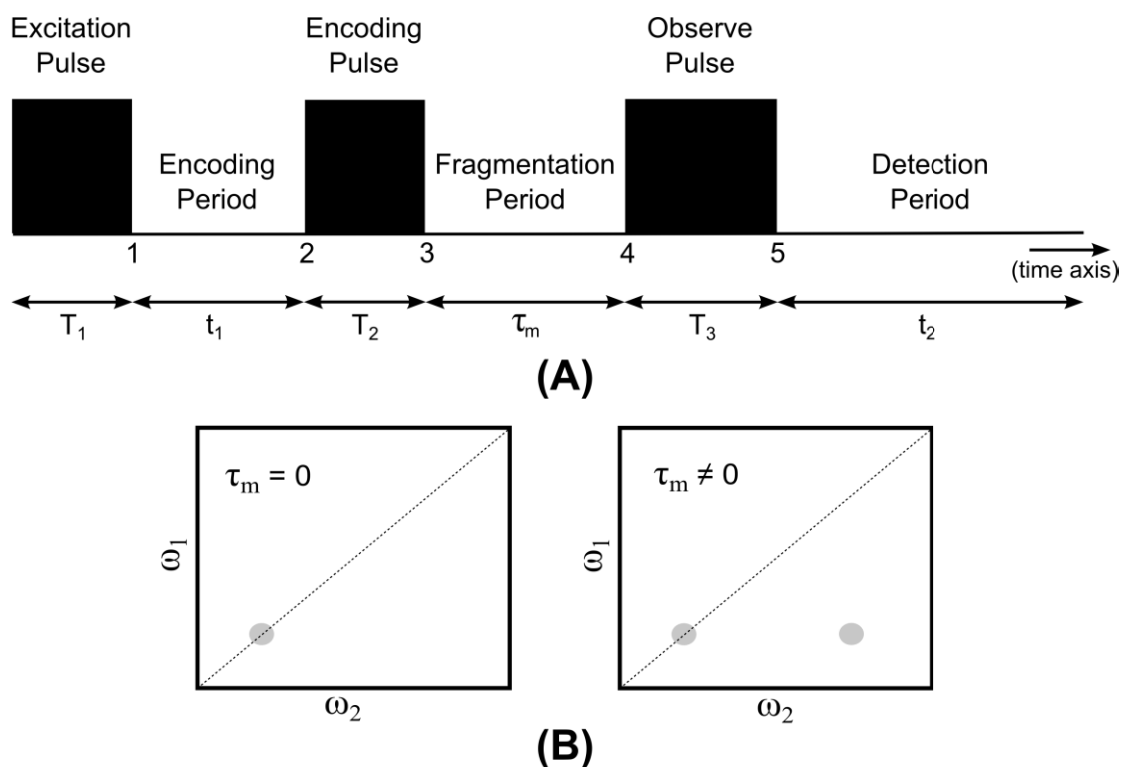


**Figure 3.2.** (A) The time axis is labelled 1, 2, etc. to distinguish the start and end of various intervals. The notations are similar to the conventions of NMR, i.e.:  $\beta - t_1 - \beta' - \tau_m - \beta'' - t_2$ , but with pulses of length  $T_1$ ,  $T_2$  and  $T_3$  rather than flip angles  $\beta$ ,  $\beta'$  and  $\beta''$ , and can thus be written  $T_1 - t_1 - T_2 - \tau_m - T_3 - t_2$  for 2D FT-ICR. (B) The left part indicates a 2D spectrum for a vanishingly short fragmentation period  $T = 0$ . The signal evolves with the same frequency for both dimensions,  $\omega_1 = \Omega^k$ ,  $\omega_2 = \Omega^k$ . For the right side, it has been assumed that some of the ion breaks up into fragments during the fragmentation period  $T$ . Some of these fragments appear at  $\omega_1 = \Omega^k$ ,  $\omega_2 = \Omega^l$ .

precursor ion  $I^k$  into a daughter ion  $I^l$  leads to a change in mass from  $m_k$  to  $m_l$  and/or to a change in charge from  $q_k$  to  $q_l$ , and hence to a jump in the ICR frequency as  $\omega_l > \omega_k$  (when ion dissociates) or  $\omega_l < \omega_k$  (when ion form adducts). This frequency jump can be characterized by 2D ICR. As the information about a precursor ion is encoded in the resulting

fragment ion, the basic mechanism underlying the complete 2D dynamics can be understood by just looking at the preparatory or encoding sequence ( $T_1-t_1-T_2$ ) of the scheme for an arbitrary precursor ion.

### 3.3 Equations of motion

In an ICR cell, the ions are subjected to a static magnetic field  $\vec{B}_0 = (0, 0, B)$  and to a perpendicular electric field  $\vec{E}(t) = (E_x, 0, 0)$ , which determines the motion of a precursor ion  $I^k$  by solving the Lorentz equation:

$$m_k \frac{d\vec{v}_k}{dt} = q_k \vec{E} + q_k (\vec{v}_k \times \vec{B}) \quad (3.1)$$

A precursor ion  $I^k$  (or another charged particle like an electron or proton) of mass  $m_k$  and charge  $q_k$  moves on a circular trajectory in a plane perpendicular to the magnetic field  $\vec{B}$ . If there is no applied electric field, the cyclotron frequency is by equation 3.2.

$$\omega_k = \frac{q_k B}{m_k} \quad (3.2)$$

To simplify the calculations, we neglected ‘magnetron’ motions along the z-axis, and assumed that the magnetic field is homogeneous across the ICR cell. We also neglected ion-ion Coulomb repulsions, although Chen and Commisarow<sup>27</sup> have shown how such effects lead to a dispersion of ion clouds, by affecting both the phases and the radii of individual ions.

The applied electric field for the FTMS is usually in the form of *rf* chirp pulses. Here, we have chosen an oscillating *rf* pulse which is ‘on resonance’, i.e., with the same frequency  $\omega_k$

as that of the cyclotron motion of the parent ion  $I^k$  during a pulse of length  $T$  (periods 0-1 and 2-3 in Figure 3.2) for the excitation.

$$E_x = \begin{cases} E_0 \sin(\omega_k t), & 0 < t < T_1 \\ 0, & T_1 < t < T_1 + t_1 \\ E_0 \sin(\omega_k t + \varphi), & T_1 + t_1 < t < T_1 + t_1 + T_2 \\ 0, & T_1 + t_1 + T_2 < t < T_1 + t_1 + T_2 + t_m \end{cases} \quad (3.3)$$

Adding a phase to the second pulse is equivalent to the ion acquiring a non-vanishing phase before the start of the second pulse for different encoding periods. The components  $v_{kx}$  and  $v_{ky}$  of the parent ion  $I^k$ , and hence its trajectory, are determined by solving equation 3.1, and substituting equation 3.2 and 3.3:

$$\frac{dv_{kx}}{dt} = \frac{q_k E_x}{m_k} + \omega_k v_{ky} \quad (3.4a)$$

$$\frac{dv_{ky}}{dt} = -\omega_k v_{kx} \quad (3.4b)$$

Taking  $E_x = E_0 \sin(\omega_k t + \varphi)$ , and solving the equation 3.4, we get:

$$v_{kx} = v_{kx0} \cos(\omega_k t) + v_{ky0} \sin(\omega_k t) + \frac{E_0 q_k t \sin(\phi) \cos(\omega_k t)}{2m_k} + \frac{E_0 q_k t \cos(\phi) \sin(\omega_k t)}{2m_k} + \frac{E_0 q_k \sin(\phi) \sin(\omega_k t)}{2m_k \omega_k} \quad (3.5a)$$

$$v_{ky} = v_{ky0} \cos(\omega_k t) - v_{kx0} \sin(\omega_k t) + \frac{E_0 q_k t \cos(\phi + \omega_k t)}{2m_k} - \frac{E_0 q_k \cos(\phi) \sin(\omega_k t)}{2m_k \omega_k} \quad (3.5b)$$

For 2D FT-ICR, we optimized the conditions for very brief pulses of the order of few  $\mu\text{s}$ . In such cases the ion fails to execute even a single complete orbit of its trajectory of an Archimedes spiral during the excitation pulse. Therefore, none of the terms of the equation 3.5 can be neglected. In the following sections, analytical solutions are obtained for the velocity components and the position coordinates for an ion up to the fragmentation period. The solution is divided into four parts: the excitation pulse period, the encoding period, the encoding pulse period and the fragmentation period.

### 3.3.1 Excitation pulse period

The ion velocity at the end of the pulse ( $t = T$ ), period 0-1 in the pulse scheme of Figure 3.2, is obtained by solving equation 3.5 for the initial condition that  $v_{kx0} = 0$  and  $v_{ky0} = 0$ . We assume that all ions are located in the centre of the ICR cell at the start of the experiment and we are not considering any ion magnetron movement for these simple trajectory calculations. The ion is assumed to be in phase with the monochromatic pulse for this period, hence  $\varphi=0$ . The corresponding x and y coordinates with respect to the centre of the ICR cell are obtained by integrating their respective velocity components.

$$v_{kx1} = \frac{E_0 q_k T \sin(\omega_k T)}{2m_k} \quad (3.6a)$$

$$x_{k1} = \frac{E_0 q_k \{\sin(\omega_k T) - \omega_k T \cos(\omega_k T)\}}{2m_k \omega_k^2} \quad (3.6b)$$

$$v_{ky1} = \frac{E_0 q_k T \cos(\omega_k T)}{2m_k} - \frac{E_0 q_k \sin(\omega_k T)}{2m_k \omega_k^2} \quad (3.7a)$$

$$y_{k1} = \frac{E_0 q_k \{2\cos(\omega_k T) + \omega_k T \sin(\omega_k T) - 2\}}{2m_k \omega_k^2} \quad (3.7b)$$

### 3.3.2 Encoding period

During the encoding period,  $E_x = 0$ , and the initial velocities at the start of this period are equal to the velocities at the end of the excitation period.

$$v_{kx2} = \frac{E_0 q_k}{4m_k \omega_k} \{ \cos[\omega_k (T + t_1)] - \cos[\omega_k (T - t_1)] + 2T\omega_k \sin[\omega_k (T + t_1)] \} \quad (3.8a)$$

$$x_{k2} = \frac{E_0 q_k}{2m_k \omega_k^2} \{ \cos(\omega_k t_1) \sin(\omega_k T) - \omega_k T \cos[\omega_k (T + t_1)] \} \quad (3.8b)$$

$$v_{ky2} = \frac{E_0 q_k}{2m_k \omega_k} \{ \omega_k T \cos(\omega_k T) \cos(\omega_k t_1) - \sin(\omega_k T) [\cos(\omega_k t_1) + \omega_k T \sin(\omega_k t_1)] \} \quad (3.9a)$$

$$y_{k2} = \frac{E_0 q_k}{4m_k \omega_k^2} \{ \cos[\omega_k (T + t_1)] - \cos[\omega_k (T - t_1)] + 4\cos(\omega_k T) - 4 + 2T\omega_k \sin[\omega_k (T + t_1)] \} \quad (3.9b)$$

### 3.3.3 Encoding pulse period

Trajectories are calculated similar to the case of the first pulse wherein the initial velocities are the same as the final velocities obtained from equations 3.8a and 3.9a. The two first

pulses of the preparatory period have equal pulse durations and amplitudes, so we also take  $T_1=T_2$ . Inserting these values into equation 3.5, we obtain:

$$v_{kx3} = \frac{E_0 q_k}{4m_k \omega_k} \{ \cos[\omega_k(2T + t_1)] - \cos(\omega_k t_1) + 2T\omega_k \cos(\omega_k T) \sin(\phi) + (T\omega_k \cos(\phi) + \sin(\phi))2 \sin(\omega_k T) + 2T\omega_k \sin[\omega_k(2T + t_1)] \} \quad (3.10a)$$

$$x_{k3} = \frac{E_0 q_k}{4m_k \omega_k^2} \{ 2 \cos(\phi) \sin(\omega_k T) - \sin(\omega_k t_1) + \sin[\omega_k(2T + t_1)] - 2\omega_k T \{ \cos[\omega_k(2T + t_1)] - \cos(\phi + \omega_k T) \} \} \quad (3.10b)$$

$$v_{ky3} = \frac{E_0 q_k}{4m_k \omega_k} \{ 2\omega_k T \{ \cos(\phi + \omega_k T) + \cos[\omega_k(2T + t_1)] \} - 2 \cos(\phi) \sin(\omega_k T) + \sin(\omega_k t_1) - \sin[\omega_k(2T + t_1)] \} \quad (3.11a)$$

$$y_{k3} = \frac{E_0 q_k}{4m_k \omega_k^2} \{ \cos[\omega_k(2T + t_1)] - \cos(\omega_k t_1) + 4 \cos(\omega_k T) - 4 \cos(\phi) + \cos(\phi - \omega_k T) + 3 \cos(\phi + \omega_k T) + 2T\omega_k \{ \sin[\omega_k(T + t_1)] + \sin(\phi + \omega_k T) \} - 4 \} \quad (3.11b)$$

The distance of the ion from the centre of the cell at the end of the preparatory period is given by:

$$r = (x_{k3}^2 + y_{k3}^2)^{1/2} \quad (3.12)$$

which is a sine and cosine function with respect to both the pulse duration ( $T$ ) and the encoding period ( $t_1$ ). Only in the case when the pulse duration  $T_{pulse}$  divided by the ion's period  $T_{Ion}$  is larger than 10, can the last term of equation 3.5b be neglected, thereby giving the distance from the centre of the cell as in the formula given by Guan and Jones.<sup>17</sup>

$$r = r_0 \{2(1 + \cos(\omega(T - t_1)))\}^{1/2} \quad (3.13)$$

### 3.3.4 Fragmentation period

The trajectories can be calculated similar to the case of the encoding period:

$$v_{kx4} = \frac{E_0 q_k}{4m_k \omega_k} \{ \cos(\omega_k(2T + t_1 + t_m)) - \cos(\omega_k(t_1 + t_m)) - \cos(\phi + \omega_k T - \omega_k t_m) \\ + \cos(\phi - \omega_k(T + t_m)) + 2T\omega_k \sin(\omega_k(2T + t_1 + t_m)) + \sin(\phi + (T + t_m)\omega_k) \} \quad (3.14a)$$

$$x_{k4} = \frac{E_0 q_k}{4m_k \omega_k^2} \{ \sin(\phi + \omega_k(T - t_m)) + \sin(\phi - \omega_k(T + t_m)) - \sin(\omega_k(t_1 + t_m)) \\ + \sin(\omega_k(2T + t_1 + t_m)) - 2\omega_k T \{ \cos(\omega_k(2T + t_1 + t_m)) + \cos(\phi + \omega_k(T + t_m)) \} \} \quad (3.14b)$$

$$v_{ky4} = \frac{E_0 q_k}{4m_k \omega_k} \{ 2\omega_k T \cos(\phi + \omega_k(T + t_m)) + 2\omega_k T \cos(\omega_k(2T + t_1 + t_m)) + \sin(\omega_k(t_1 + t_m)) \\ - \sin(\omega_k(2T + t_1 + t_m)) - \sin(\phi + \omega_k(T - t_m)) + \sin(\phi - \omega_k(T + t_m)) \} \quad (3.15a)$$

$$y_{k4} = \frac{E_0 q_k}{4m_k \omega_k^2} \{ -4\cos(\phi) + 4\cos(\omega_k T) - \cos(\omega_k(t_1 + t_m)) + \cos(\omega_k(2T + t_1 + t_m)) + 4\cos(\phi + \omega_k T) - \\ \cos(\phi + \omega_k(T - t_m)) + \cos(\phi - \omega_k(T + t_m)) - 4 + 2\omega_k T \sin(\omega_k(2T + t_1 + t_m)) + 2\omega_k T \sin(\phi + \omega_k(T + t_m)) \} \quad (3.15b)$$

## 3.4 Trajectory mapping

The trajectory of the ions in every part of the preparatory period can be calculated by plotting the  $x$  and  $y$  coordinates from the equations calculated above. For mapping the trajectories we

varied the phase  $\varphi$  of the second pulse from 0 to  $\pi$ . We mapped the trajectory for the following four cases.

### 3.4.1 Case I: $\omega_k t_1 = 2n\pi$ and $\omega_k T = 2\pi$

In this case, the lengths of the first two pulses ( $T_1 = T_2 = T$ ) are chosen to match the period of precession of a parent ion  $I^k$  with a frequency  $\omega_k$ , so that  $\omega_k T = 2\pi$ . We shall refer to this case as a ‘pulse of matched duration’, or a ‘matched pulse’ for short. We shall assume that the evolution interval  $t_1$  has a duration that also matches the period of precession of the ion, so that  $\omega_k t_1 = 2\pi n$ , where  $n$  is an integer. In such a case, the ion travels through an integer number of complete circles about the centre of the cell in the interval  $t_1$ . The trajectories are shown in Figure 3.3. Here, the ion’s trajectory is centred in the middle of the ICR cell. During the first pulse, the ion’s radius increases and then it evolves on a circle during the encoding period. We changed the phase of the second pulse from 0 to  $180^\circ$ . The distance of the ion from the centre is maximum after the evolution period if the ion is in-phase with respect to the second pulse and decreases to zero, i.e., the ion comes back to the centre of the ICR cell, when it is completely out-of-phase with respect to the second pulse.

### 3.4.2 Case II: $\omega_k t_1 < 2\pi k$ and $\omega_k T = 2\pi$

In this case, the ion does not travel through an integer number of complete circles about the centre of the cell in the interval  $t_1$ . The trajectory is indeed centred because it depends on the duration of the pulses. But for a phase difference of  $\pi$ , rather than returning to the centre of the cell, the ion’s radius increases and it transcribes a larger circle (Figure 3.4).

### 3.4.3 Case III: $\omega_k t_1 = 2n\pi$ and $\omega_k T < 2\pi$

Here, pulses shorter than a single period of  $2\pi/T\omega_k$  are considered. The encoding period is taken to be such that ion executes multiple circles; perpendicular to the direction of the velocity at the instant the *rf* electric field is removed. The trajectories are plotted in Figure 3.5. As can be seen from the figure, due to a non-matched pulse, the ion's trajectory gets off-centre and is pulled in the direction of the applied electric field. After the preparatory period, depending upon the phase of the second pulse and the pulse duration, the ion orbits in contracting/enlarging circles with the centre oscillating about the true centre of the cell as per equation 3.16 as plotted in Figure 3.6.

$$shift = \frac{E_0 q_k}{m_k \omega_k^2} \{1 + \cos(\phi) - \cos(\omega_k T) - \cos(\phi + \omega_k T)\} \hat{j} \quad (3.16)$$

The centre of the ion's trajectory coincides with the centre of the cell if the phase difference between the ion and the second pulse is  $\pi$ .

### 3.4.4 Case IV: $\omega_k t_1 < 2\pi k$ and $\omega_k T < 2\pi$

This is the general case of non-matched pulse and a non-matched encoding period. The ion's trajectory after the first pulse becomes off-centred as shown in Figure 3.7. The shift of the centre follows a similar trend as for case III because the shift is independent of  $t_1$ .

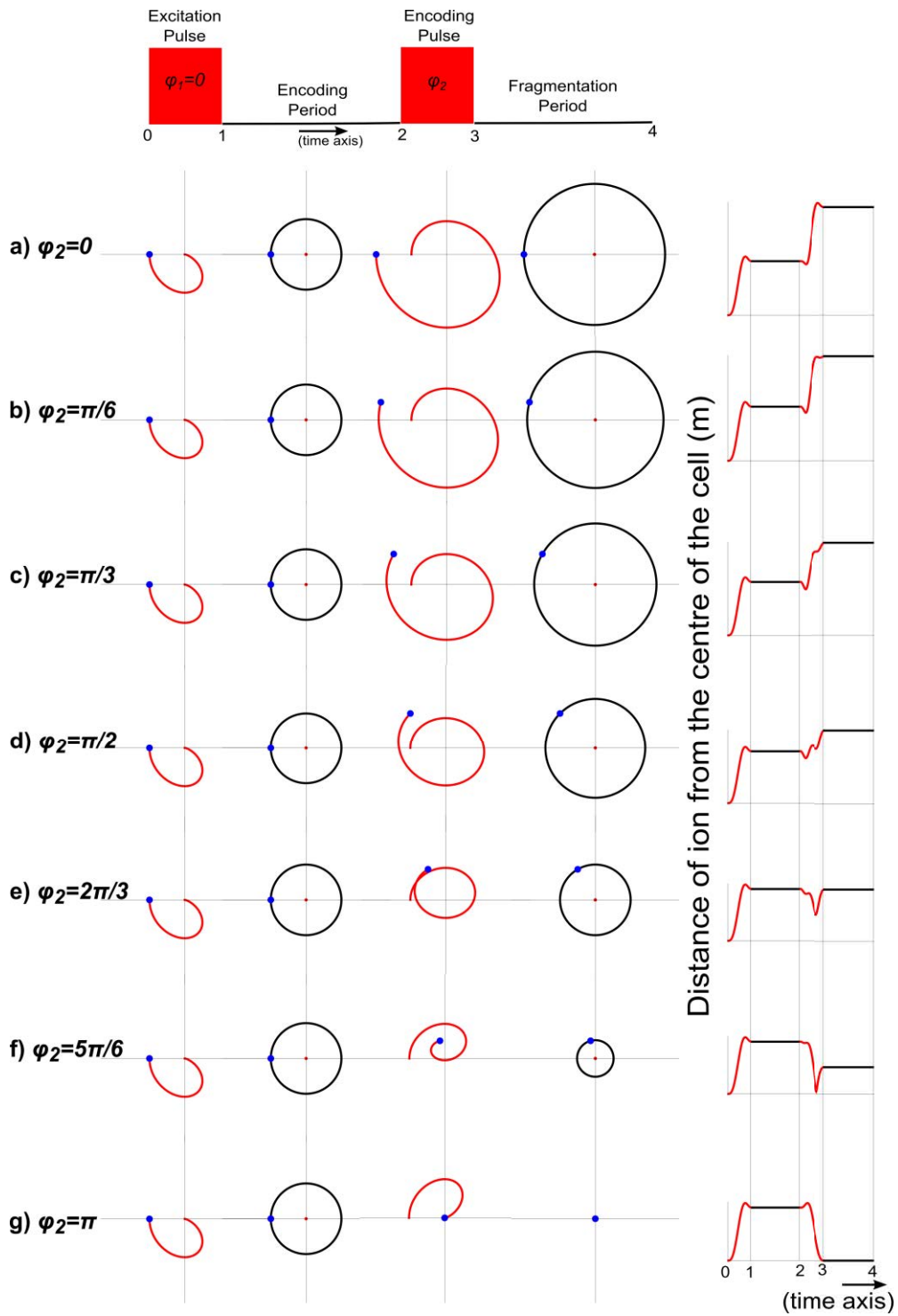


**Figure 3.3.** Representation of Case I of a matched pulse and matched encoding period  $t_1$ . Blue bullets represent the ion, red bullets the centre of the trajectory during the encoding period and black bullets the centre of the trajectory during the fragmentation period  $T$ .

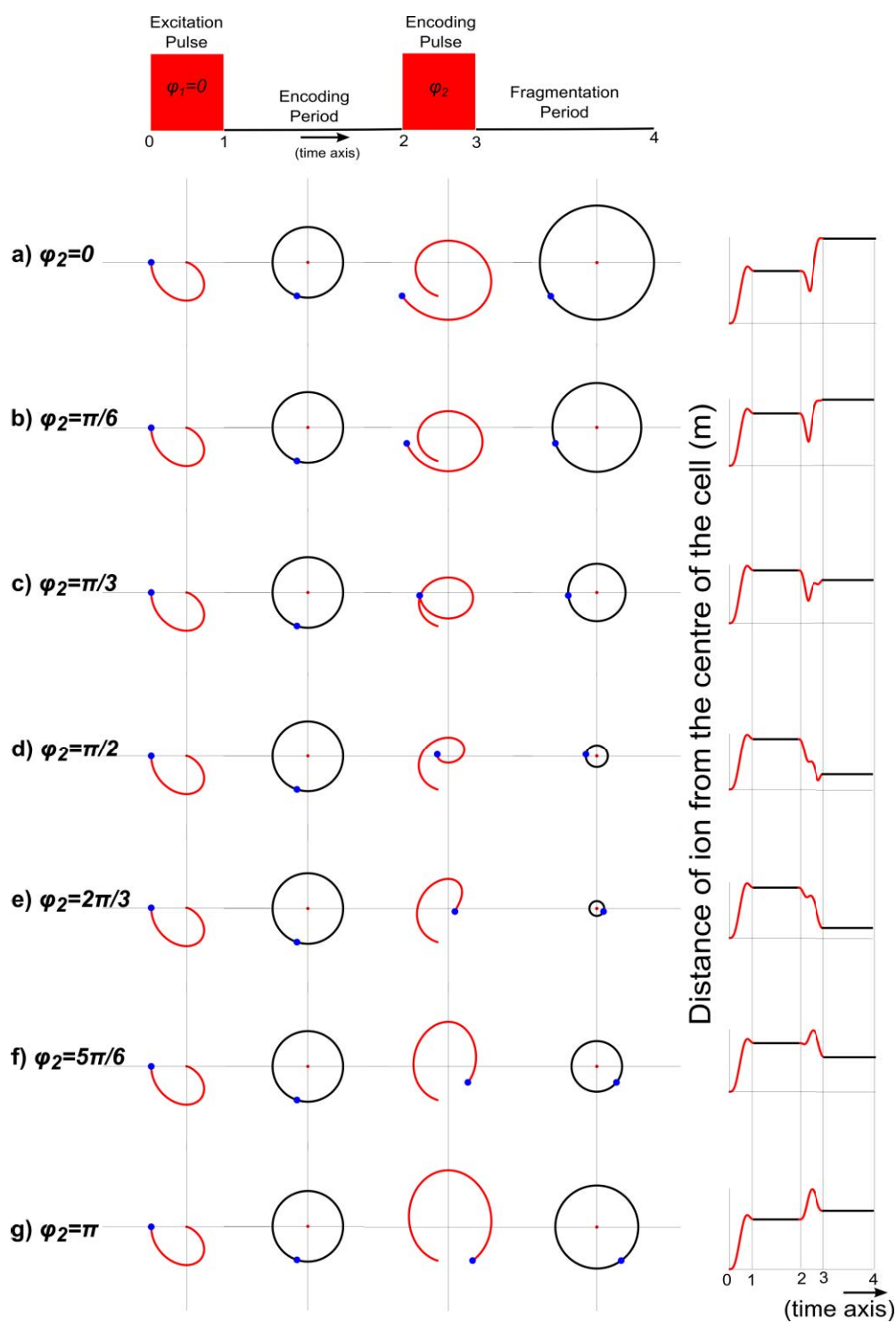


**Figure 3.4.** Representation of Case II. Blue bullets represent the ion. The centre of the trajectory does not shift if the encoding period  $t_1$  is not matched to the frequency but does affect the trajectory during the second pulse.

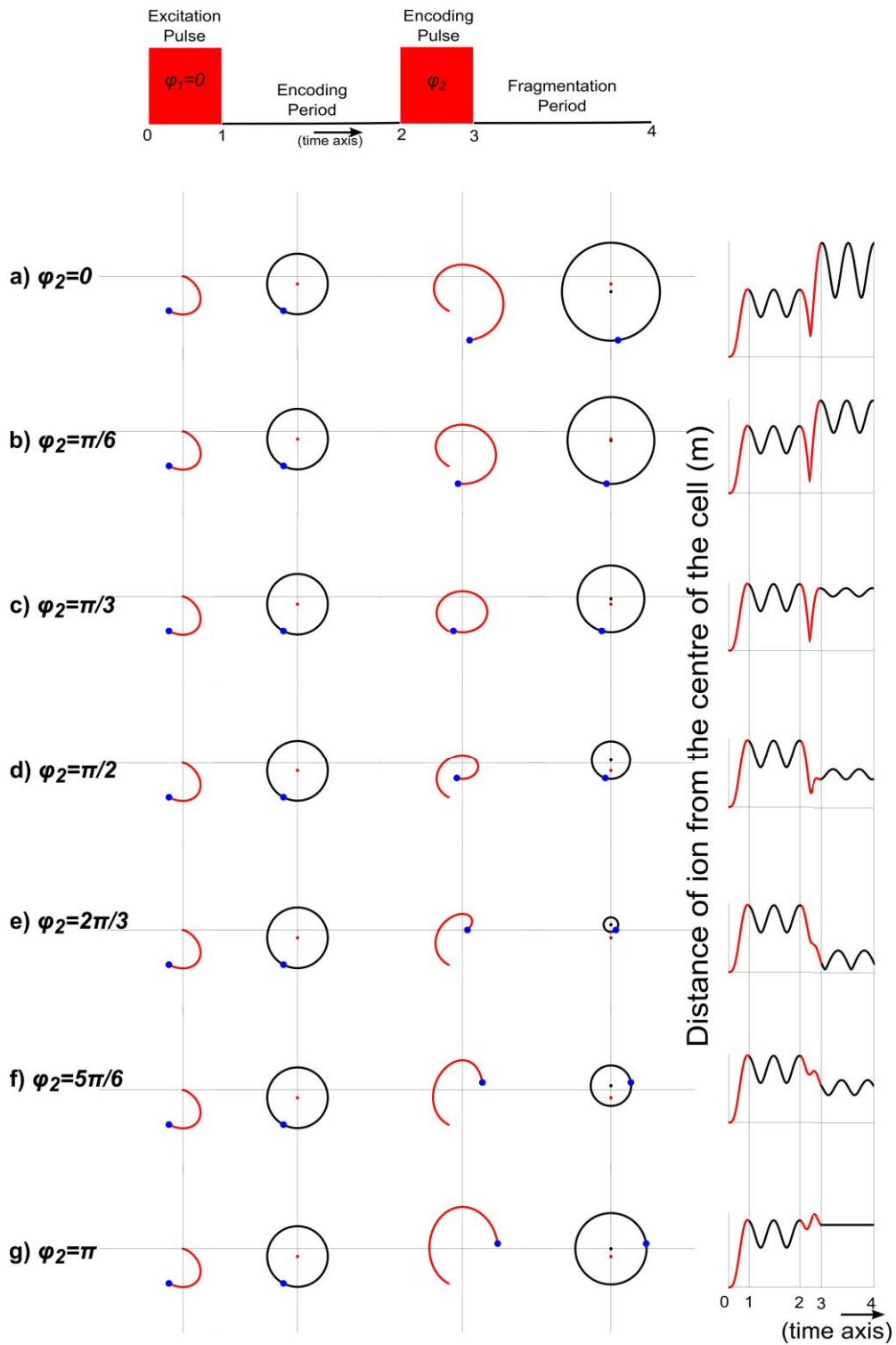


**Figure 3.5.** Trajectories for  $\omega_k t_1 = 2\pi k$  and  $\omega_k T < 2\pi$ . Blue bullets represent the ion, red bullets the centre of the trajectory during encoding period  $t_1$  and black bullets the centre of the trajectory during the fragmentation period  $T$ .

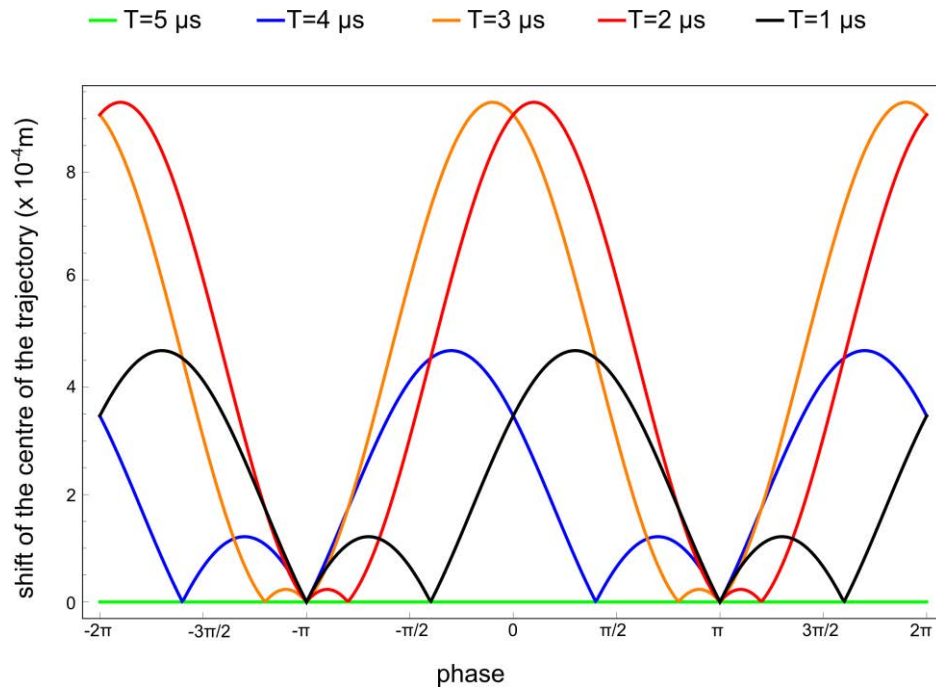


**Figure 3.6.** Variation of the shift with respect to the centre of the cell as a function of the phase of the second pulse for different pulse durations.

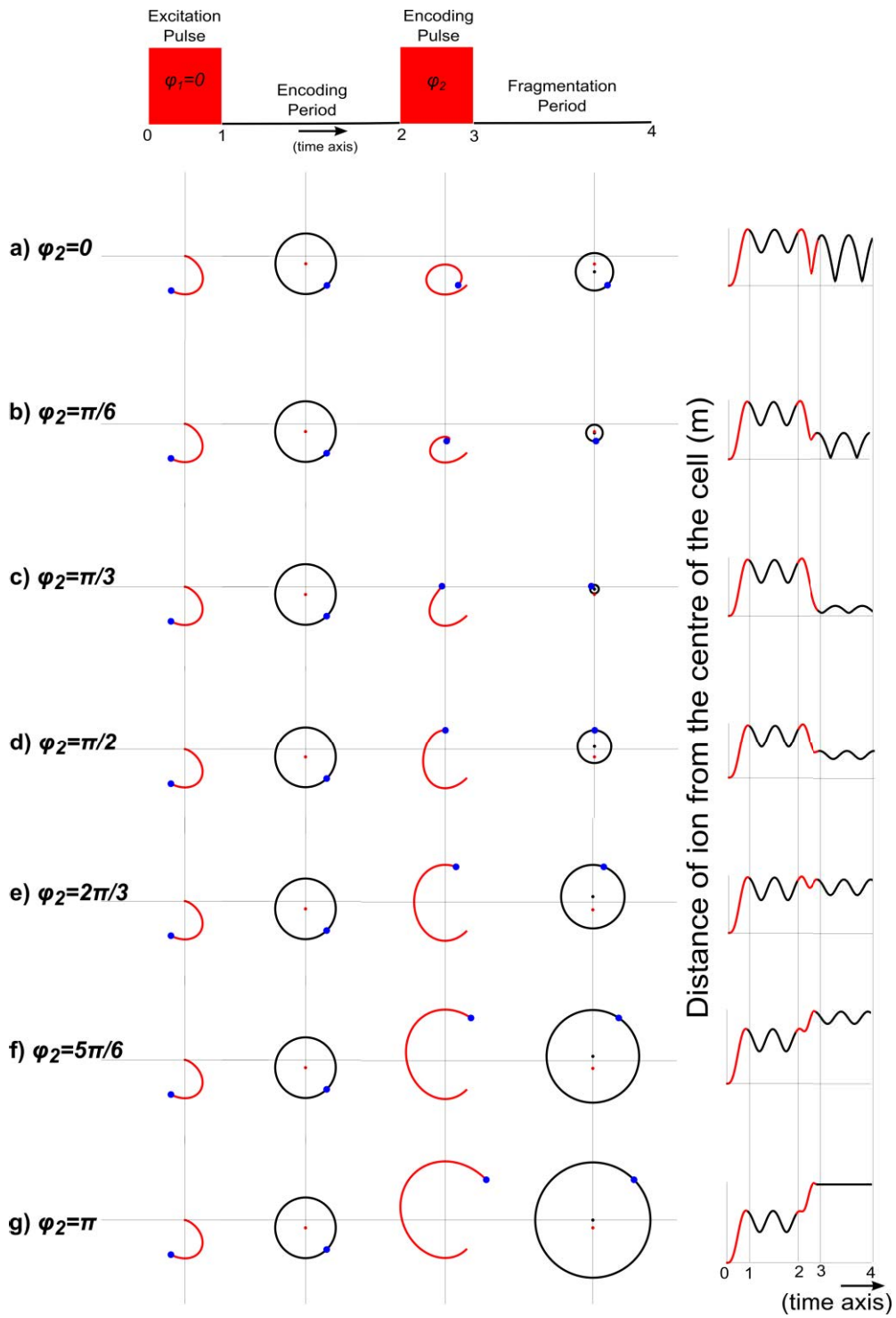


**Figure 3.7.** Trajectories for  $\omega_k t_1 < 2\pi k$  and  $\omega_k T < 2\pi$ . Blue bullets represent the ion, red bullets the centre of the trajectory during the encoding period and black bullets the centre of the trajectory during the fragmentation period.

Our simulations show ion trajectories after the encoding pulses by solving the equations of ion movements in an ideal Penning cell using Mathematica for simple monochromatic pulses. Such trajectories help in developing a better understanding of the availability of ions for efficient fragmentation by cell-centred techniques like IRMPD. As can be seen from the Figure 3.8, for the Case I of matched pulses and matched encoding period, when the phase difference is an odd multiple of  $\pi$  (i.e. the second pulse is anti-phase with the ion motion), the ions are de-excited back to the centre of the ICR cell by the second pulse. For Case II and III the minimum distance of the ion from the centre of the cell happens to occur when the phase of the second pulse is equal to an odd multiple of  $2\pi/3$ . For case IV of short non-matched pulses and a non-matched encoding period, the minimum is shifted further to the right at odd integrals of  $\pi/2$ . The displacements of ICR orbit centres for Cases III and IV are very similar to the ion-lock events which were proposed by Chen *et al.*<sup>28,29</sup> Such an idea can be used to develop 2D ion lock experiments wherein the reluctance of the ions to fragment can be manipulated for the advantage of selectively sequestering them and observing them gradually with other combinations of pulses. This we plan to probe in the near future.

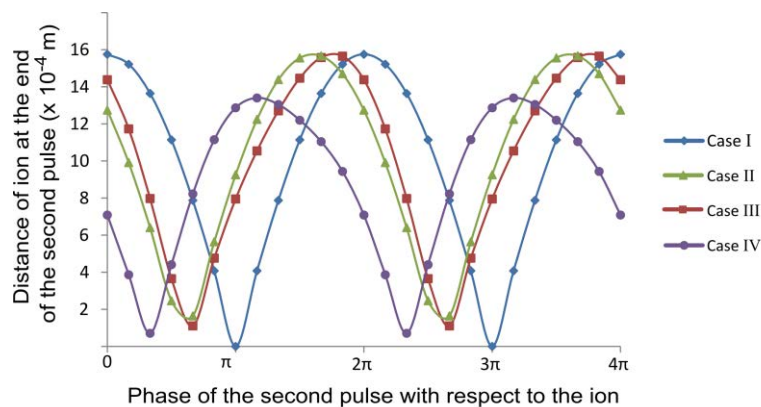


**Figure 3.8.** Distance of the ion from the centre of the cell versus the phase of the second pulse for the four cases discussed before.

### 3.5 Harmonics in 2D spectra

As the modulation of the ionic radii is non-sinusoidal, 2D FT-ICR mass spectra is overwhelmed with intense harmonics in the vertical dimension, both for precursor and fragment ion peaks which leads to complications of 2D mass spectra by reducing the signal amplitude and the readability of the spectra.<sup>17</sup> In a recent work published by our group, precursor and fragment ions were excited to smaller radii than in routine MS or MS/MS conditions by using pulses of smaller duration for the preparatory period. In the work it was experimentally shown that harmonics decrease for smaller pulses.<sup>18</sup> Herein, we plot the patterns of the harmonics for pulses in the range of 1-5  $\mu\text{s}$  (i.e., 0.05-0.25 times the ion's period) for ions excited by monochromatic pulses as shown in Figure 3.9. For such a simplified case, where both pulses of the preparatory period are identical, we observe that in-between the quadrants of ion's period, the distance variation of the ion after the preparatory period versus encoding period tends to become sinusoidal and the intensity of the harmonics therefore decreases.

Though, pulses which do not have durations equal to integrals numbers of one-quarter of an ion's period cause the trajectories to be off-centred, but as shown in Figure 3.9, they can contribute to decreasing the harmonics in the spectra. The variation of distance with the encoding period goes from non-sinusoidal to sinusoidal and back to non-sinusoidal in one quadrant in case of pulses smaller than one period of the ion's frequency.

To probe the relationship of the phase of the ion during the encoding period with respect to the phase of the encoding pulse, we changed the phase of the second pulse by  $\varphi$ . Ions starting in the centre of the ICR cell are sensitive to the product of the pulse amplitude and the duration. Therefore, for all simulations of harmonics, we kept this product to be constant (equal to the default operating condition of the spectrometer:  $100 V_{p-p}$  for 20  $\mu\text{s}$ ).

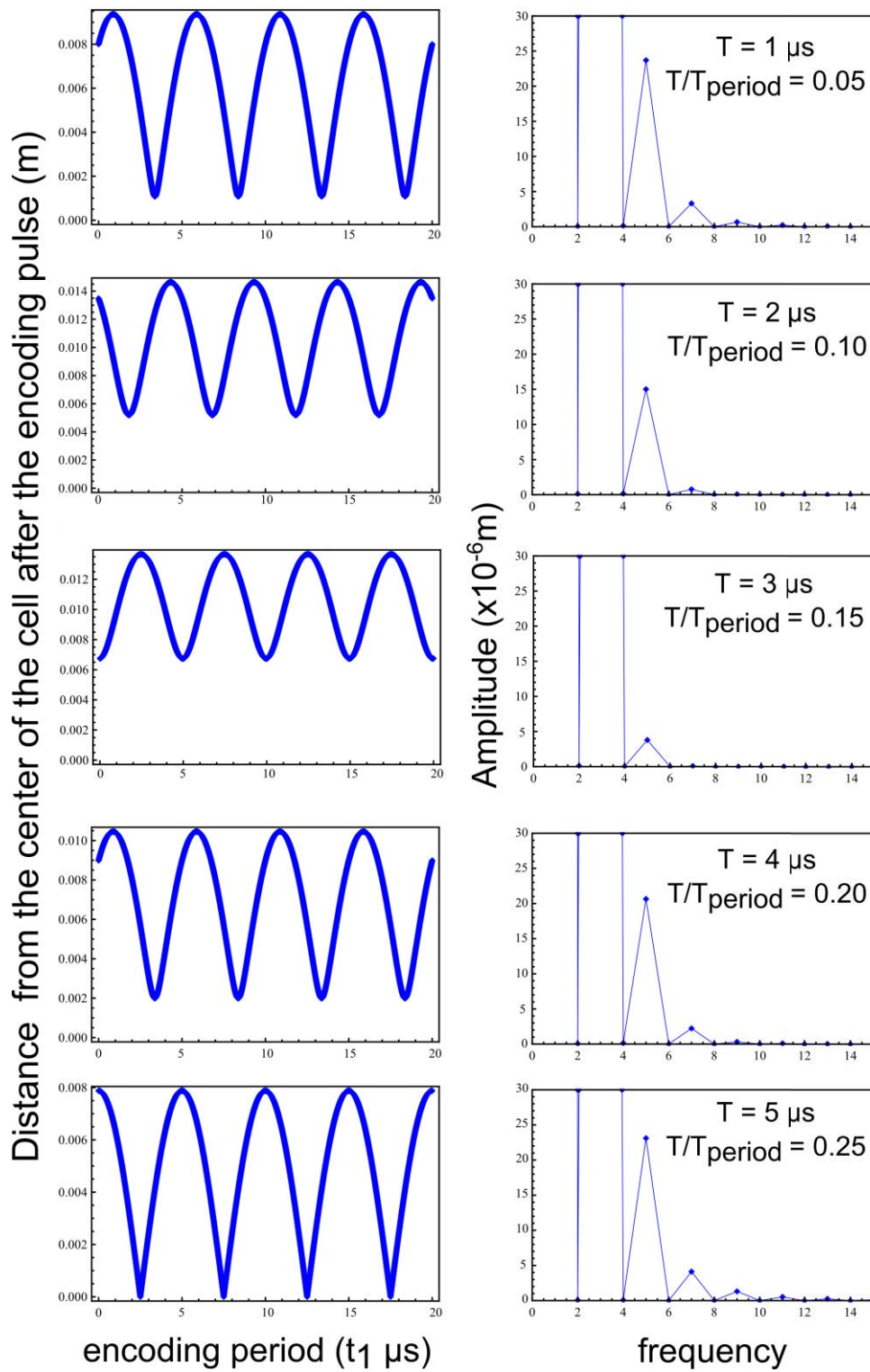


**Figure 3.9.** The left figure indicates the variation of distance of the ion from the centre after the encoding pulse as a function of the encoding period and the right figure shows the respective Fourier transform profiles.

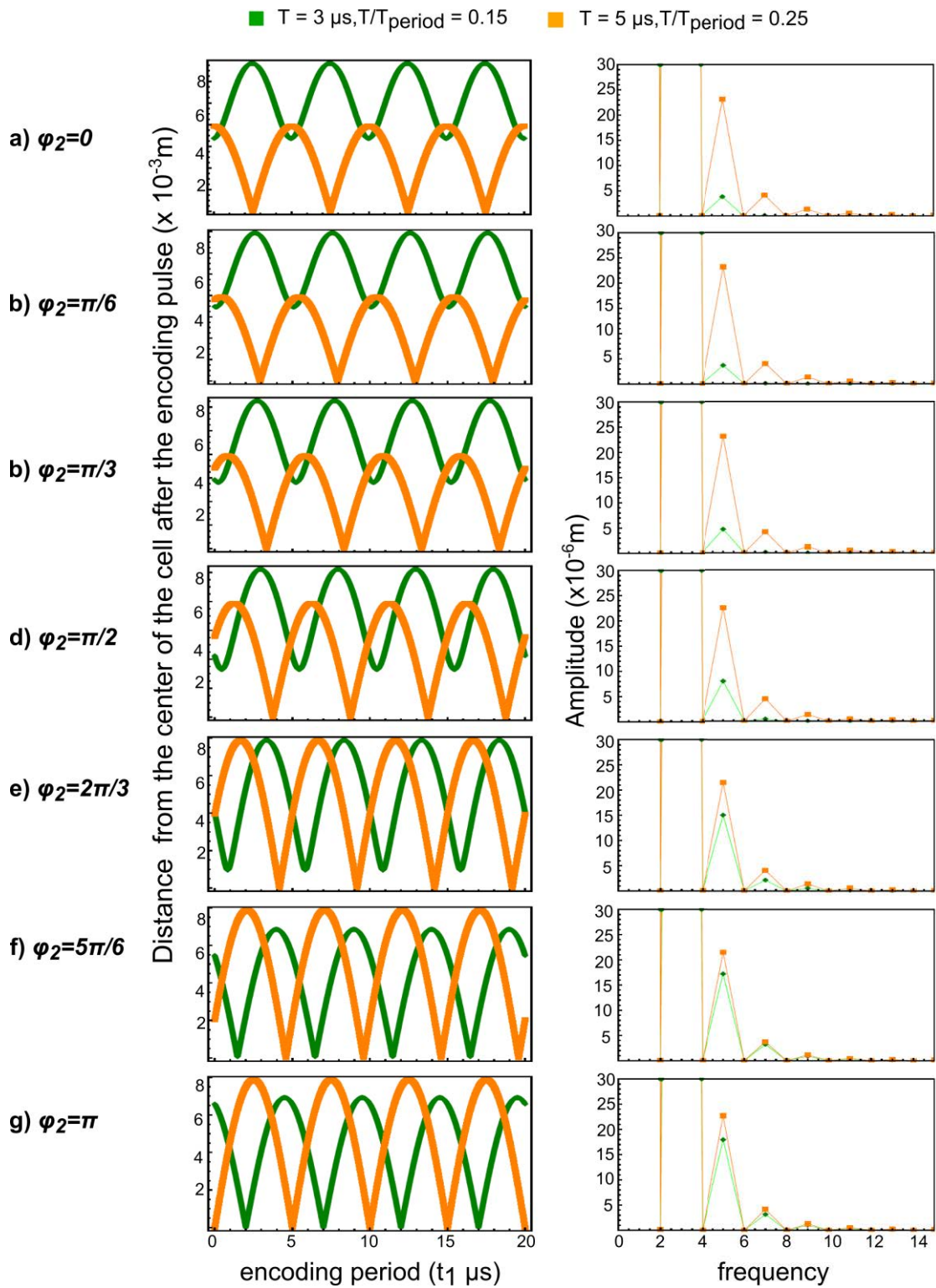


**Figure 3.10.** The left figure indicates the variation of distance of the ion after the encoding pulse as a function of the encoding period and the right figure shows the respective Fourier transform profiles.

The duration of the pulses are taken for two cases: matched pulses (5  $\mu\text{s}$ ) and non-matched pulses (3  $\mu\text{s}$ ), as shown in Figure 3.10. As we have seen before in Figure 3.5, that non-matched pulses for a 0 phase is off-centred and it becomes centred for a phase change of  $\pi$ . The pattern of the plot of variations of the distance of the ion from the centre with  $t_1$  goes from sinusoidal to non-sinusoidal in the same way. The harmonics are small for sinusoidal patterns and the amplitude of harmonics converges to similar values as for a centred trajectory.

### 3.7 Conclusions and Perspectives

Two-dimensional (2D) Fourier Transform Ion Cyclotron Resonance mass spectrometry pursues similar objectives as MS/MS experiments which are done one ion at a time. 2D FT ICR can examine all possible fragmentation correlations (precursor, fragment and neutral loss spectra) in one experiment. We revisited the original 2D FT-ICR experiment which did not lead to any significant analytical applications until now due to technical limitations. These should currently be much less of a nuisance due to improved FT-ICR instrumentation and computer hardware and software. We sought here to achieve a better understanding of the intricacies of the behaviour of ions during the three-pulse scheme used for two-dimensional ICR. Through our simulations we mapped the ion trajectories for different pulse durations and for different phase relations. We also extended our studies to analyse the contribution of off-axis excitation to harmonics in the 2D spectra.

When optimizing the pulse sequence, we found that the best results were obtained when using the smallest possible duration for each frequency step within the linearly frequency swept “chirp” pulses (0.5  $\mu\text{s}$  versus 20  $\mu\text{s}$  for standard excitation pulses). We initially

believed that the phase difference between the ion and the encoding pulse  $P_2$  varies only with the cyclotron frequency and  $t_1$ , so that if the ion is in-phase with the second pulse  $P_2$ , the ion is propelled onto a higher radius, whereas if the ion is out-of-phase with respect to with  $P_2$ , it is brought back to the centre of the cell.<sup>30</sup> However, this only occurs if the ions are excited during several tens of radio-frequency periods, which is not the case when frequency steps within the chirp pulses are of very short duration. We simulated the ion trajectories during encoding pulses by solving equations of ion movements in an ideal Penning cell. For monochromatic pulses that are on-resonance with the ion's frequency, we observed that during the first pulse the ion gains in kinetic energy, moving in spirals away from the centre. The movement of the ion during the subsequent evolution period  $t_1$  follows an orbit which is off-centre, unless the product of the duration  $T_1$  of the excitation pulse  $P_1$  and the frequency  $\omega$  of the ion is exactly a multiple of  $2\pi$ . Hence, the second pulse  $P_2$ , even when it is perfectly out-of-phase with the ion, fails to bring the ion back exactly to the centre of the cell which is essential for performing fragmentation by the IRMPD technique. We obtained the conditions for which the ion will actually fragment for all durations of pulses and encoding periods. We also showed how the displacement of the ions reduces harmonics and pulses with smaller durations can be a simple way forward with 2D ICR without requiring any sophisticated de-noising techniques.

In the future work we intend to extend the study of ion trajectories and ion behaviour with chirp pulses as the monochromatic pulses and the theory developed on its ground is a preliminary step and moreover on the spectrometers, chirp pulses are employed. We intend to study the effect of harmonics due to the off-axis excitation of the chirp pulses. We will also explore new chirp pulses in contrast to the conventional pulses used on the machine. The conventional chirp pulses are of the types where for every frequency in the chirp the duration

of the frequency step and the intensity are same for the entire range being probed. This provides a uniform excitation profile as the radius of the ion acquired due to the excitation is proportional to the product of intensity and the duration of the pulse. Therefore, during a chirp excitation all ions acquire the same radius but as the phase acquired by the ion depends on the product of the respective ion's frequency with the pulse duration, ions acquire different phases. As seen in this chapter such different phases can lead to all complex variations of ion's position, leading to off-centre excitation. We plan to implement pulses such that the duration of the pulse is inversely and the amplitude of the pulse is directly proportional to the respective frequency as shown in the Figure 3.11.

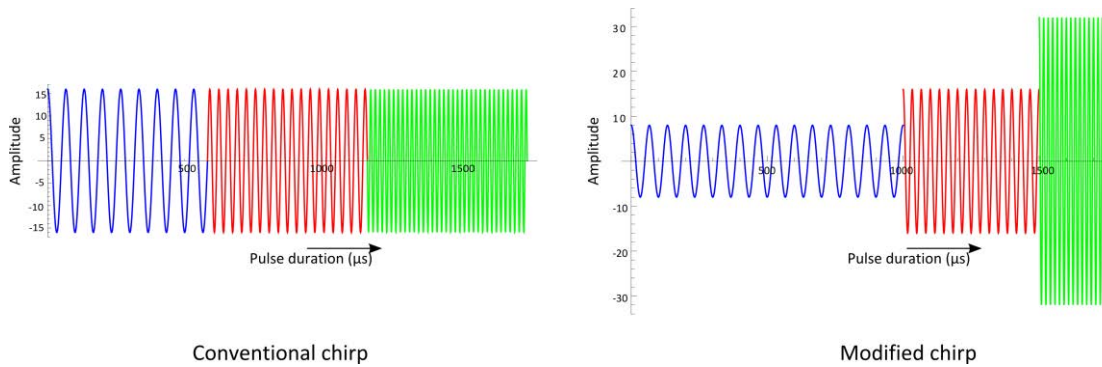


**Figure 3.11.** The left figure is the conventional chirp pulse and the right figure is the modified chirp pulse which provides a constant phase. For explanation here we have taken just three frequencies ( $\omega$ ,  $2\omega$ ,  $4\omega$ ). The total duration of the pulse is  $7t/4$  s, with every frequency for the conventional chirp being of the duration of  $7t/12$  s and for modified chirp of  $t$ ,  $t/2$  and  $t/4$  s respectively. The amplitude for the conventional pulse is taken to be  $2E$  and for the chirp pulse it's taken to be  $E$ ,  $2E$  and  $4E$ . (For this example, we took  $t = 1.75$  ms ,  $E=8$  and  $\omega = 2\pi$  MHz).

This will not only lead to the ion acquiring a constant radius but also a constant phase. Because of this, we will be able to refocus all ions to the exact same point with the second

pulse of an opposite phase, thus overcoming off-centeredness and the distribution of ion to all random phases and locations in the cell.

There exists an ample scope of trying new things for the development of 2D FT-ICR. This work is just a tip of a proverbial iceberg which needs to be comprehended and analysed.

## References

- (1) Noda, I. *J. Am. Chem. Soc.* **1989**, *111*, 8116.
- (2) Gorcester, J.; Freed, J. H. *J. Chem. Phys.* **1988**, *88*, 4678.
- (3) Pfandler, P.; Bodenhausen, G.; Rapin, J.; Houriet, R.; Gaumann, T. *Chem. Phys. Lett.* **1987**, *138*, 195.
- (4) Hybl, J. D.; Ferro, A. A.; Jonas, D. M. *J. Chem. Phys.* **2001**, *115*, 6606.
- (5) Jonas, D. M. *Annu. Rev. Phys. Chem.* **2003**, *54*, 425.
- (6) Aue, W. P.; Bartholdi, E.; Ernst, R. R. *J. Chem. Phys.* **1976**, *64*, 2229.
- (7) Pfandler, P.; Bodenhausen, G.; Rapin, J.; Walser, M.-E.; Gaumann, T. *J. Am. Chem. Soc.* **1988**, *110*, 5625.
- (8) Bensimon, M.; Zhao, G.; Gaumann, T. *Chem. Phys. Lett.* **1989**, *157*, 97.
- (9) Williams, E. R.; Loh, S. Y.; McLafferty, F. W.; Cody, R. B. *Anal. Chem.* **1990**, *62*, 698.
- (10) McLafferty, F. W.; Stauffer, D. B.; Loh, S. Y.; Williams, E. R. *Anal. Chem.* **1987**, *59*, 2212.
- (11) Ross, C. W.; Guan, S.; Grosshans, P. B.; Ricca, T. L.; Marshall, A. G. *J. Am. Chem. Soc.* **1993**, *115*, 7854.
- (12) Van der Rest, G.; Marshall, A. G. *Int. J. Mass Spectrom.* **2001**, *210-211*, 101.
- (13) Ross, C. W.; Simonsick; Aaserud, D. J. *Anal. Chem.* **2002**, *74*, 4625.
- (14) Agthoven, M. A. Van; Delsuc, M.; Rolando, C. *Int. J. Mass Spectrom.* **2010**.

- (15) Agthoven, M. A. Van; Chiron, L.; Coutouly, M.; Delsuc, M.; Rolando, C. *Anal. Chem.* **2012**, *84*, 5589.
- (16) Agthoven, M. A. Van; Coutouly, M. A.; Rolando, C.; Delsuc, M. A. *Rapid Commun. Mass Spectrom.* **2011**, *25*, 1609.
- (17) Guan, S.; Jones, P. R. *J. Chem. Phys.* **1989**, *91*, 5291.
- (18) Agthoven, M. van; Chiron, L.; Coutouly, M. A.; Sehgal, A. A.; Pelupessy, P.; Bodenhausen, G.; Delsuc, M.; Rolando, C. *Int. J. Mass Spectrom.* **2014**, *Accepted*.
- (19) Marshall, A. G. *Acc. Chem. Res.* **1996**, *29*, 307.
- (20) Marshall, A. G.; Chen, T. *Int. J. Mass Spectrom.* **2014**, *In press*.
- (21) Marshall, A. G.; Wang, T.-C. L.; Ricca, T. L. *Chem. Phys. Lett.* **1984**, *105*, 233.
- (22) Zubarev, R. A.; Kelleher, N. L.; McLafferty, F. W. *J. Am. Chem. Soc.* **1998**, *120*, 3265.
- (23) Syka, J. E. P.; Coon, J. J.; Schroeder, M. J.; Shabanowitz, J.; Hunt, D. F. *Proc. Natl. Acad. Sci. U. S. A.* **2004**, *101*, 9528.
- (24) Little, D. P.; Speir, J. P.; Senko, M. W.; O'Connor, P. B.; McLafferty, F. W. *Anal. Chem.* **1994**, *66*, 2809.
- (25) Schnier, P. D.; Price, W. D.; Jockusch, R. A.; Williams, E. R. *J. Am. Chem. Soc.* **1996**, *118*, 7178.
- (26) Wells, J. M.; McLuckey, S. A. *Methods Enzymol.* **2005**, *402*, 148.
- (27) Chen, S.-P.; Comisarow, M. B. *Rapid Commun. Mass Spectrom.* **1991**, *5*, 450.
- (28) Ruidan, C.; Marshall, A. G.; Wang, M. *Chem. Phys. Lett.* **1991**, *18*, 168.
- (29) Mciver, R. T. *Int. J. Mass Spectrom. Ion Process.* **1989**, *89*, 343.

(30) Marshall, A. G.; Roe, D. C. *J. Chem. Phys.* **1980**, 73, 1581.

## GLOSSARY: Part-II

---

**Archimedes Spiral:** It is an Archimedean spiral also known as the arithmetic spiral or the spiral of Archimedes, named after the Greek Mathematician who first discussed it in 225 BC, in his work *On Spirals*. The equation of such a spiral in polar coordinates  $(r, \theta)$  is given as:

$$r = a + b\theta$$

where  $a$  and  $b$  can be any real numbers. The parameter  $a$ , drives the turns of the spiral and  $b$  controls the distance between the successive turns.

Source: Wolfram Math world.

**Bloch sphere:** The Bloch representation was developed by Felix Bloch in 1946 to explain many NMR phenomena. The superposition of two spin states can be represented as:

$$|\psi\rangle = c_1|1\rangle + c_2|2\rangle$$

where,  $c_1$  and  $c_2$  are normalised.

$$c_1^2 + c_2^2 = 1$$

This suggests that the state of the wave function can be represented by a vector of unit length starting from the origin. The geometric representation of states of coherent superposition is called the Bloch representation, with the vector defining the state called the Bloch vector, and the sphere, known as the Bloch sphere, as shown in the figure, can be represented in spherical coordinates of  $(r, \theta, \varphi)$ . The north and south poles represent the two states  $|1\rangle$  and  $|2\rangle$ , which

can also be assumed to have spin up and spin down. Points on the surface of the sphere represent pure states, whereas points in the interior of the sphere represent mixed states.

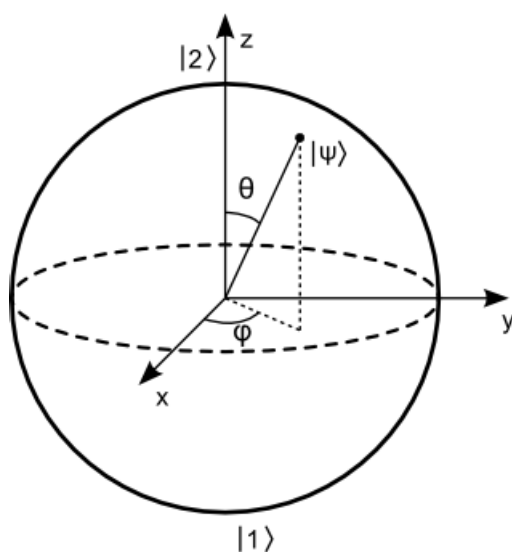
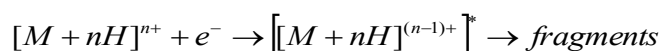


**Figure 1.** 2D Pictorial representation of Bloch sphere.

Source: Quantum Optics: An Introduction by *M.Fox*, OUP Oxford.

**ECD (Electron Capture Dissociation):** It is a method of fragmenting gas phase ions for mass spectrometric analysis. ECD involves the direct introduction of low energy electrons into a trap with ions in gas phase, forming an odd-electron ion which dissociates to form fragments:



The liberation of the internal energy results in fragmentation of the product ion without randomization of its energy.

Source: Mass Spectrometry: Principles and Applications by *E de Hoffmann and V. Stroobant*, Wiley

**IRMPD (Infrared Multiphoton Dissociation):** It is a method of fragmentation of ions in gas phase by using an infrared laser which is directed through a window into the vacuum chamber of a mass spectrometer where the ions are situated. It typically uses a CO<sub>2</sub> laser of 10.6 μm wavelength with a power of 25-50 W. The mechanism involves the absorption of multiple infrared photons by a given ion. The internal energy accumulates in various vibration modes, eventually breaking the bonds to form fragments of the precursor ion.

Source: Mass Spectrometry: Principles and Applications by *E de Hoffmann and V. Stroobant*, Wiley

**Isotopologue:** Isotopologues are molecules that differ only in their isotopic composition.

Source: Compendium of Chemical Terminology by *A.D. McNaught and IUPAC*, Blackwell Science Inc

**LC-MS (Liquid chromatography–mass spectrometry):** For analysis of complex mixtures, chromatographic separation techniques are combined with analytical capabilities of mass spectrometry. LC-MS is used in bioanalysis and in studies of proteomics and metabolomics.

Source: Mass Spectrometry: Principles and Applications by *E de Hoffmann and V. Stroobant*, Wiley.

**Mathieu Stability diagram:** The stability of the motion of a particle in a quadrupole analyzer is obtained by solving the differential Mathieu equation, for a function  $u$ , with  $a$  and  $q$  as constants:

$$u'' + (a - 2q \cos(2v))u = 0$$

For the quadrupole analyzer, the constants  $a$  depends on  $dc$  voltage and  $q$  depend on the  $rf$  voltages applied on the rods, and these parameters are also determined by the angular frequency, and  $m/z$  ratio. The solutions obtained are of two types: (i) periodic but unstable and (ii) periodic and stable which determines the motion of ions in the quadrupole analyzer. The stability curve is produced by plotting  $q$  against  $a$ . The  $rf$  voltage is usually kept constant and the stable trajectories for a given  $m/z$  are determined by observing various voltage combinations. These areas in the Mathieu stability diagram are termed stability regions, and are labeled A, B, C, and D in the figure shown below.

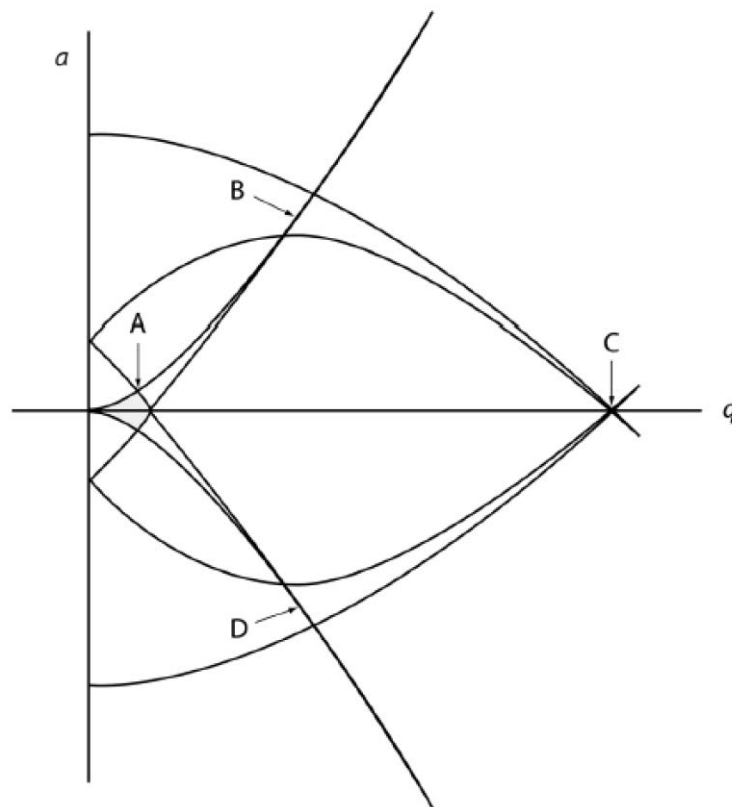


**Figure 2.** Mathieu stability diagram with the stability regions labelled as A, B, C and D.

Source: An introduction to quadrupole ion trap mass spectrometry, *R.E.March, Journal of mass spectrometry*, 32, 351-369 (1997), Mass Analysis by *G. H. Smith and S.J. Blanksby*, Wiley.

**Penning trap:** The Penning Trap was built by Hans Georg Dehmelt who named it after F. M. Penning from whose work on vacuum gauges he obtained his inspiration. A Penning trap is a device to store charged particles by applying a magnetic and electric field. The magnetic field prevents the escape of the ions perpendicular to the field and the ion thereby possesses a cyclotron motion represented by the unperturbed cyclotron frequency,  $\omega_c$ . The ions are confined in the direction of the magnetic field by applying voltages  $V_T$  to electrodes. The resulting ion motion thus can be described by three uncoupled harmonic oscillations determined by the reduced cyclotron frequency  $\omega_+$ , the axial or trapping frequency  $\omega_z$ , and the magnetron frequency  $\omega_-$ :

$$\omega_c = \frac{qB}{m}, \quad \omega_z = \sqrt{\frac{2qV_T\alpha}{md^2}}, \quad \omega_+ = \frac{\omega_c}{2} + \sqrt{\left(\frac{\omega_c}{2}\right)^2 - \frac{\omega_z^2}{2}}, \quad \omega_- = \frac{\omega_c}{2} - \sqrt{\left(\frac{\omega_c}{2}\right)^2 - \frac{\omega_z^2}{2}}$$

where,  $m$  is the mass of ion,  $q$  is its charge,  $d$  is depth of the trap and  $\alpha$  is a characteristic trap parameter. The magnetron and trapping frequencies are usually much lower than the cyclotron frequency. They are generally not detected unless there is a small misalignment of the instrument axis with respect to the magnetic field, or the amplitude of the ion motion is so large that it becomes comparable with the dimensions of the ICR cell.

Source: Fourier Transforms in NMR, optical and mass spectrometry: A User's Handbook by *A.G.Marshall* and *F.R. Verdun*, Elsevier

**Resolution:** It refers to the ability to distinguish two peaks of slightly different mass-to-charge ratios in a mass spectrum. The resolution is defined as:

$$R = \frac{m}{\Delta m}$$

where,  $m$  represents the observed peak and  $\Delta m$  represents the full width at half maximum (FWHM) of the peak.

Source: Mass Spectrometry: Principles and Applications by *E de Hoffmann and V. Stroobant*, Wiley.

**SRM (Selected reaction monitoring)**: It is a method used in MS/MS techniques where a particular precursor ion is selected and fragmented and then, in a next step, one of its fragment ions is monitored. When SRM is applied in three or more stages, rapidly examining different precursor/fragment pairs, then it is called as ***multiple reaction monitoring (MRM)***.

Source: Tandem mass spectrometry: a primer, *E. de Hoffmann, Journal of Mass Spectrometry*, 31, 129–137,(1996), Spectrometry: Principles and Applications by *E de Hoffmann and V. Stroobant*, Wiley.



## APPENDIX-I

Ion isolation experiments were performed for the following samples utilizing 2 step ejection-isolation pulse as shown in Figure 1, instead of the 3 step pulse discussed in the chapter 2.

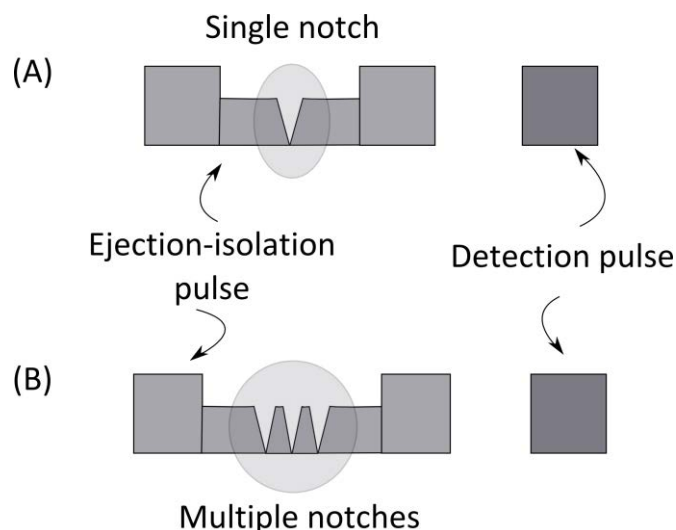


**Figure.1.** Two-stepped schemes for ion ejection by lowering the sweep rate for part of the ejection pulse: (A) for one ion, (B) for multiple ions.

Ubiquitin (8.6 kDa): Isolated peaks from the  $m/z$  cluster of  $MH_7^{7+}$ ,  $MH_8^{8+}$ ,  $MH_9^{9+}$ ,  $MH_{10}^{10+}$ ,  $MH_{11}^{11+}$ . The pulse parameters for ejection isolation pulse for all the isolation experiments were {78 V for 10 $\mu$ s and 1 V for 15000  $\mu$ s} and for detection a pulse of {78 V for 4  $\mu$ s} was used.

Ribonuclease A (13.7 kDa): Isolated various combinations of  $MH_{11}^{11+}$  and  $MH_{13}^{13+}$  simultaneously (Figure 2). For the same sample we succeeded in isolating the most abundant ions of three consecutively charged states ( $z = +11, +12$  and  $+13$ ) with a peak resolution of about 15000 and with an intensity of about 1/10th of the intensity of the peak in the conventional mass spectrum (Figure 3). Pulse parameters were same as used for ubiquitin.

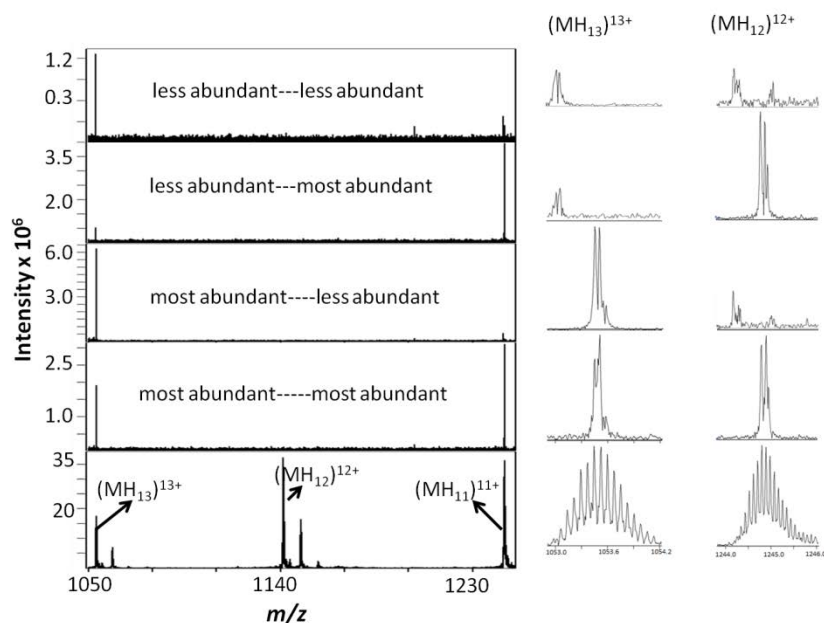


**Figure.2.** Isolated two charged states of ribonuclease A with different mass-over-charge combinations  $(MH_{13})^{13+}$  and  $(MH_{11})^{11+}$ . On the right side: expansions of the spectra shown on the left side.

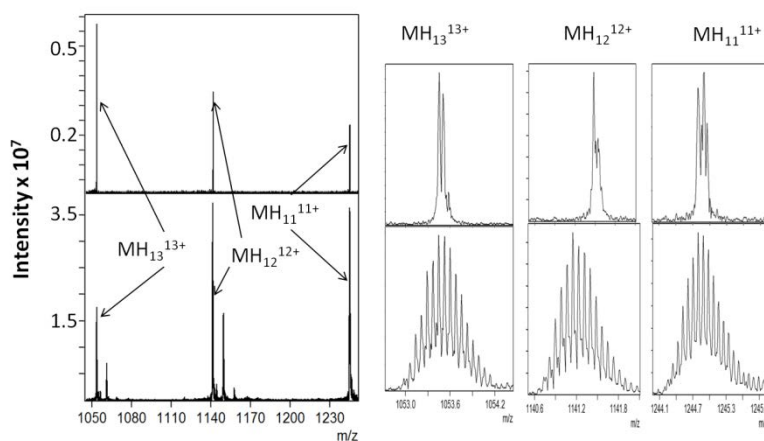


**Figure.3.** Simultaneous isolation of charged isotopic peaks of three consecutive ions of ribonuclease A. On the right side: expansions of the spectra shown on the left side.

These experiments were performed while optimising the conditions for ion isolation. A three stepped ejection-isolation pulse improved the resolution of the peaks isolated and also the isolation efficiency.



## RESUME DE LA THESE

---

Pendant ma thèse de doctorat, j'ai eu la grande chance de travailler sur le développement de nouvelles méthodes de deux techniques spectroscopiques complètement différentes : la Résonance Magnétique Nucléaire (RMN) et la Spectroscopie de Masse par Résonance Cyclotronique Ionique à Transformée de Fourier (FT-ICR/MS). En tant que méthodologiste, mon but principal a été d'améliorer les méthodes existantes et la théorie. En RMN, l'outil fantastique de la manipulation des spins permet la mise en place des séquences d'impulsions, et en FT-ICR, les rapports masse sur charge ( $m/z$ ) des ions et des fragments d'ions obtenus par différents chemins de fragmentation peuvent être appliqués à des problèmes en chimie, biochimie et médecine.

Le manuscrit de ma thèse de doctorat comporte deux parties. Les sujets abordés étant différents, ce manuscrit a été rédigé pour que chaque chapitre puisse être lu indépendamment. La première partie aborde la RMN dans le chapitre I. Dans ce chapitre, nous avons amélioré une méthode développée précédemment dans l'équipe pour l'étude de l'échange rapide des protons par RMN. Nous avons adapté la méthode à l'étude de l'acide aminé histidine, système en apparence simple mais qui s'est avéré très compliqué à l'étude. La nouveauté de cette étude consiste dans la détermination des vitesses d'échange sans connaître *a priori* ni les déplacements chimiques des protons labiles ni les constantes scalaires à une liaison. L'histidine est un acide aminé essentiel qui est souvent localisé dans les sites actifs des enzymes et d'autres protéines impliquées dans la catalyse, la régulation du pH, la liaison avec des métaux et la phosphorylation. Le caractère acido-basique de l'histidine rend cet acide aminé unique. En effet, l'histidine est le seul acide aminé comportant une chaîne latérale

imidazole qui agit soit comme un acide soit comme une base à pH physiologique. Cette propriété a une importance considérable pour la fonction de nombreuses protéines. Par exemple, la RMN a confirmé le rôle catalytique de His-12 et His-119 dans la ribonucléase A (RNase A), la fonction de régulation de His-146 dans l'hémoglobine humaine, le rôle de His-37 dans le transport des protons dans le virion par protonation et déprotonation de l'imidazole. Des études RMN pionnières basées sur la détection directe du proton ont montré que les protons  $H^{\epsilon 2}$  and  $H^{\delta 1}$  du cycle imidazole présentent des vitesses d'échange lentes dans la RNase et l'anhydrase carbonique humaine. Alors que la spectroscopie RMN a été utilisée pour déterminer les déplacements chimiques des noyaux  $^{15}\text{N}$  et les couplages scalaires  $^2J_{\text{NC}}$  and  $^3J_{\text{NC}}$  dans les cycles imidazole de l'histidine sur une large plage de pH, à notre connaissance, les vitesses d'échange des protons labiles dans l'histidine en solution n'ont pas encore été étudiées. La spectroscopie RMN en phase solide a été utilisée pour étudier les déplacements chimiques  $^{15}\text{N}$  and  $^{13}\text{C}$  de cristaux uniques d'histidine mais aussi de l'histidine lyophilisée ou microcristalline. De plus, les déplacements chimiques isotropes et anisotropes de  $^{15}\text{N}$  ont été exploités pour caractériser les équilibres tautomère et acido-basiques dans l'histidine. Cela a permis de trouver une corrélation linéaire entre les déplacements chimiques isotropes  $^{15}\text{N}$  de l'imidazole et le degré d'élongation de la liaison induit par la liaison d'hydrogène. Il a été également observé que les déplacements chimiques  $^{13}\text{C}$  du cycle imidazole de l'histidine lyophilisée à partir de solutions à différents pH conservaient la même information sur les  $\text{pK}_a$  que les solutions initiales.

Bien que la RMN soit sans égal dans la détermination des vitesses d'échange grâce à sa capacité de fournir des informations spécifiques site par site, son application est jusqu'à récemment restée limitée à la mesure de vitesses d'échange allant jusqu'à quelques centaines de  $\text{s}^{-1}$  dans des conditions favorables. Cette limite a pu être récemment repoussée par

plusieurs ordres de grandeur grâce à une méthode indirecte qui permet de déterminer avec précision les effets induits par l'échange rapide des protons sur la relaxation scalaire des noyaux  $^{15}\text{N}$ . Cette méthode a ainsi permis de mesurer des vitesses d'échange allant jusqu'à  $10^5 \text{ s}^{-1}$  pour un groupement NH. Elle exploite la décroissance de l'aimantation  $^{15}\text{N}$  sous l'effet d'un train d'impulsions de refocalisation du type Carr-Purcell-Meiboom-Gill (CPMG) en présence ou en l'absence du découplage des protons. Pendant ma thèse, j'ai étendu l'application de cette méthode à la mesure des vitesses d'échange des deux protons  $\text{H}^{\delta 1}$  and  $\text{H}^{\epsilon 2}$  du cycle imidazole et des protons  $\text{NH}_3^+$  de l'histidine en fonction du pH et de la température. De plus, nous avons déterminé les constantes de couplage scalaire à travers une liaison  $^1J_{\text{NH}_i}$  et les déplacements chimiques  $\Omega_{\text{H}_i}$  des protons « invisibles »  $\text{H}^{\delta 1}$ ,  $\text{H}^{\epsilon 2}$  et  $\text{NH}_3^+$  de l'histidine.

Il est important de remarquer que notre méthode permet de mesurer les vitesses d'échange  $k_{ex}$  des protons invisibles de l'histidine sans aucune connaissance préalable des déplacements chimiques  $\delta_{\text{H}}$  et des couplages scalaires  $^1J_{\text{NH}}$ . Plus précisément, notre approche permet de déterminer ces paramètres de façon indirecte. Les vitesses d'échanges pour les groupements  $\text{NH}^{\delta 1}$ ,  $\text{NH}^{\epsilon 2}$  et  $\text{NH}_3^+$  de l'histidine ont été mesurées à différents pH et températures. Cela nous a permis d'accéder aux énergies d'activation apparentes des processus d'échange en fonction du pH. Cette méthode peut être appliquée à l'étude des histidines dans des protéines à condition que les vitesses de relaxation transverse des  $^1\text{H}$ ,  $^{13}\text{C}$  et  $^{15}\text{N}$  ne soient pas trop rapides. L'ensemble de ces résultats fournit des informations précieuses sur le rôle essentiel du pH dans la chimie de l'histidine.

La deuxième partie de ma thèse de doctorat aborde la spectroscopie de masse et comprend deux chapitres. Dans le chapitre II, nous avons essayé de faire revivre et de mettre en œuvre une méthode longtemps oubliée ; il s'agit de la méthode d'isolement d'ions par éjection sélective ('notch ejection') par spectroscopie de masse FT-ICR. Nous avons montré que la technique peut être appliquée à des rapports élevés  $m/z$  sans perdre pour autant en résolution, paramètre tant convoité en spectroscopie de masse.

La spectrométrie de masse a fait un long chemin depuis sa découverte par J. J. Thompson en 1912, qui a étudié le flux d'ions positifs de néon à travers des champs magnétique et électrique en mesurant leur déflexion sur une plaque photographique et qui a pu observer les deux isotopes du néon  $^{20}\text{Ne}$  et  $^{22}\text{Ne}$ , puis la FT-ICR par Comisarow et Marshall en 1974, et l'état actuel de la FT-ICR, qui permet des développements dans des domaines comme la protéomique, métabolomique, et pétroléomique. L'isolation des ions a aussi fait d'énormes progrès depuis l'étude de la charge d'une gouttelette isolée d'huile ou d'alcool pour déterminer sa charge par Millikan en 1911 jusqu'aux techniques modernes pour la sélection et l'isolation d'ions dans des expériences MS/MS qui permettent l'étude de réactions ion/molécule, l'analyse de protéines, de séquences de peptides, l'élucidation de structures chimiques, etc. De nos jours, sur un spectromètre commercial Bruker FT-ICR, l'isolation des ions se fait de façon routinière en utilisant deux techniques discutées ci-après.

Des pièges d'ions quadrupolaires sont utilisés en association avec les spectromètres de masse FT-ICR pour sélectionner les ions précurseurs et pour effectuer une analyse 'tandem' de ions qui ont des rapports  $m/z$  dans une plage donnée. Ce type de pièges représente une approche relativement simple pour isoler les ions, car les ions peuvent être sélectionnés en appliquant des potentiels modulables à souhait avant leur entrée dans la cellule ICR. Les potentiels du

courant continu (*dc*) et du champ radio-fréquence (*rf*) laissent sortir du piège seulement les ions ayant des trajectoires bien stables alors que tous les ions ayant interagi avec le piège sont éliminés. Bien que l'utilisation de cette technique soit simple, tous les isotopologues, à savoir toutes les entités qui diffèrent dans leur composition isotopique, sont isolées ensemble ce qui ne conduit pas à une sélection propre, si bien que les pièges ne permettent pas de sélectionner de ions multiples dans des régions de rapports  $m/z$  différents dans une même expérience ; de plus, l'élimination d'une partie des ions conduit à une réduction de l'efficacité de l'isolation.

Les spectromètres de masse ICR sont facilement modulables. Cette versatilité vient du fait que les ions piégés peuvent être manipulés à souhait grâce à des impulsions *rf*. Cela conduit à une deuxième méthode pour l'isolation des ions qui est disponible sur les spectromètres de masse FT-ICR : la technique d'isolation dans la cellule, connue aussi comme technique CHEF (Correlated Harmonic Excitation Fields), qui utilise des impulsions d'excitation *rf* pour la sélection des ions. Dans cette méthode, une excitation balayée en fréquence du type CHIRP est utilisée pour mettre tous les ions non-désirés sur des orbites de rayon de plus en plus grand jusqu'à ce qu'ils entrent en collision avec les parois de la cellule, *i.e.*, avec les plaques de détection. À la place d'une impulsion CHIRP avec une variation de fréquence monotone, la fréquence peut être ajustée pour 'sauter' la fréquence cyclotronique de l'ion à isoler. Cette approche a le désavantage que les bandes latérales inhérentes aux balayages en fréquence peuvent conduire à l'excitation d'ions ayant un rapport  $m/z$  proche de celui des ions à éjecter. Une telle méthode n'est donc pas adaptée à l'étude de la fragmentation d'ions ni par dissociation multiphotonique infrarouge (IRMPD) ni par capture d'électron dissociative (ECD). Il faut savoir que, pendant le processus d'éjection, les ions vont acquérir

une énergie cinétique axiale et vont ainsi s'éloigner de plus en plus du centre ; cela rend la fragmentation par IRMPD difficile et, de plus, conduit à une interférence avec la fragmentation par ECD car, comme le laser est appliqué au centre de la cellule, on a une faible superposition des faisceaux d'électrons avec les ions décentrés.

Une autre méthode qui s'affranchit de tous ces désavantages de l'isolation quadrupolaire en cellule est la méthode appelée SWIFT de Marshall et de ses collaborateurs. Introduite en 1985, cette méthode 'stored waveform inverse Fourier transform' est encore considérée aujourd'hui comme la technologie la plus avancée pour l'isolation des ions. Dans cette méthode, le domaine d'excitation de fréquence est défini a priori et l'onde d'excitation est calculée en conséquence. En pratique, une impulsion d'excitation avec une forme d'onde définie est créée dans le domaine temps par transformée de Fourier inverse pour avoir un profil désiré dans le domaine de fréquence (ou rapport  $m/z$ ), ce qui permet une sélection d'ions très précise. Bien que SWIFT soit encore une technique de pointe, elle peut s'avérer lourde à mettre en œuvre en pratique car elle nécessite des interfaces et des logiciels adaptés.

Une autre méthode existe qui permet aussi d'éviter l'excitation hors-résonance. Elle a été initialement proposée par Noest et Kort en 1983. Les détails de cette méthode, qui est maintenant connue comme '*notch ejection*' (ce qui pourrait se traduire par « éjection à encoche »), ont été exposés dans la thèse de doctorat de A. J. Noest. Cette thèse n'a été publiée que plus tard et la méthode a été appliquée sur un spectromètre de masse commercial à l'étude de l'échange hydrogène-deutérium en isolant des hydroxides dans de petites molécules comme les phényl éthers. Des applications de la méthode ont été décrites par Vulpius *et al.* et par Farrell *et al.* et leurs collaborateurs. Les premiers ont pu isoler des ions peu abondants avec un rapport signal-sur-bruit remarquable et un pouvoir séparateur plus grand que 1 Da sur des fragments d'ions de 1-nonène ( $m/z$  68 et 54) générés par ionisation

par impact électronique. Farrell et ses collaborateurs ont appliqué la '*notch ejection*' à la séparation sélective d'ions dans une double cellule et ont ainsi isolé des ions avec des rapports  $m/z = 183$  dans un phosphate de triéthyl protoné.

Comme cette méthode simple d'isolation d'ions ne peut pas être appliquée à des systèmes ayant des rapports  $m/z$  grands sans une perte en résolution, elle n'est pas très populaire. En principe, elle demande l'excitation d'ions pendant la première moitié de balayage suivie d'une désexcitation des ions après inversion de la phase *rf*. On part de l'idée que la méthode nécessite une amplitude *rf* symétrique de part et d'autre de la fréquence sélectionnée, ce qui est difficile à réaliser à cause des caractéristiques défavorables des générateurs *rf*.

Pendant ma thèse, nous avons essayé de nous affranchir de toutes ces difficultés de la technique '*notch ejection*' et nous avons amélioré la méthode en modifiant le profile d'amplitude *rf* pendant le balayage en fréquence. Nous avons ainsi obtenu une grande résolution pour les échantillons de grande masse avec une isolation efficace et propre. La méthode a pu être facilement implémentée sur des spectromètres de masse FT-ICR car elle ne nécessite ni matériel ni logiciel supplémentaire.

Cette technique améliorée exploite l'inversion de la phase de l'impulsion *rf* lorsque le balayage de la fréquence *rf* est proche de la fréquence cyclotronique des ions à sélectionner, ce qui conduit à une sélection précise et propre sans perte d'intensité. Une isolation efficace d'un seul pic isotopique avant la fragmentation réduit la complexité des spectres de fragments d'ions, ce qui permet d'identifier plus facilement ces fragments. En utilisant trois niveaux d'amplitude, le temps expérimental a été considérablement réduit. Si la méthode classique exploitant un seul niveau d'amplitude dure des heures, la nouvelle approche ne prend que quelques minutes. Cette réduction du temps expérimental donne beaucoup de liberté sur la manipulation multiple des ions et permet ainsi une meilleure efficacité d'isolation. Une telle

approche à l'isolation d'ions peut être facilement utilisée sur les spectromètres commerciaux. Cependant, si l'on pouvait introduire une liste de fréquences, cela permettrait une utilisation encore plus efficace de la méthode. De plus, si l'on avait une meilleure connaissance du comportement des ions dans la cellule lors de l'inversion de la phase, on pourrait mieux optimiser les conditions, ce qui conduirait à une amélioration de la technique proposée.

Expérimentalement, nous avons obtenus des bons résultats non seulement pour l'isolation de fragments d'ions, isolation qui était très propre, mais aussi pour l'isolation des précurseurs. On a ainsi pu isoler les ions souhaités d'un complexe mixte de protéines marquées en  $^{13}\text{C}$  et  $^{15}\text{N}$  et étendre la méthode à une mesure quantitative de peptides, sans recours à la chromatographie, en utilisant la technique dite de quantification absolue (AQUA).

Un autre sujet abordé pendant ma thèse, qui est décrit dans le chapitre III, concerne l'utilisation de trois impulsions *rf* dans une expérience à deux dimensions (2D) ICR. Notre objectif a été de mieux comprendre la complexité du comportement des ions pendant cette expérience 2D ICR, en particulier pour le cas d'impulsions courtes. Les expériences à deux dimensions en RMN ont inspiré le développement de techniques 2D dans de nombreux autres domaines comme l'infrarouge, la résonance paramagnétique électronique de spins électroniques, la résonance cyclotronique ionique et la spectroscopie UV rapide à l'échelle des femtosecondes. Jusqu'à maintenant, ces techniques 2D n'ont eu ni l'impact ni l'étendue remarquables qu'elles ont eues en RMN. La technique 2D FT-ICR/MS a été introduite il y a environ 27 ans par les efforts communs d'un groupe de RMN dirigé par le Prof. Bodenhausen et d'un groupe de spectrométrie de masse dirigé par le Prof. Gäumann. Cette idée a été inspirée par deux expériences RMN 2D d'échange : la spectroscopie d'échange à deux

dimensions (EXSY) et la spectroscopie de l'effet nucléaire Overhauser, qui ont été exploités pour obtenir des informations sur des processus dynamiques tels que l'échange, l'isomérisation ou la structure. Dans une expérience 2D FT-ICR, des méthodes à une et deux fréquences ont été initialement utilisées pour cartographier des réactions ion-molécule dans des composés de petite taille. Pour s'affranchir des limitations de largeur de bande d'excitation des impulsions monochromatiques, les expériences ont été améliorées en utilisant des impulsions balayées en fréquence *rf* du type CHIRP. Ainsi, une dépendance du signal en fonction du temps d'évolution indirecte appelé  $t_1$  a été observée pour des ions de méthane ( $\text{CH}_3^+$ ,  $\text{CH}_4^{*+}$  et  $\text{CH}_5^+$ ) et du méthane deutérié ( $\text{CHD}_2^+$ ,  $\text{CHD}_3^+$  et  $\text{CD}_3^+$ ). Pfändler *et al.* avaient déjà observé que les expériences 2D FT-ICR/MS n'étaient pas limitées aux techniques de fragmentation en phase gazeuse comme la dissociation induite par collision (CID). Ils ont en effet enregistré un spectre de masse 2D FT-ICR en utilisant la méthode IRMPD pour la fragmentation. Deux autres méthodes ont été proposées pour enregistrer des spectres de masse FT-ICR à plusieurs dimensions : 2D Hadamard Transform/Fourier Transform (HT/FT) et SWIM (Stored Waveform Ion radius Modulation). Dans la première méthode, environ la moitié des ions précurseurs est sélectionnée, et les ions sont dissociés de façon simultanée en utilisant une excitation en forme de peigne; le processus est répété pour sélectionner l'autre moitié des précurseurs ( $N$  est aussi le nombre de précurseurs). La technique SWIM, développée par Ross *et al.*, combine des caractéristiques des deux méthodes HT/FT-ICR et de la séquence Pfändler-Bodenhausen-Gäumann. Alors que Pfändler *et al.* ont utilisé deux impulsions balayées en fréquence pour la modulation des rayons cyclotroniques, Ross *et al.* ont combiné ces deux impulsions dans une seule et varié l'amplitude de l'impulsion sinusoïdale en fonction de la fréquence en suivant un principe similaire proposé par McLafferty et ses collaborateurs. Dans cette technique, la fréquence de

la variation est conçue pour augmenter linéairement. Pour chaque spectre enregistré en domaine fréquence, la transformée de Fourier inverse est calculée et le voltage  $rf$  résultant est appliqué aux plaques d'excitation pour  $N$  formes d'onde, toutes différentes, avant l'injection du gaz dans la cellule ICR. Au lieu de calculer la transformée de Fourier en fonction de l'intervalle  $t_I$ , le signal est calculé en fonction du nombre des formes d'onde  $n = 1, 2, \dots N$ . En 2001, van der Rest a utilisé la méthode SWIM FT/FT-MS pour étudier des mélanges complexes, à savoir des dimères d'acides aminés liés soit par des protons soit par des ions de sodium. En 2002, Ross et ses collaborateurs ont appliqué SWIM à des produits de synthèse combinatoire ayant un intérêt pharmaceutique et à des produits d'intérêt pour l'industrie automobile.

Depuis 2010, l'intérêt pour les expériences 2D FT-ICR a été réanimé par l'équipe de C. Rolando qui a utilisé la méthode IRMPD pour la fragmentation de peptides. Ensuite, la technique de fragmentation ECD a été incorporée pour l'analyse 2D de complexes de protéines. Des algorithmes de débruitage comme celui de Cadzow et le rQR, qui sont fréquemment utilisés dans l'analyse des données RMN, ont été adaptés aux données 2D FT-ICR afin de réduire le bruit de scintillation dans la dimension indirecte. La méthode 2D FT-ICR/MS a le potentiel de devenir une méthode viable pour l'analyse chimique. Cependant, à part l'article de Guan et Jones sur la théorie de la méthode 2D, très peu d'articles traitent de cette technique dans la littérature. Ce travail théorique trouve des solutions élégantes et décrit les trajectoires des ions pour des impulsions  $rf$  longues ; en pratique, l'utilisation des impulsions longues conduit à une perte en sensibilité et, par conséquent, un tel modèle théorique ne semble pas adapté aux conditions expérimentales optimales. Pendant ma thèse, nous avons essayé de mettre les bases d'une théorie qui décrit le comportement des ions pour des cas pratiques, utilisant des impulsions courtes qui conduisent à une grande sensibilité.

Les méthodes 2D FT-ICR/MS ont les mêmes objectifs que les expériences MS/MS qui sont effectuées ion par ion. Le grand avantage de la méthode 2D FT-ICR est de permettre l'analyse des corrélations de tous les fragments possibles (les spectres des précurseurs, des fragments et des molécules neutres) dans une seule expérience. Nous avons revisité l'expérience originale 2D FT-ICR qui n'a pas conduit à de nombreuses applications analytiques à cause de limitations techniques à l'époque de sa conception. De nos jours, les nombreuses améliorations tant au niveau de l'instrumentation FT-ICR qu'au niveau du matériel informatique et des logiciels font que les obstacles initiaux ne sont plus un facteur limitant. Nous avons tenté d'aboutir à une meilleure compréhension de la complexité du comportement des ions pendant une expérience 2D à trois impulsions utilisée pour enregistrer des spectres ICR à deux dimensions. Par des simulations, nous avons cartographié les trajectoires des ions pour différentes relations entre la longueur des impulsions et leur phase. Nous avons également étendu nos études à l'analyse des contributions aux harmoniques dans les spectres 2D d'ions déplacés par rapport au centre de la cellule ICR.

Lors de l'optimisation des séquences d'impulsions, nous avons observé que les meilleurs résultats étaient obtenus en utilisant les intervalles les plus courts possibles pour chaque palier de fréquence au cours d'impulsions du type CHIRP. Nous avons initialement pensé que la différence de phase entre l'ion et la deuxième impulsion varie seulement avec la fréquence cyclotronique et  $t_1$  et conduit ainsi à propulser les ions sur des trajectoires de plus grand rayon. D'autre part, si l'ion et la deuxième impulsion sont en opposition de phase, l'ion est alors ramené au centre de la cellule. Cependant, cela ne peut arriver que si les ions sont excités pendant plusieurs dizaines de périodes  $rf$ , ce qui est impossible pour des intervalles très courts entre les impulsions CHIRP. Nous avons simulé les trajectoires des ions pendant les impulsions de codage en résolvant les équations des mouvements d'ions pour le cas idéal

d'une cellule de Penning. Pour des impulsions monochromatiques appliquées en résonance avec la fréquence des ions, nous avons observé que pendant la première impulsion l'ion gagne une certaine énergie cinétique et s'éloigne ainsi du centre par un mouvement en spirale. Le mouvement de l'ion pendant la période d'évolution ultérieure  $t_I$  suit une orbite qui est décalée par rapport au centre de la cellule sauf pour le cas où le produit entre la longueur de la première impulsion et la fréquence de précession de l'ion est un multiple exact de  $2\pi$ . Ainsi, même lorsqu'elle est en complète opposition de phase avec l'ion, la deuxième impulsion n'arrive pas à ramener l'ion exactement au centre de la cellule, ce qui est pourtant essentiel pour les expériences de fragmentation en utilisant la technique IRMPD. Une telle approche nous a permis d'obtenir les conditions de fragmentation des ions pour un ensemble de longueurs d'impulsions et de délais d'encodage. Nous avons également montré comment le déplacement des ions par rapport au centre de la cellule réduit les harmoniques ce qui permet d'utiliser des impulsions plus courtes dans l'expérience 2D FT-ICR sans avoir recours à des techniques sophistiquées de débruitage.

## Curriculum Vitae

### Research Interest

---

Development of methodology for Fourier Transform Ion Cyclotron Resonance (FT-ICR) mass spectrometry and Nuclear Magnetic Resonance (NMR) and analytical/biological applications of these techniques in proteomics, metabolomics, petroleomics etc.

### Career Recital

---

#### 1. PhD Research Scholar (Ecole Normale Superieure, Paris – July 2011 to present)

**Thesis title:** Methodology for Nuclear Magnetic Resonance (NMR) and Ion Cyclotron Resonance (FT-ICR) mass spectrometer.

**Thesis supervisor:** Prof. Geoffrey Bodenhausen

**Project Description:**

- a) *Fast proton exchange in histidine: measurement of rate constants through indirect detection by NMR spectroscopy.*
- b) *High-resolution ion isolation in FT-ICR Mass Spectrometry by modulating the radio-frequency (RF) phase during the frequency sweep.*
- c) *Spiraling ion trajectories in two-dimensional ICR mass spectrometry.*

#### 2. M.Sc. Dissertation (Indian Institute of Technology Roorkee, India – Jan. – June 2011)

**Project:** Interaction of DNA hexamer sequence d-(CGATCG)<sub>2</sub> with berberine by two-dimensional Nuclear Magnetic Resonance spectroscopy and restrained molecular dynamics

**Project Supervisors:** Dr. Maya S. Nair and Prof. Tashi Nautiyal

**Project Description:**

The project dealt with studying the interaction of anti cancerous drug with a hexamer DNA sequence through NMR and molecular dynamics (MD) simulations.

#### 3. M.Sc. Project (Indian Institute of Technology Roorkee, India – Jan – March 2011)

**Project:** Revisiting Planck and Bohr's correspondence principle

**Project Supervisors:** Prof. Tashi Nautiyal

**Project Description:**

Theoretical project to study the convergence and divergence of correspondence principle in the realms of classical and quantum mechanics.

#### 4. Summer Internship (University of Fribourg, Switzerland – May – July 2010)

**Project:** Analysis of photoinduced superconductivity in ferromagnetic (LCMO)/high temperature superconductors (YBCO) heterostructure.

**Project Supervisors:** Prof. Christian Bernhard and Dr. Vivek Kumar Malik

**Project Description:**

Charge transfer phenomenon at interfaces between complex oxides may lead to photoinduced superconductivity in heterostructures. We observed photogenerated effects in multilayer of YBCO LCMO YBCO heterostructure. We found transient photoconductivity with larger enhancements ( $T_c$  of 22.9 K) of superconductivity.

**5. Undergraduate Project (University of Lucknow, India – May – July 2008)**

**Project:** Review project on quantum dot fabrication techniques and application as a drug delivery device.

**Project Supervisor:** Dr. B. C. Yadav

---

## Academic and Professional Credentials

---

<b>Ph. D.</b> Ecole Normale Superieure, Paris, France	<b>2014</b>
<b>Master of Science (Physics)</b> [CGPA: 8.55/10] Indian Institute of Technology Roorkee, India	<b>2011</b>
<b>Bachelor of Science, (Physics and Nanotechnology)</b> [72.72%] University of Lucknow, India	<b>2009</b>

---

## Awards and Honors

---

- Student travel stipend award from 55<sup>th</sup> ENC, Boston (2014).
- National Agency of Research (ANR) funded grant for the doctoral studies since 2011-2014.
- Selected for "International Doctorate Program NanoBioTechnology" of Center for NanoScience in Munich in 2011.
- Amongst top 5 students in all Masters of Science courses of IIT Roorkee (2009-2011).
- Top 1% rank in Joint Admission test for Masters (JAM) conducted by IITs in 2009 amongst few thousand of applicants.
- Highest percentage of marks in university merit in B.Sc. (Physics and Nanotechnology) and amongst top 10 students in all undergraduate studies of university (2006-2009).
- 28<sup>th</sup> rank in National Science Talent Search Examination in 2004.
- Selected for the SIA Youth Scholarship, Ministry of Education, Singapore in 2004.

---

## Publications

---

1. **Sehgal A.A.**, Duma L., Bodenhausen G., Pelupessy P. (2014). Fast proton exchange in histidine: measurement of rate constants through indirect detection by NMR spectroscopy. *Chem. Eur. J.*, 20(21), 6332-6338.

2. van Agthoven M.A., Chiron L., Coutouly M.A., **Sehgal A.A.**, Pelupessy P., Delsuc M.A., Rolando C. (2014) Optimization of the Discrete Pulse Sequence for Two-Dimensional Fourier Transform Ion Cyclotron Resonance Mass Spectrometry. Accepted in *IJMS*, 370,114-124.
3. **Sehgal A.A.**, Pelupessy P., van Agthoven M.A., Bodenhausen G., Rolando C. (2014). High-resolution ion isolation in Fourier Transform Ion Cyclotron Resonance (FT-ICR) Mass Spectrometry by modulating the RF phase during the frequency sweep. (Under pre-submission review for *JASMS*).
4. **Sehgal A.A.**, Pelupessy P., Bodenhausen G., Rolando C. (2014). Spiraling ion trajectories in two-dimensional Ion Cyclotron Resonance Mass spectrometry. (Manuscript under preparation).

### Oral Presentations

1. **Sehgal A.A.**, van Agthoven M.A., Pelupessy P., Bodenhausen G., Rolando C., *Ion isolation in Fourier Transform Ion Cyclotron Resonance Mass Spectrometry by phase reversal of the sweep frequency*, the theme day of Doctoral School ED 388 on June 2012 at UPMC, Jussieu, Paris, France.
2. **Sehgal A.A.**, van Agthoven M.A., Pelupessy P., Bodenhausen G., Rolando C., *Ion isolation in Fourier Transform Ion Cyclotron Resonance Mass Spectrometry by phase reversal of the sweep frequency*, at the summer school on mass spectrometry by 'Jeunes de la Société Française de Spectrométrie de Masse (SFMS)', April 2012, La Bresse, France.
3. van Agthoven M.A., **Sehgal A.A.**, Chiron L., Coutouly M.A., Pelupessy P., Bodenhausen G., Delsuc M.A., Rolando C., *2D FT-ICR MS: New Instrumental and Software Developments for Peptide and Protein Analysis*, April 2012, Warwick, UK.
4. **Sehgal A.A.**, van Agthoven M.A., Pelupessy P., Bodenhausen G., Rolando C., *Ion isolation in Fourier Transform Ion Cyclotron Resonance Mass Spectrometry by notch ejection*, the theme day of the Chemistry Department, 'Journée des Jeunes Chercheurs', March 2012, ENS, Paris, France.

### Poster Presentations

1. **Sehgal A.A.**, van Agthoven M.A., Pelupessy P., Bodenhausen G., Rolando C., *Understanding the ion motion for 2D- Fourier Transform Ion Cyclotron Resonance Mass Spectrometer*, 11<sup>th</sup> European Fourier Transform Mass Spectrometry, April 2014, Paris, France.
2. **Sehgal A.A.**, van Agthoven M.A., Pelupessy P., Bodenhausen G., Rolando C., *High-resolution ion isolation by reversing the phase of frequency sweep in Fourier Transform Ion Cyclotron Resonance Mass Spectrometer*, 11<sup>th</sup> European Fourier Transform Mass Spectrometry, April 2014, Paris, France.
3. **Sehgal A.A.**, Duma L., Bodenhausen G., Pelupessy P., *Measurements of fast exchange rates by indirect detection in NMR: the case of histidine*, 55<sup>th</sup> Experimental Nuclear Magnetic Resonance Conference, March, 2014, Boston, MA, USA.

4. **Sehgal A.A.**, Duma L., Bodenhausen G., Pelupessy P., *Fast exchange rate constants of protons measured through indirect detection via  $^{15}\text{N}$  nuclei in histidine by NMR spectroscopy*, EUROMAR, July 2013, Hersonissos, Crete, Greece.
5. **Sehgal A.A.**, van Agthoven M.A., Pelupessy P., Bodenhausen G., Rolando C., *High-resolution ion isolation in Fourier Transform Ion Cyclotron Resonance Mass Spectrometry by reversing the phase of sweep frequency*, Société Française de Spectrométrie de Masse' (SFSM) Conference, September 2012, Orleans, France.
6. **Sehgal A.A.**, van Agthoven M.A., Pelupessy P., Bodenhausen G., Rolando C., *High-resolution ion isolation in Fourier Transform Ion Cyclotron Resonance Mass Spectrometry by reversing the phase of sweep frequency*, 10<sup>th</sup> European Fourier Transform Mass Spectrometry, April 2012, Warwick, UK.
7. **Sehgal A.A.**, Yadav A., Srivastava R., Yadav B.C. *Quantum dots: fabrication techniques and applications*, Symposium on current trends in Nanoscience and Technology (CTNT-09), ABV-IITM, Gwalior, India, January 2009.

## Summer Schools

---

- Alliance summer school on science and policy organized by Columbia University, New York and SciencePo, Paris from 18<sup>th</sup> – 26<sup>th</sup> June, 2013 at SciencePo, Paris, France.
- Mass spectrometry summer school organised by the Jeunes de la Société Française de Spectrométrie de Masse (SFMS) from 2<sup>nd</sup> - 06<sup>th</sup> April, 2012 at La Bresse, France.

## Technical Skills

---

- Technical language and softwares: Mathematica, Matlab, Origin, Qtiplot, Inkscape, mMass, Bruker Data Analysis, MS Office, Libre Office.
- Operating Systems: Linux, Windows.
- Lab skills: Instrument handling of NMR and FT-ICR mass spectrometer, wet-lab sample preparations, nanoparticle synthesis.

## Other Activities

---

- Student representative for Pierre and Marie Curie University (UPMC) at LERU (League of European Research Universities) Bright Conference (2013) from 12<sup>th</sup> – 16<sup>th</sup> August at University of Freiburg, Germany and University of Strasbourg, France.
- Managed the web-page of the group (2011-2013).
- Member of Babel Tower Club (book club) at Institute Curie, Paris, France (2012-2014).
- Member of Art of Living, Paris (Life member).

## Personal details

---

Name : Akansha Sehgal  
Father's Name : Ashvani Kumar Sehgal  
Mother's Name : Seema Sehgal  
Date of Birth : 28-04-1987  
Sex : Female  
Marital status : Single  
Languages : Hindi, Punjabi and English  
Nationality : INDIAN

## References

---

### **Prof. Geoffrey Bodenhausen**

Professor  
Département de Chimie,  
Ecole Normale Supérieure,  
24, rue Lhomond,  
75231 Paris cedex 05, France.  
Phone: +33 (0)1 44 32 34 02  
Email: geoffrey.bodenhausen@ens.fr  
geoffrey.bodenhausen@epfl.ch

### **Dr. Christian Rolando**

Research Director  
Miniaturisation pour la Synthèse, l'Analyse & la Protéomique (MSAP),  
USR CNRS 3290,  
Université de Lille-1, Sciences et Technologies,  
59655 Villeneuve d'Ascq, France  
Phone: +33 (0)3 20 43 49 77  
Email: christian.rolando@univ-lille1.fr

### **Dr. Philippe Pelupessy**

Research Engineer  
Département de Chimie,  
Ecole Normale Supérieure,  
24, rue Lhomond,  
75231 Paris cedex 05, France.  
Phone: +33 (0)1 44 32 33 44  
Email: philippe.pelupessy@ens.fr